AFRL-IF-RS-TR-2003-125
Final Technical Report
May 2003

USING A RECIRCULATING FIBER LOOP TO DETERMINE THE LIMITATIONS PLACED ON ULTRA-HIGH-PERFORMANCE SOLITON AND LINEAR OPTICAL SYSTEMS BY POLARIZATION MODE DISPERSION

University of Southern California

Sponsored by
Defense Advanced Research Projects Agency
DARPA Order No. J167

AIR FORCE RESEARCH LABORATORY
INFORMATION DIRECTORATE
ROME RESEARCH SITE
ROME, NEW YORK

This report has been reviewed by the Air Force Research Laboratory, Information Directorate, Public Affairs Office (IFOIPA) and is releasable to the National Technical Information Service (NTIS). At NTIS it will be releasable to the general public, including foreign nations.

AFRL-IF-RS-TR-2003-125 has been reviewed and is approved for publication.

APPROVED: 

PAUL SIERAK
Project Engineer

FOR THE DIRECTOR: 

WARREN H. DEBANY JR., Technical Advisor
Information Grid Division
Information Directorate

REPORT DOCUMENTATION PAGE

Form Approved
OMB No. 074-0188

1. AGENCY USE ONLY (Leave blank)	2. REPORT DATE	3. REPORT TYPE AND DATES COVERED
	MAY 2003	Final May 98 – Nov 02

4. TITLE AND SUBTITLE
USING A RECIRCULATING FIBER LOOP TO DETERMINE THE LIMITATIONS PLACED ON ULTRA-HIGH-PERFORMANCE SOLITON AND LINEAR OPTICAL SYSTEMS BY POLARIZATION MODE DISPERSION

5. FUNDING NUMBERS
C - F30602-98-1-0196
PE - 62110E
PR - G150
TA - 00
WU - 01

6. AUTHOR(S)
Allan E. Willner and Paniz Ebrahimi

7. PERFORMING ORGANIZATION NAME(S) AND ADDRESS(ES)
University of Southern California
Optical Communications Laboratory
Los Angeles California 90089-1147

8. PERFORMING ORGANIZATION REPORT NUMBER
N/A

9. SPONSORING / MONITORING AGENCY NAME(S) AND ADDRESS(ES)
Defense Advanced Research Projects Agency
3701 North Fairfax Drive
Arlington Virginia 22203-1714

AFRL/IFGA
525 Brooks Road
Rome New York 13441-4505

10. SPONSORING / MONITORING AGENCY REPORT NUMBER
AFRL-IF-RS-TR-2003-125

11. SUPPLEMENTARY NOTES
AFRL Project Engineer: Paul Sierak/IFGA/(315) 330-7346/ Paul.Sierak@rl.af.mil

12a. DISTRIBUTION / AVAILABILITY STATEMENT
APPROVED FOR PUBLIC RELEASE; DISTRIBUTION UNLIMITED.

12b. DISTRIBUTION CODE

13. ABSTRACT ***(Maximum 200 Words)***
System effects of Polarization Mode Dispersion (PMD) were investigated both experimentally and theoretically. Several novel methods for PMD emulation, compensation and monitoring were developed, theoretically analyzed and experimentally investigated.

14. SUBJECT TERMS
Single Mode Fiber, Polarization Mode Dispersion, PMD Compensation

15. NUMBER OF PAGES
76

16. PRICE CODE

17. SECURITY CLASSIFICATION OF REPORT	18. SECURITY CLASSIFICATION OF THIS PAGE	19. SECURITY CLASSIFICATION OF ABSTRACT	20. LIMITATION OF ABSTRACT
UNCLASSIFIED	UNCLASSIFIED	UNCLASSIFIED	UL

Table of Contents

List of Figures and Tables

List of Tables

1. Introduction

Polarization Mode dispersion (PMD) has emerged as one of the critical hurdles for next generation high bit-rate transmission systems (≥10GB/s/channel). To first order, PMD can be represented by a differential group delay (DGD) between the two principal states of polarization.

For a fixed average PMD value, DGD is a random variable that has a Maxwellian probability density function. A critical aspect of PMD compensation is to account for the low probability but high-degradation tails of this distribution. PMD is a stochastic, random process because: (i) each short discrete length of fiber will have a slightly different core asymmetry, (ii) the extent of the signal degradation caused by PMD is dependent on the state of polarization of light at a given point in the fiber link, and (iii) the state of polarization of an optical signal will wander randomly due to temperature changes and mechanical stress.

Fibers links deployed before 1996 may have a PMD value that is perhaps >100 times greater than present-day fiber. Even with new fiber, PMD, remains a major problem since: (i) there is still a small residual asymmetry in the fiber core, and (ii) slight PMD exists in discrete in-line components, such as isolators, couplers, filters, Erbium-doped fiber (EDF), modulators, and multiplexers. Therefore, even under the best of circumstances, PMD will still significantly limit the deployment of 40Gbit/s systems.

PMD issues can be categorized in 4 different sections: System issues, emulation, compensation and monitoring. Using this grant we have researched all these different issues which will be explained in more detail in their corresponding sections.

System Issues: In contracting the deleterious effects of PMD, it is important for systems designers to determine the relative merits of using several possible data formats for high-speed systems that use the embedded fiber base. The formats considered are non-return-to-zero (NRZ), return-to-zero (RZ), solitons—and specifically dispersion-managed solitons (DMS), and pre-chirped RZ (CRZ). Many signal degrading effects evolve quite differently in the regime of high PMD— PMD > 0.5 ps/km$^{1/2}$—as compared to the regime of low PMD—PMD << 0.5 ps/km$^{1/2}$—at 10 Gbit/s. In particular, although soliton pulses might be less affected at low PMD due to the pulse stability and trapping in one state-of-polarization, solitons tend to become unstable under high PMD conditions. We compared the performance of NRZ, RZ, dispersion-managed solitons, and pre-chirped RZ in the presence of high PMD for 10 Gbit/s terrestrial systems. Fiber nonlinearities and signal chirp interacted with PMD-induced pulse distortion to generate clear trends in system power penalties. The chirped RZ pulses seemed to be the most tolerant to high PMD values.

Another important issue to take into consideration is the interaction between fiber nonlinearities and the PMD especially in the presence of several WDM channels. We show that in a WDM system, where different channels experience phase changes due to nonlinear interactions between the channels, first-order PMD compensation is not as effective as in the case of a single channel system. The phase change due to XPM can introduce bit-pattern-dependent variations of the principal states of polarization (PSP), therefore making it impossible to fully compensate for first-order PMD.

Another important issue is the interaction between PMD and Polarization Dependent Loss (PDL) of the components in the system. In most of the analysis for a system with PMD, PDL is considered to be zero, but when PDL is not negligable the PMD effect (pulse broadening) can be severely magnified. We investigated the statistical properties of the interactions between PMD and PDL using a 10-Gb/s, 8×82-km, recirculating fiber-loop testbed. As average PDL varied from 1.0 to 2.1 dB with a fixed average PMD of 18 ps, the power penalty at 2% probability increased from 2.5 to 4.3 dB.

PMD Emulation: High PMD fiber is not commercially available, and even if it were, it would not be able to rapidly explore a large number of different fiber conditions. For testing of optical systems that may be affected by PMD and especially for the characterization of PMD compensators and PMD monitors, it is critical to be able to accurately emulate first and higher-order PMD and quickly cycle through a large number of different fiber PMD states. In addition the frequency autocorrelation function of the emulators should ideally follow the real fiber and quadratically tend to zero. This will accommodate correct PMD emulation of several WDM signals simultaneously. We have investigated a technique to accurately emulate PMD using multiple sections of PM fiber with rotatable connectors. Also we have come up with a method to emulate PMD in a short circulating fiber loop using loop-synchronous polarization scrambler.

PMD Compensation: It is usually considered that the maximum tolerable PMD is between 10-20% of the bit duration. Typical PMD values of installed fibers are greater than 1.5ps/√km, which limits to a few 100km the transmission distance at 10Gb/s the maximum tolerable PMD value without compensation is rapidly reached. For higher values compensation is required. We have proposed several schemes to increase the tolerable PMD value. We have looked at first order Fiber Bragg Grating (FBG) Compensator, WDM compensation using a single module, combined effect of Forward Error Correction and first order compensation, higher order compensation, PDL compensation and the effect of nonlinearities (specifically XPM) on successful compensation.

PMD Monitoring: Since the birefringence of a fiber changes randomly along a fiber link and the state-of-polarization of an optical signal changes with environmental conditions, PMD effects on the data signal are stochastic and time varying. Therefore, any PMD compensator at a receiver must track the degrading effects of PMD and dynamically adjust the amount of compensation. Such tracking requires accurate monitoring of these ≥ms-time-scale effects. In addition, even if the PMD compensation is implemented after the receiver and in the electrical domain, still optical PMD monitors will be crucial in compensation. Several methods for monitoring PMD have been investigated and are discussed further throughout this report.

2. PMD systems effects

The following system effects were investigated.

(a) The performance of NRZ, RZ, dispersion-managed solitons, and pre-chirped RZ in the presence of high PMD was compared for 10 Gbit/s terrestrial systems. Fiber nonlinearities and signal chirp interacted with PMD-induced pulse distortion to generate clear trends in system power penalties. The chirped RZ pulses are shown to be the most tolerant to high PMD values.

(b) In a WDM system, where different channels experience phase changes due to nonlinear interactions between the channels, first-order PMD compensation is not as effective as in the case of a single channel system. The phase change due to XPM can introduce bit-pattern-dependent variations of the principal states of polarization (PSP), therefore making it impossible to fully compensate for first-order PMD. In fact, for optical power as low as 3 dBm/channel in systems where PMD is not uniformly distributed along the transmission link, first-order PMD post-compensation can be ineffective.

(c) The combined statistical effect of PMD and PDL was investigated in a 10-Gb/s, 8×82-km, recirculating fiber-loop testbed. As average PDL varies from 1.0 to 2.1 dB with a fixed average PMD of 18 ps, the power penalty at 2% probability increases from 2.5 to 4.3 dB.

(d) It is shown that polarization dependent gain (PDG) in Raman fiber amplifiers is a statistical parameter that depends on the PMD of the fiber. The PDG distribution is characterized by simulation and verified by experiment.

2.1 Comparison of different modulation formats in terrestrial systems with high polarization mode dispersion

The performance of NRZ, RZ, dispersion-managed solitons, and pre-chirped RZ in the presence of high PMD was compared for 10 Gbit/s terrestrial systems. Fiber nonlinearities and signal chirp interacted with PMD-induced pulse distortion to generate clear trends in system power penalties. The chirped RZ pulses are shown to be the most tolerant to high PMD values.

In contracting the deleterious effects of PMD, it is important for systems designers to determine the relative merits of using several possible data formats for high-speed systems that use the embedded fiber base. The formats considered are non-return-to-zero (NRZ), return-to-zero (RZ), solitons—and specifically dispersion-managed solitons (DMS), and pre-chirped RZ (CRZ). Many signal degrading effects evolve quite differently in the regime of high PMD— PMD > 0.5 ps/km$^{1/2}$—as compared to the regime of low PMD—PMD << 0.5 ps/km$^{1/2}$—at 10 Gbit/s. In particular, although soliton pulses might be less affected at low PMD due to the pulse stability and trapping in one state-of-polarization, solitons tend to become unstable under high PMD conditions. Previously published analyses of optical pulse propagation along a fiber link have

generally been limited to the statistical average time evalution of these pulses. However, there has been little system study of the limitations placed on terrestrial systems by considering the complete statistical characteristics of PMD.

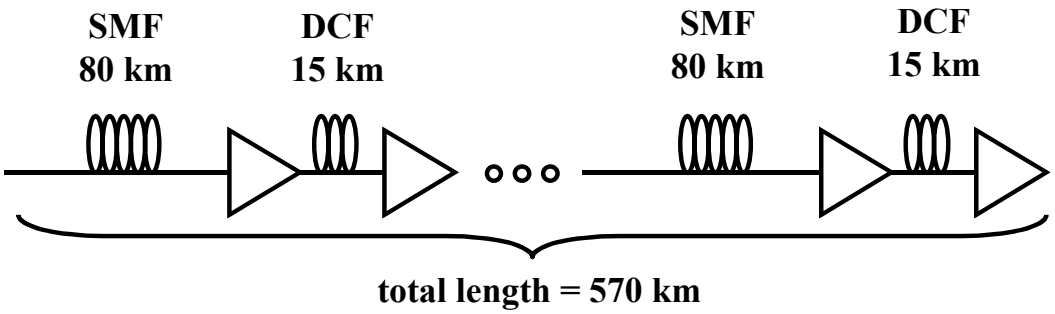

Figure 1. Model used for terrestrial system. Dispersion of the SMF = 17 ps/nm/km, loss of SMF = 0.25 dB/km, loss of DCF = 0.5 dB/km

We concentrated our model on terrestrial systems operating at 10 Gbit/s. Figure 1 shows the setup of our model. We consider a dispersion map that consists of 80 km of single-mode fiber (SMF), 15 km of dispersion compensation fiber (DCF), and 2 optical amplifiers. This is a commonly used dispersion map for terrestrial systems. The average input power is set to 5 dBm and –1 dBm for SMF and DCF fibers respectively. Six stages of this dispersion map are considered, totaling 570 km of transmission. We assumed zero average dispersion for NRZ and RZ (50% duty cycle) formats, and approximately 0.4 ps/nm/km for DMS format. For CRZ (chirp=1) format, the total residual dispersion of the link is assumed to correspond to the maximum pulse compression at the end of transmission with no PMD in the link—i.e. approximately 150 ps/nm. The full width at half-maximum power of DMS pulses was optimized for the best performance with no PMD in the link—i.e. approximately 25 ps.

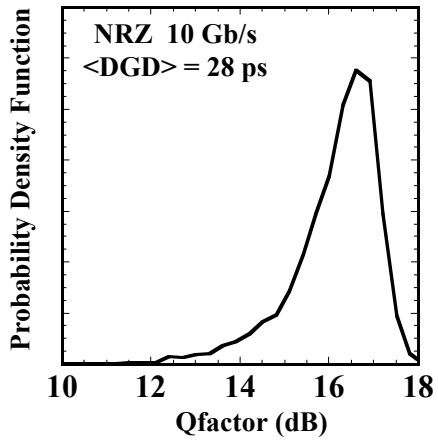

Figure 2. Q factor distribution for 10,000ensembles of fibers. Average accumulatedDGD is 28 ps.

For each PMD value, an ensemble of 10,000 fibers is evaluated using the coarse step method. An ideal integrate-and-dump receiver is considered, and the best sampling time is searched within a bit-time window to take into account the PMD-induced pulse shifts. Amplified spontaneous emission noise is assumed as the dominant noise source. Figure 2 shows the Q-factor probability density function for a 10 Gbit/s NRZ system with 28 ps of average differential group delay (DGD). The Q-factor can vary over a wide range depending on the birefringence of different segments of transmission fiber. Since it is insufficient to consider the average system performance, we take into account the worst case Q-factor that appears in the tail of its distribution.

Figures 3(a) and 3(b) show average and worst case—with probability of 0.001—PMD-induced power penalties for different PMD values (average DGD) and different modulation formats at 10 Gbit/s. There is a large differential in power penalties between the worst case and average case scenarios. In general, pulses with shorter duty cycles—including RZ, DMS and CRZ—perform better than NRZ because they have a wider margin which makes them more tolerant to pulse broadening. In NRZ format, PMD-induced inter-symbol interference causes a rapidly increasing "0" level. Higher "0" levels induce higher amplifier-generated noise on the "0" bits and increase the power penalty. DMS and RZ tend to perform similarly for high-PMD values. It should be noted that soliton trapping, in which soliton energy remains in a single polarization, can not prevent PMD-induced distortion as PMD values considered here are higher than the trapping limit.

It is well known that chirped pulses in the presence of the chromatic dispersion undergo initial compression if the signs of the chirp and dispersion are the same. Knowing this fact, we introduced chirped super-gaussian RZ pulses (CRZ) as the input signal and took advantage of the pulse compression to negate PMD-induced pulse broadening. This type of signal format would have a similar pulse width as RZ format but it has a specific phase change—i.e. chirp—at the edges of the pulse. It is important that the signal chirp and the residual chromatic dispersion of the transmission link are matched to generate the maximum pulse compression at the receiver end. Due to PMD-induced pulse broadening, some part of the pulse energy leaks to the neighboring bits, and causes inter-symbol-interference and high power penalty. Chirp-induced pulse compression helps the pulse energy to remain in its bit time, and therefore decreases the power penalty. This leads to a superior performance for CRZ pulses over other data formats at higher PMD values.

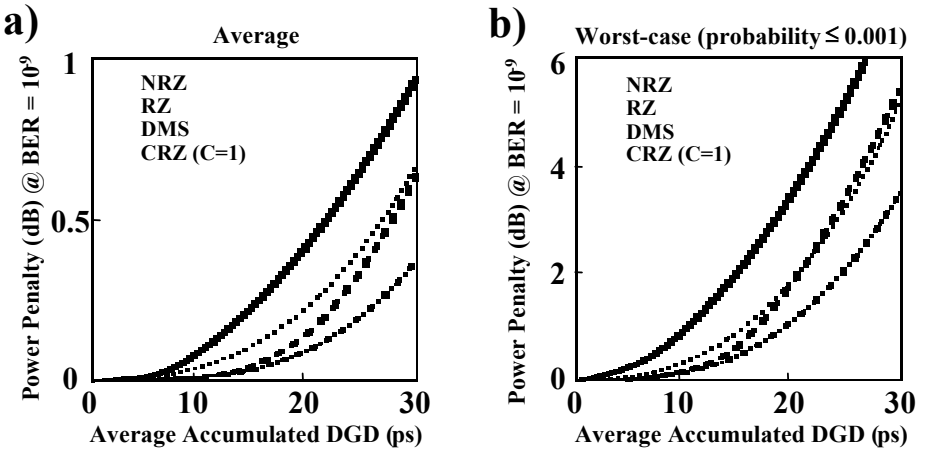

Figure 3. PMD-induced power penalty @ BER=10^{-9} for different PMD values in an ensemble of 10,000 fiber after 570km transmission, a) average power penalty, b) worst case power penalty (probability ≤ 0.001).

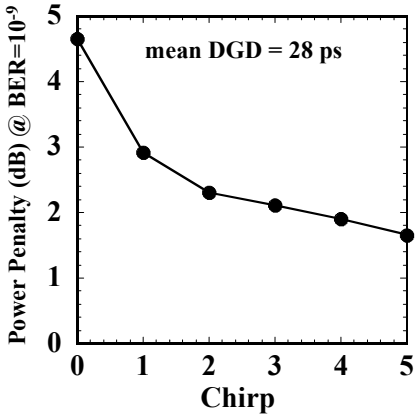

Figure 4. Chirp effect on 10 Gbit/s RZ systems with 28 ps average accumulated DGD after 570 km transmission.

Figure 4 shows the influence of chirp on power penalty for RZ pulses at 28 ps average DGD. For different chirp values, the residual dispersion of the transmission link is assumed to match for the maximum pulse compression at the receiver end with no PMD in the link. It is shown that pre-chirping can greatly reduce the power penalty caused by PMD. For chirp=1, ~1.7 dB improvement compared to un-chirped RZ is obtained. Although the result is shown for a super-Gaussian chirped RZ pulses, we also evaluated the performance improvement for linearly chirped RZ pulses (chirp=1) and found similar improvement. By increasing the chirp to 5, the power penalty improves by ~ 3 dB. However, large chirp values result in much higher bandwidths than the un-chirped signal.

2.1.1 Experimental Penalty distribution comparison for different data formats under high PMD values

The performance of conventional and chirped versions of RZ and NRZ was experimentally compared in 10-Gbit/s systems that have high average DGD of >40 ps. It was found that the RZ formats have a significantly smaller power variance (~2 dB) between the peak and the 2-% tail of the power distribution than the NRZ formats, which reduces the probability of link outage. Furthermore, chirped-NRZ (CNRZ) provides a significant increase (>2 dB) in baseline sensitivity relative to NRZ. Overall, chirped-RZ (CRZ) provides the best performance.

Figure 5 shows the experimental setup used to compare the four different data formats in the presence of high PMD (average DGD ~42.6 ps). An external-cavity laser at 1556.7 nm is externally modulated with two cascaded electro-optic (EO) modulators to achieve NRZ and RZ intensity modulation at 10-Gbit/s (2^{15}-1 PRBS). The phase-adjusted 10-GHz clock signal is applied at the second EO-modulator to obtain RZ data. A phase modulator, also driven with the clock signal, is used to introduce a sinusoidal chirp after intensity modulation. The PMD emulator consists of 15 sections of polarization-maintaining (PM) fiber, with 9 polarization controllers distributed between the sections to realize different polarization coupling and therefore closely emulate the Maxwellian distribution of DGD. The measured average DGD value of the emulator is ~42.6 ps.

After the PMD emulator, 16 km of dispersive single-mode fiber (SMF) is used to compress the pulses for CNRZ and CRZ data. The amount of the applied chirp for CNRZ and CRZ is optimized based on bit error rate (BER) performance after the 16 km of SMF, with a resulting modulation depth at the phase modulator of about 0.5 for both cases.

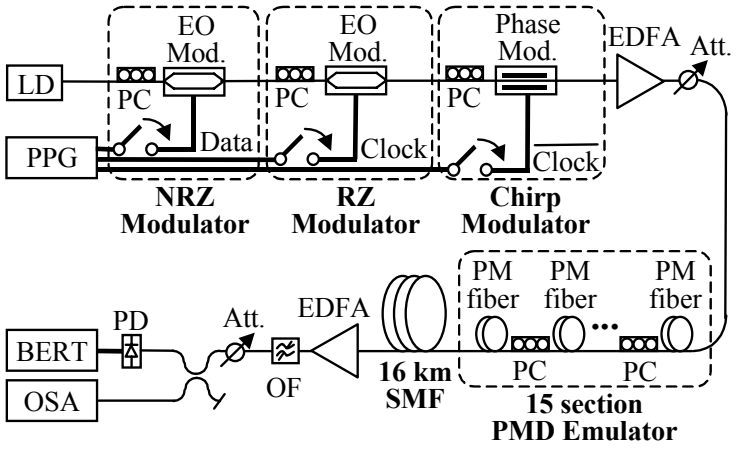

Figure 5. Experimental setup (PPG: pulse pattern generator, OF: optical filter, Att. :variable attenuator)

The distribution of the received optical power at BER=10^{-9} in the presence of PMD is measured for the four different data formats by randomly changing the polarization coupling inside the PMD emulator using the polarization controllers. Figure 6 shows the measured distribution of the received optical power at BER=10^{-9} for (a) NRZ, (b) CNRZ,

(c) RZ, and (d) CRZ (500 distinct emulator states for each data format). The general shape and tail of the NRZ distribution is similar to the CNRZ distribution, and the general shape and tail of the RZ distribution is similar to the CRZ distribution.

For a given data format, the power variance between the peak and the 2-% tail (corresponding to the 10 worst out of the 500 samples) position provides crucial information about the sensitivity of that format to PMD-related effects. The positions of the peak and the 2-% tail of the power distributions for the four data formats are listed in Table 1. The RZ and CRZ data formats achieve a ~2 dB lower power variance than the corresponding NRZ formats (measured between the peak and the 2-% tail position of the distribution). Due to their narrower pulse widths, RZ and CRZ data formats have a greater tolerance for pulse spreading at larger DGD values (i.e., at the tail of the DGD distribution) than NRZ and CNRZ data formats. This results in less increase in the "0"-level caused by inter-symbol-interference, and hence in less signal-spontaneous beat noise for the RZ formats. For both RZ and NRZ, chirping the signal results in a higher baseline sensitivity.

Figure 7 shows measured eye diagrams for NRZ, CNRZ, RZ, and CRZ: without PMD (top), at the peak of the distribution with PMD (middle) and at the tail end of the received optical power distribution with PMD (bottom). Severe distortion of the received eye diagrams at the tail of the power distribution can be observed for all four formats, but the CRZ and RZ formats show a better eye opening compared to NRZ.

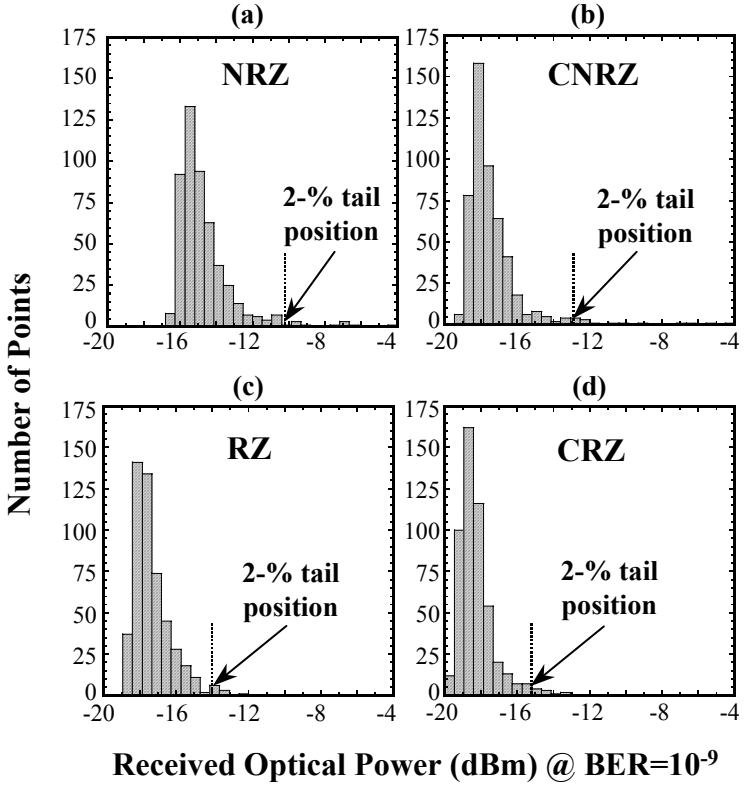

Figure 6. Measured distribution of the received optical power at BER=10-9 for (a) NRZ, (b) CNRZ, (c) RZ, (d) CRZ data formats (average DGD ~42.6 ps).

Table 1. Received optical peak power, 2-% tail power, and power variance between peak and 2-% tail at BER=10^{-9} for NRZ, CNRZ, RZ, and CRZ data formats (average DGD ~42.6 ps).

	RZ		NRZ	
	with chirp	without chirp	with chirp	without chirp
Peak power (dBm)	-18.6	-17.9	-18.1	-15.7
2-% tail power (dBm)	-15.2	-14.0	-12.7	-10.0
Variance between peak and 2-% tail (dB)	3.4	3.9	5.4	5.7

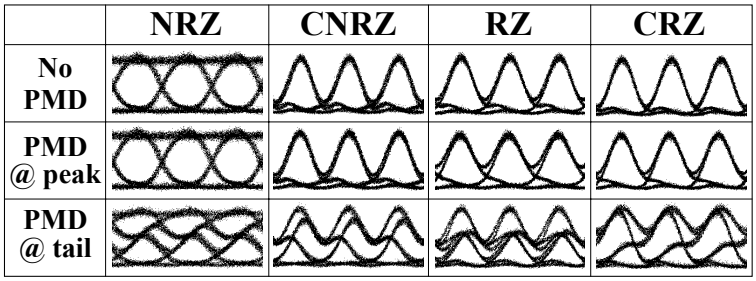

Figure 7. Measured eye diagrams for different data formats.

2.2 Limitations to First-Order PMD Compensation in WDM Systems Due to XPM-Induced PSP Changes

We show both numerically and experimentally that the nonlinear phase change due to XPM induces a bit-pattern-dependent change in the state-of-polarization that translates to uncertainty in the PSP. This effect severely limits the effectiveness of first-order PMD post-compensation and suggests the use of in-line compensation.

First-order PMD compensation is the simplest technique to compensate for PMD. It is accomplished by simply delaying one state-of-polarization (SOP) with respect to the other by the amount of DGD. There have been several experiments to demonstrate first-order PMD compensation. However, nearly all of these experiments only used single-channel PMD compensation, and the potentially significant effects of fiber nonlinearities in WDM systems on first-order PMD compensation were overlooked.

We show that in a WDM system, where different channels experience phase changes due to nonlinear interactions between the channels, first-order PMD compensation is not as effective as in the case of a single channel system. We show that the phase change due to XPM can introduce bit-pattern-dependent variations of the principal states of polarization (PSP), therefore making it impossible to fully compensate for first-order PMD. In fact, for optical power as low as 3 dBm/channel in systems where PMD is not uniformly distributed along the transmission link, first-order PMD post-compensation can be ineffective.

Nonlinear Transformation of the SOP

The index of refraction can be changed by the optical power in a specific polarization state, resulting in a nonlinear birefringence. In WDM systems, cross-phase modulation (XPM) induces a nonlinear, bit-pattern-dependent phase change in an optical signal whenever there is optical power present at other wavelengths, causing a bit-pattern-dependent variation in the SOP. Figure 8 illustrates this concept for a simple 2-channel system. The bits at wavelength λ_1 that propagate alongside a long series of "1"s in the channel at λ_2 experience a small change in the birefringence of the fiber that changes their original SOP. This effect becomes significant when the relative SOPs of the channels are preserved over a distance that is long enough for nonlinear interactions to accumulate, implying that the nonlinear change in the SOPs is more prevalent in fibers with very low PMD, in which the relative polarization states of the channels remain correlated over long distances.

If the PMD is not uniformly distributed along the transmission fiber (e.g., high PMD sections of fiber are followed by low PMD sections of fiber), the overall link will still require compensation. However, the nonlinear change of the SOPs in the low PMD fiber sections can seriously reduce the effectiveness of PMD compensators, due to the fact that the overall PSP is dependent on the power of the other optical channels and their SOPs. Since first-order PMD compensation depends on applying the appropriate amount of DGD, aligned with the PSPs of the signal, it follows that if the PSP is bit-pattern-dependent, PMD compensation cannot be effectively realized.

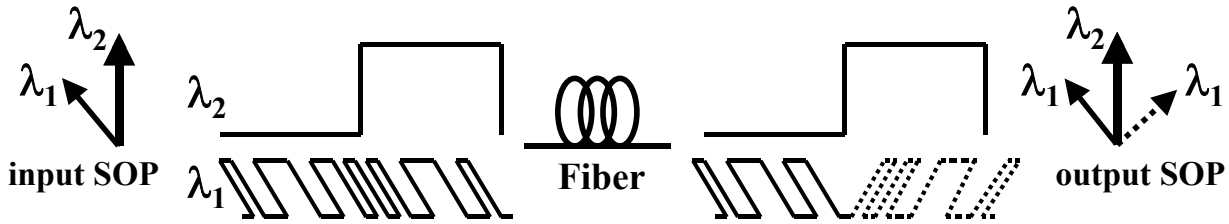

Figure 8. Optical power induces a small nonlinear birefringence that randomizes the SOP, limiting the effectiveness of first-order PMD compensation.

Numerical System Model and Experimental Set-up

Our simulations concentrated on terrestrial systems operating at 10 Gbit/s. Each dispersion map consists of 85 km of single-mode fiber (SMF), 15 km of dispersion compensating fiber (DCF), and two gain stages. The average input powers are set to 5 dBm and –2 dBm for the SMF and DCF fibers, respectively. We considered six stages of dispersion-map transmission, totaling 600 km. The WDM channel spacing is considered to be 0.8 nm. A low-pass filter with a 6 GHz cut-off frequency is used at the receiver. The sampling time and decision threshold are optimized to account for PMD-induced bit-pattern shifts. Amplified spontaneous emission noise is assumed as the dominant noise source.

For our experiment, we used an optical recirculating loop, which consists of ~82 km SMF and ~12 km DCF. The signal passed a single-section PMD compensator with ~76 ps DGD after 6 passes through the loop.

Results

To evaluate the effects of XPM on PMD compensation, we first consider the simple case of a 2-channel system. The first channel contains a random 64-bit signal, with 50 ps of DGD applied to its two orthogonal polarization components, and is transmitted over 600 km of low PMD fiber [0.1 ps/(km)$^{1/2}$]. First-order PMD compensation is used at the end of the transmission link. The second channel is used to induce XPM, and consists of a long series of "1"s followed by a long series of "0"s to take into account the worst case patterns.

Figure 9(a) shows the power penalty distributions for a 2-channel system with different average optical power levels in the XPM-inducing channel. Figure 9(b) shows the 10% worst-case penalty for different initial DGD values and different average XPM-inducing optical powers. These results show that although in a single channel system without XPM the initial DGD can be fully compensated after transmission, in a WDM system with XPM, the first-order PMD compensator can not fully compensate for the initial DGD due to uncertainty in the PSP. Higher initial DGD values are more susceptible to the uncertainty in the PSP, as small deviations in the PSP result in higher penalties after compensation. It can be seen that average optical powers as low as 3 dBm can cause severe penalties after first-order PMD compensation.

It is important to note that if the PMD of the link is not small, the different SOPs of the WDM channels become uncorrelated and change quickly over a very short distance. This results in an averaging of the nonlinear effects on the SOPs which reduces the impact of XPM-induced PSP variations. Figure 10(c) shows the power penalty caused by XPM-induced PSP variations for a signal with 50 ps initial DGD after first-order compensation. It can be seen that the penalty is initially reduced as PMD increases. However, as PMD continues to increase, an additional penalty is induced due to higher-order PMD, which can not be fully compensated with a first-order PMD compensator.

In order to support our simulation result, we set up an experiment as shown in Fig. 2(d). We transmitted two optical signals (one with modulated data and the other as a continuous wave). By adjusting the polarization controller (PC1) before the PM fiber, we first optimized the performance of the system and measure the bit-error-rate (BER) curve. Then we changed the relative polarization between the two optical signals by changing PC2 to get the worst performance. The BER curves for different optical powers on the XPM-inducing channel are shown in Figure 9(e), indicating a significant change in the performance of the system.

Figure 10 shows the Q-factor distribution for an 8-channel system with 3 dBm/channel optical power, before and after first-order PMD compensation. Again, it is assumed that all channels but one consist of a long series of "1"s followed by a long series of "0"s to simulate worst-case XPM. The first 100 km of the link is assumed to have a high PMD of 3 ps/(km)$^{1/2}$, and the remaining 500 km has a low PMD of 0.1 ps/(km)$^{1/2}$. It is clearly seen that XPM has little effect on the Q-factor distribution without first-order PMD compensation, but causes significant distortion (> 4 dB penalty) after compensation.

Because fiber nonlinearities can limit the performance of first-order PMD post-compensation, in-line compensation may be necessary to avoid accumulation of PSP uncertainties over the link.

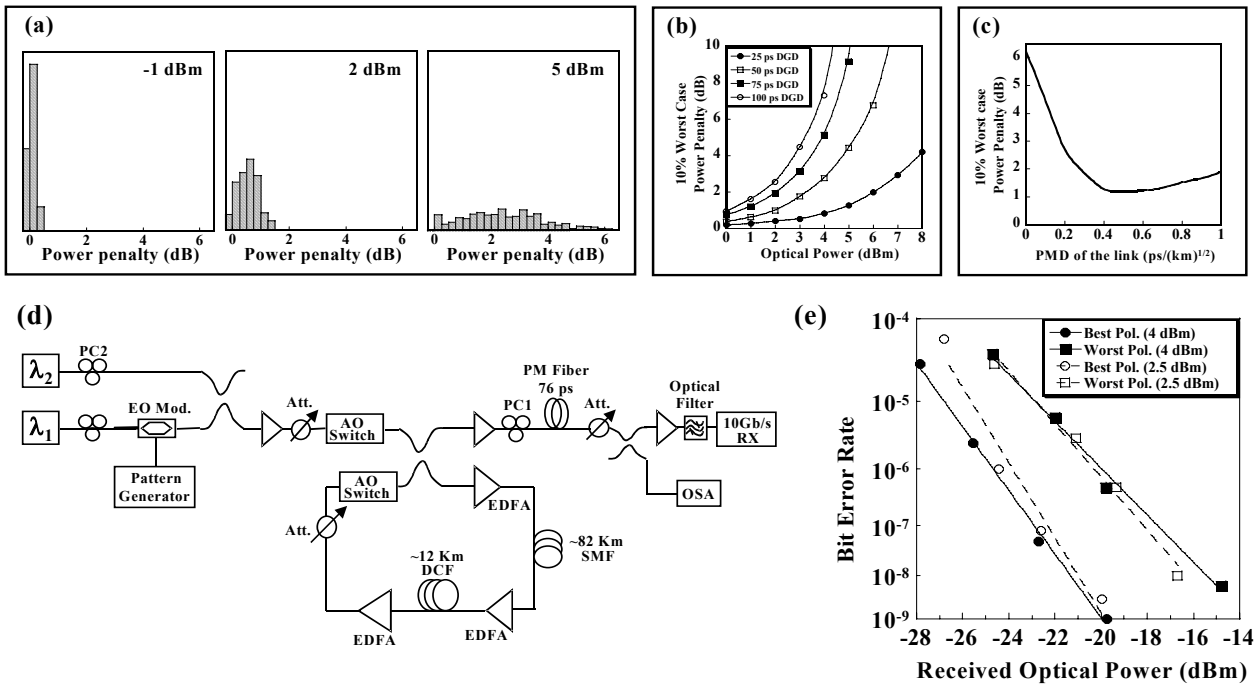

Figure 9. SIMULATION—600 km transmission, 2-channel 10 Gb/s system, 0.8 nm channel spacing—(a) Power penalty distributions due to different XPM-inducing optical powers (average power = –1 dBm, 2 dBm, 5 dBm) after first-order PMD compensation, 50 ps initial DGD, (b) 10% worst-case penalty after first-order PMD compensation for different initial DGD values and different average XPM-inducing optical powers, (c) 10% worst-case penalty after first-order PMD compensation vs. PMD of the link, 50 ps initial DGD, 5 dBm/channel; EXPERIMENT—6 times re-circulation in the loop, 0.8 nm channel spacing—(d) Experimental set-up, (e) BER curves for the best and worst relative polarization between the two signals for 2.5 dBm and 4 dBm input power on the XPM-inducing channel to the SMF.

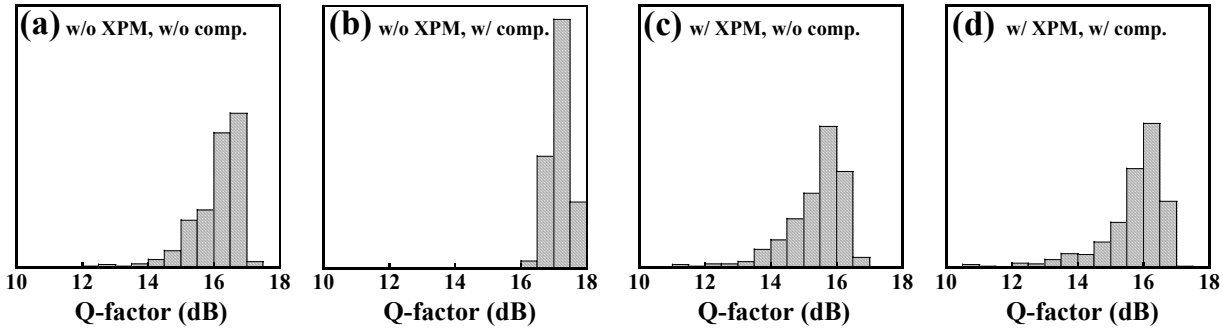

Figure 10. Q-factor distribution for a 10 Gb/s signal (8-channels) after 600 km transmission. The first 100 km of the link has a high PMD of 3 ps/(km)$^{1/2}$, and the remaining 500 km has a low PMD of 0.1 ps/(km)$^{1/2}$. (a) No XPM, before PMD compensation, (b) No XPM, after PMD compensation, (c) with XPM, before PMD compensation, and (d) with XPM, after PMD compensation.

2.3 Statistical Measurement of the Combined Effect of PMD and PDL Using a 10-Gb/s Recirculating Loop Testbed

The combined effect of PMD and PDL was investigated statistically using a 10-Gb/s, 8×82-km, recirculating fiber-loop testbed. As average PDL varied from 1.0 to 2.1 dB with a fixed average PMD of 18 ps, the power penalty at 2% probability increased from 2.5 to 4.3 dB.

Fiber-optic communication systems and networks are vulnerable to problems arising from various fiber polarization effects, particularly, polarization mode dispersion (PMD) and polarization dependent loss (PDL). To first order, PMD induces pulse broadening by creating a delayed copy of the original signal. PDL has also been recognized as a critical issue because various optical networking components, such as isolators, filters, and switches, may have non-negligible PDL. It is well known that PDL, as well as polarization dependent gain (PDG) of optical amplifiers, can induce a random fluctuation of the optical signal-to-noise-ratio (OSNR), which leads to a significant performance degradation in long-distance systems. Furthermore, theoretical analysis has shown that PDL can enhance pulse broadening when combined with PMD. A recent experiment reported bit-error-rate (BER) degradation and instability due to a lumped PDL placed after a PMD emulator in 2.5 Gb/s system. However, investigation of the combined effects of PMD and PDL in an experiment that closely approximates a real optical amplifier system has never been reported.

Recirculating fiber loop testbeds are powerful tools in the research and development of optical amplifier systems. However, conventional recirculating loops are inadequate in the presence of non-negligible polarization-dependent effects, specifically PMD, because a recirculating loop exhibits some measure of periodic behavior that artificially produces an unrealistic PMD distribution that is skewed towards higher differential group delays (DGDs). Our solution to this problem is to employ loop-synchronous polarization scrambling inside the loop. This technique provides an effective tool to measure statistically the effects of PMD and/or PDL on system performance.

In this paper, we measure the probability distribution of power penalties for a 10-Gb/s, 8×82-km recirculating fiber loop that represents a typical terrestrial system. For this system, with an average PMD of 18 ps, the penalty distribution tail at 2% probability increases from 2.5 to 4.3 dB as the average PDL increases from 1.0 to 2.1 dB. In the absence of PMD (PDL only), we observe much lower power penalties. As the number of optical components increases in the links, this problem will become more severe.

Experimental Setup

Figure 11 shows the experimental setup. An external cavity laser at 1557 nm is modulated at 10 Gbit/s (215-1 PRBS). The dispersion-managed recirculating loop consists of three EDFAs operating in the saturated regime, 82 km of single-mode fiber (SMF), and 12 km of dispersion-compensating fiber (DCF) with a chromatic dispersion of -1348 ps/nm. The input powers to the SMF and DCF are fixed at 3.0 dBm and -1.0 dBm, respectively. In order to emulate the statistical distribution of PMD and PDL in real systems, a loop-synchronous LiNbO3 polarization controller (PC), a polarization-

maintaining (PM) fiber, and a PDL emulator are used inside the loop. The polarization transfer matrix of the LiNbO3 PC is controlled by six input voltages and can be set to a random state during each loop period. These decorrelated polarization states are repeated after a certain number of loops as determined by the loop control circuitry. The PDL emulator can be adjusted from 0.15 dB to 0.9 dB per pass. The background PDL, mainly due to the LiNbO3 PC, is about 0.25 dB per loop. We use 8 passes through the loop, corresponding to about 650-km transmission.

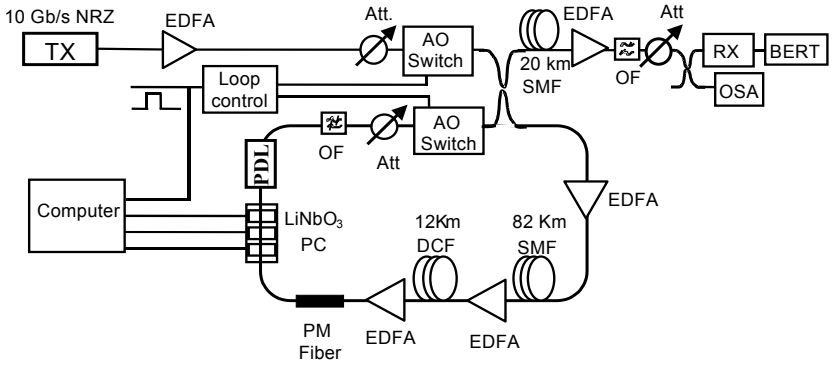

Figure 11. Setup of our recirculating fiber loop with loop-synchronous polarization scrambling.

Results and Discussion

Figure 12 shows the standard deviation of the received power penalty after 650-km transmission under different conditions of combined PMD and PDL, with each point in the figure measured from 200 samples. Here, the power penalty is determined by comparing the receiver sensitivity at 10^{-9} BER with the back-to-back sensitivity measured at 25-dB OSNR. The intrinsic penalty without the PM fiber and PDL emulator is about 0.8 dB. TThe average PDL is estimated as $\sqrt{Loop\ number} \times (PDL/\ loop)$, where in this case the loop number is 8. Without the PM fiber, the standard deviation of power penalties comes from fluctuations in the received OSNR. This is a relatively small effect. PMD is introduced by including a piece of PM fiber in the loop. Two spools of PM fiber with 6.9-ps and 8.4-ps DGD are used, corresponding to average system PMD (8 loops) of 18 ps and 22 ps, respectively. Also shown in Fig. 2 is a comparison between measured data and estimated results under the assumption that PDL and PMD affect system performance independently. When the average PDL is lower than 1.0 dB (0.35 dB/loop), the interaction between PMD and PDL is not obvious. However, when PDL is greater than 2.1 dB (0.75 dB/loop), serious performance degradation is observed, e.g., the power penalty standard deviation changes from 0.8 dB to 1.9 dB as the average PDL varies from 0.7 dB to 2.5 dB with 22-ps PMD.

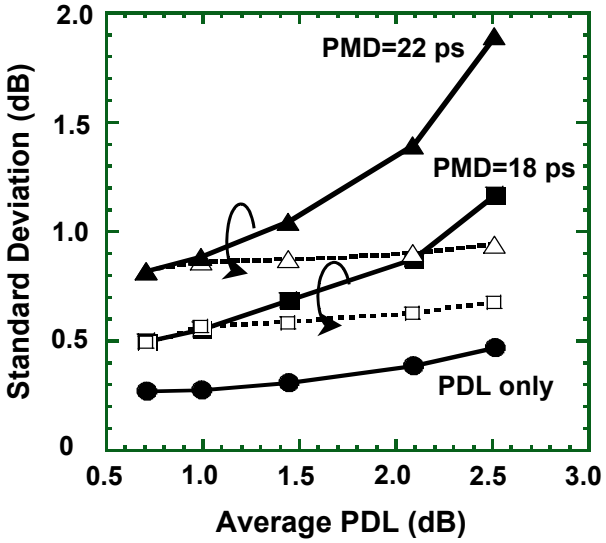

Figure 12. Standard deviation of power penalty versus average PDL after 650-km fiber transmission. Solid line: measurement (each point obtained from 200 samples) Dashed line: estimated results assuming PMD and PDL are statistically independent

To further compare system performance under conditions of small and large PDL, we measure the histogram of power penalties with the results shown in Figure 13. Here, each histogram is drawn from 500 samples. Without incorporating PMD into the loop, the power penalty for 500 samples is bounded by 2.5 dB even when the average PDL is 2.1 dB, as shown in Figures 13(a) and (b). We assume a system outage happens when the power penalty is greater than 4 dB. Only 2 outages are observed when the system has a PMD of 18 ps and a relatively small PDL of 1 dB (0.35 dB/loop), as shown in Figure 13(c). This agrees with the 0.3% outage probability obtained from a simulation assuming that PDL is negligible. However, when the PDL increases to 2.1 dB (0.75 dB/loop), the number of outages increases to 13 out of 500 samples, as shown in Figure 3(d). Such an outage probability (2.6%) far exceeds the result expected under the assumption that the effects of PMD and PDL are statistically independent, confirming that the performance degradation is due to the combined effect of PMD and PDL. In addition, the power penalty distribution tail at 2% probability increases from 2.5 dB to 4.3 dB as the PDL increases from 1.0 dB to 2.1 dB for 18-ps PMD.

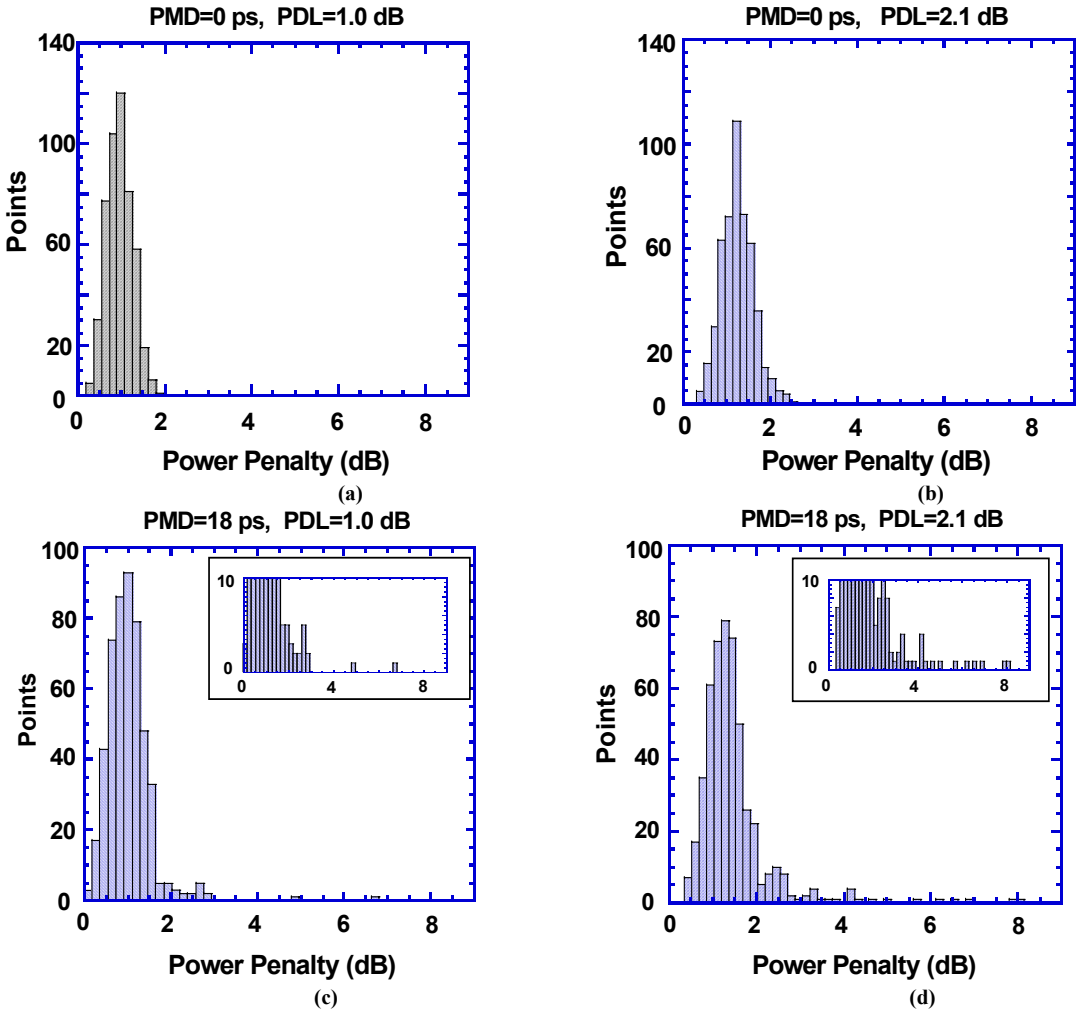

Figure 13. Histograms of power penalty of PDL only and combined PMD/PDL (500 samples each). Here PDL value is average PDL. (a) PMD=0 ps/PDL=1.0 dB (b) PMD=0 ps/PDL=2.1 dB (c) PMD=18 ps/PDL=1.0 dB (d) PMD=18 ps/PDL=2.1 dB

2.4 Statistics of Polarization Dependant Gain in Raman Fiber Amplifiers due to PMD

Polarization dependent gain (PDG) in Raman fiber amplifiers is shown to be a statistical parameter that depends on the PMD of the fiber. The PDG distribution was characterized by simulation and verified by experiment.

With the recent availability of high power pump lasers, Raman amplification has become feasible for commercial DWDM fiber-optic communication systems. Raman fiber amplifiers are highly attractive for their low equivalent noise figure and wideband gain. However, the Raman gain coefficient is polarization sensitive and can be up to 10 times higher when the signal and pump polarization states are parallel rather than perpendicular. Previous studies of this polarization dependent gain (PDG) investigate its relationship with the polarization mode dispersion (PMD) of the fiber, and the degree of

the polarization (DOP) of the pump laser. These studies show that when the average PMD of the fiber becomes high enough, or if the pump DOP is very low, then the PDG becomes negligible. But these studies do not investigate the statistical behavior of the polarization dependant gain.

There are two ways of characterizing polarization sensitivity in Raman amplifiers. One is to measure the PDG at a given point in time, which is determined by varying either the pump or signal polarization and recording the difference between the maximum and minimum gains. Alternatively, one can monitor how the instantaneous gain varies over time due to both PMD induced variations and changes to the signal's input state of polarization (SOP). In this paper we investigate the statistical characteristics of both of these parameters theoretically and experimentally.

Since PDG is greatly reduced for counterpropagating pump schemes, we use a copropogating configuration in our experimental setup to magnify the polarization effects. Copropogating amplifiers have certain improved amplification characteristics and may be useful in some system applications, and for these, a quantitative understanding of PDG statistics may be critical. Our results show how the mean and standard deviation of the PDG decreases with increasing values of PMD.

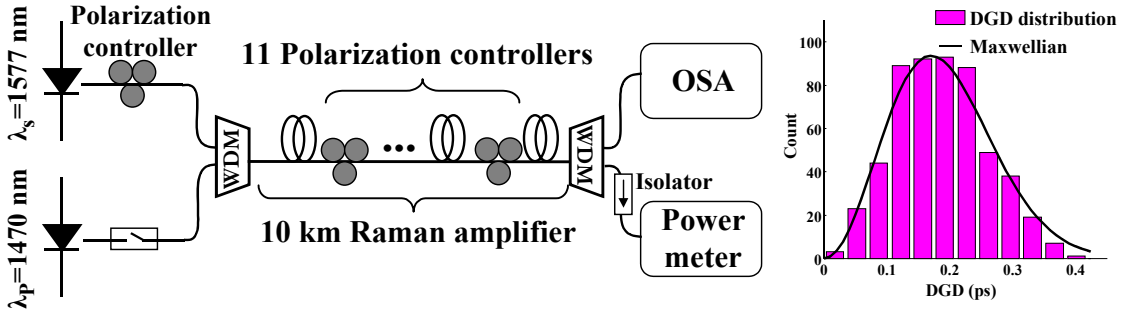

Figure 14. Raman amplifier setup and measured DGD distribution; <DGD>= 0.19ps, PMD=0.06ps/km1/2.

Experimental setup

Figure 14 depicts the experimental setup. The Raman amplifier consists of 10 km of unspooled dispersion shifted fiber. The input pump power is 205mW and the average gain is 3.4 dB. The signal passes through a computer controlled polarization controller to vary the signal's input SOP. The switch in the pump path is used to "turn off" the pump for gain measurements. The pump and signal are separated at the output where the signal power fluctuations are monitored with an optical spectrum analyzer (OSA).

Within the amplifier, 11 polarization controllers (PCs) are placed at approximately 800m intervals. By changing these PCs between measurements, we induced random variations in the polarization mode coupling within the transmission fiber that would otherwise only occur over a long period of time. We verified this technique by taking 500 samples of instantaneous differential group delay (DGD) at our signal wavelength while randomly changing the PCs between measurements. The resulting DGD distribution (figure 14) closely approximates the expected Maxwellian and yields an

average PMD of 0.06 ps/km^{½}. It should also be noted that the PDL of our setup is ≤0.33dB, which is about 1 dB less than our average PDG.

Results

Figure 15(a) shows the measured PDG distribution. The 11 PCs were varied randomly between each of the 500 samples. During each measurement, the output signal power was monitored while the input signal SOP was varied randomly. The maximum achieved power fluctuation determines the PDG since the average Raman gain, which was also measured at each data point, remained constant at 3.4±0.15 dB (variation due to PDL). To further verify our measurement technique, another 500 samples were taken without changing the 11 PCs at all (over a period of only four hours to avoid the natural evolution of polarization coupling within the fiber). The resulting PDG remained constant within ±0.2 dB, adding validity to our method. Figure 15(b) shows the cumulative distribution functions (cdf) for the measured and simulated PDG for 0.06 ps/km$^{1/2}$ PMD. Note the simulated and experimental results closely agree. Similarly, figures 15(c) and (d) show the measured and simulated distributions of the instantaneous Raman gain. Again, the simulated and experimental results are in agreement.

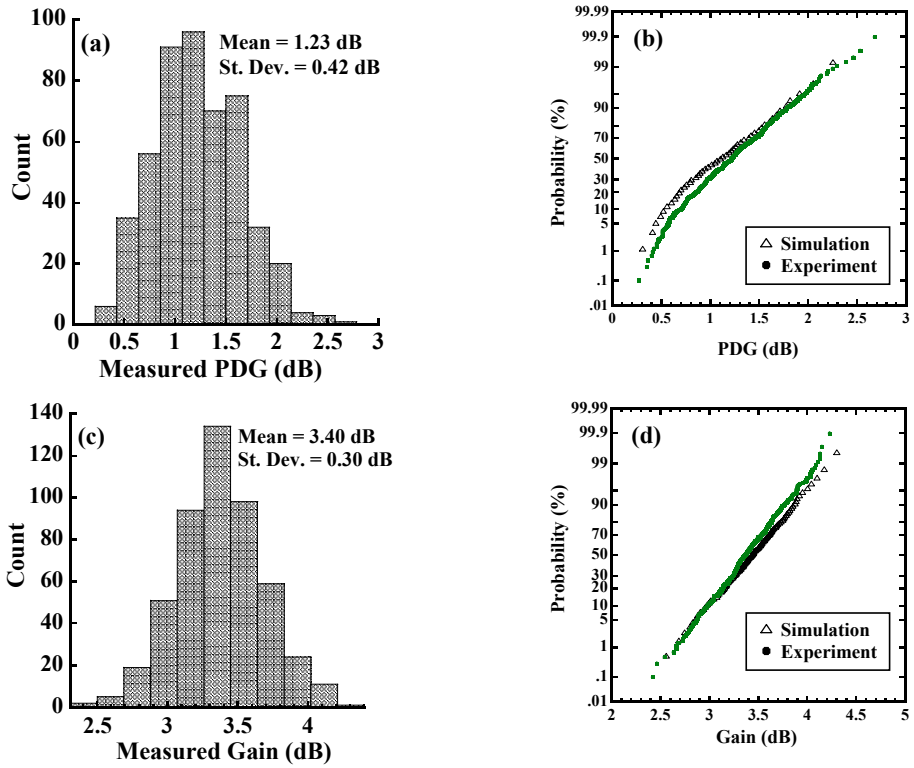

Figure 15. (a) Measured histogram of PDG, (b) simulated vs. experimental cumulative distribution functions of PDG; (c) and (d) show the same plots for the Raman gain (for PMD=0.06 ps/km½).

Since our experimental results are presently limited to only a single PMD value (we are looking for higher PMD fibers to further our experiments), the simulation was used to investigate how the PDG statistics vary for different values of PMD. Our simulation models a fiber with PMD as a series of 1000 equal length sections with random polarization mode coupling between them. The Raman gain of each section depends on the relative polarizations of the signal and pump. Figure 16(a) shows that even modest increases in the PMD reduce both the average and spread of the PDG distribution. Figure 16(b) shows the normalized variation of the mean PDG versus PMD. The results show that a total PMD of 0.66 ps ($0.2 ps/km^{1/2}$ x $(10km)^{1/2}$) is enough to reduce the mean PDG to as low as 10% of the average gain. Figure 16(c) shows the normalized variation of the standard deviation of the Raman gain versus PMD. Also note that the constant slope in figure 16(b) shows that the product of the mean PDG and the PMD of the link remains constant, as does σ_{Gain} x PMD (figure 16(c)).

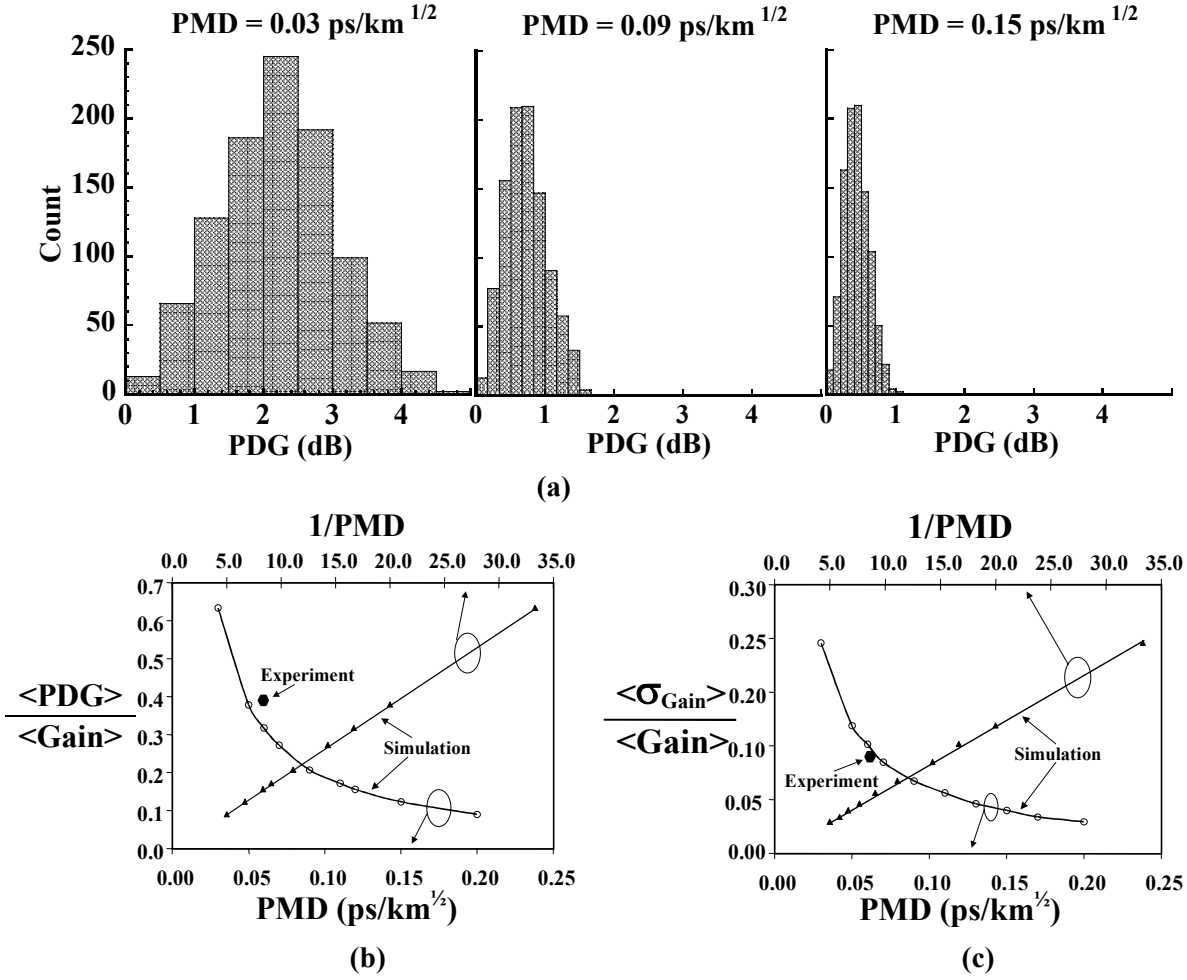

Figure 16. (a) Histograms showing how the mean and standard deviation of the Raman PDG decrease as the PMD is increased from 0.03 to 0.09 to 0.15 ps/km$^{1/2}$; (b) and (c) show the mean PDG and the standard deviation of the Raman gain versus PMD (and 1/PMD) for a 10-km Raman amplifier (where the PDG and gain are normalized to the average gain).

3. PMD Emulation

For testing of optical systems that may be affected by PMD and especially for the characterization of PMD compensators, it is critical to be able to accurately emulate first and higher-order PMD and quickly cycle through a large number of different fiber PMD states. Any PMD emulator should meet the following three key performance metrics:

(1) The DGD should be Maxwellian-distributed over an ensemble of fiber realizations at any fixed optical frequency.
(2) The emulator should produce accurate higher-order PMD statistics and should be able to reach any combination of first and higher-order PMD values.
(3) When averaged over an ensemble of fiber realizations, the frequency autocorrelation function of the PMD emulator should tend towards zero outside a limited frequency range.

In addition to the above performance requirements, a PMD emulator should ideally exhibit the following features to act as a practical measurement tool:

(1) Stability – the PMD of the emulator should remain stable over the measurement period, which may last minutes to hours.
(2) Repeatability and predictability – it should be possible to "dial in" any desired PMD state of the emulator.
(3) Simplicity – the implementation of the emulator should be simple and power efficient, and it should be easy to quickly vary the emulator's PMD state. Furthermore, the emulator should ideally have low loss and exhibit negligible polarization dependent loss (PDL).

The first two requirements, stability and repeatability, are very difficult to achieve since most emulators are constructed of several birefringent elements which tend to be extremely sensitive to environmental changes, causing the polarization state at the emulator output to vary over short periods of time even though the control parameters are held constant (such as polarization controller settings, crystal rotations, etc.).

With this grant,

(a) Both experimentally and theoretically a new technique was investigated to realistically emulate polarization mode dispersion. It was demonstrated that 15 sections of polarization-maintaining fiber with randomly rotatable connections emulate an almost ideal Maxwellian differential group delay (DGD) distribution and close to ideal frequency auto correlation function whereas fixed connections is inadequate.

(b) A compact, all-fiber PMD emulator with accurate first and higher order PMD statistics was constructed using electrically controllable thin-film micro-heaters to temperature tune the birefringence of multiple PM fiber sections spliced at 45° angles. The advantages over the previous emulator were low loss, negligible PDL, simple construction, no internal reflections, and no moving parts.

(c) A short recirculating fiber loop (~100 km) that can emulate PMD with Maxwellian statistics was realized by loop-synchronous polarization scrambling inside the loop. The performance of the distribution-correct PMD loop was compared both experimentally and numerically to that of a distribution-incorrect PMD loop. This achievement enabled correct PMD experiments in the recirculating fiber loops.

3.1 Emulator with Polarization Controllers or Rotatable Connectors between Sections

Our initial investigations of PMD emulators focused on the study of the number sections required to produce accurate first and higher order statistics, on the differences between full polarization scattering and simple polarization rotation between sections, and on obtaining a frequency autocorrelation function that quadratically falls to zero after a short bandwidth. Both simulation and experimental investigations were performed. In addition, an analytical formula for the probability density function of an emulator with polarization scattering between sections was developed.

Figure 17(a) shows simulated probability density functions for 3- and 15-section emulators with polarization controllers between each section of PM fiber. It was observed that utilizing unequal lengths of PM fibers increases the rate of convergence of DGD to a Maxwellian distribution. In practice, an emulator with polarization controllers is difficult to build and control. Thus, our experimental implementation used rotatable connectors that change the polarization orientations but not their relative phases.

DGD density functions were obtained using Monte Carlo simulations based on the coarse step method. Figure 17(b) shows the DGD pdfs of 3- and 15-section PMD emulators. The shape of the DGD density function converges to a Maxwellian pdf for emulators with more than 10 sections of PM fiber. Figure 17(c) shows the worst case eye diagram (with probability 0.001, a point in the tail of the distribution) of a 10 Gb/s signal with 30 ps average DGD, for a real fiber and a 3-section PMD emulator. It is apparent that a 3-section PMD emulator cannot reproduce realistic PMD degradation. We numerically verified that with 15 sections of PM fiber, a Maxwellian pdf is achieved out to 3 times the average DGD in the tail of the pdf.

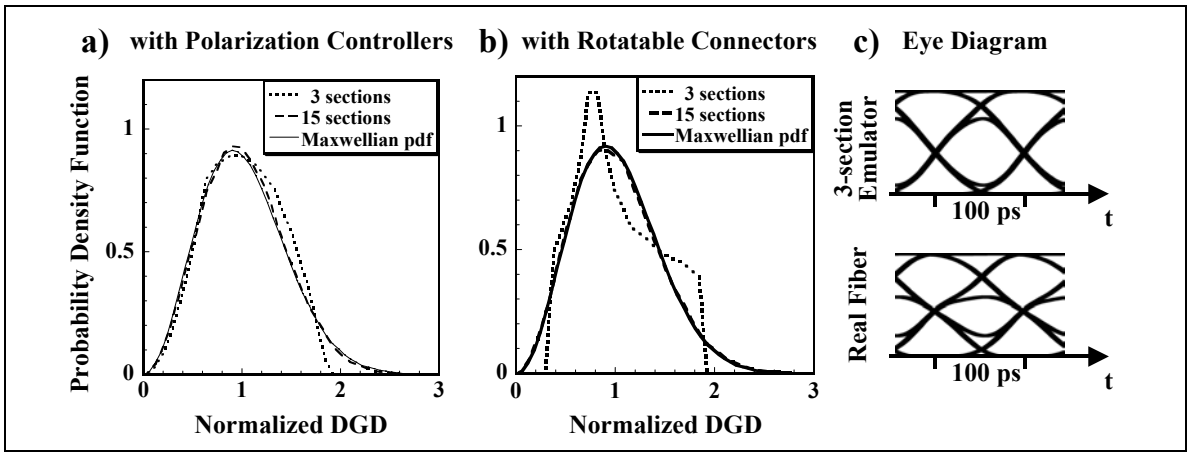

Figure 17. Simulation results. a) DGD distribution for a 3- and 15-section PMD emulator with a polarization controller between each section (unequal lengths of PM fiber), b) with a polarization rotation between each section, c) the worst case eye diagram (with probability 0.001) of a 10 Gb/s signal with 30 ps average DGD, for a real fiber and a 3-section PMD emulator.

The experimental emulator was constructed using 15 sections of PM fiber connected by rotatable-key connectors. Rotatable connectors allow the polarization axes of any two adjacent fibers to be rotated with respect to each other. The length of the PM fibers were chosen randomly, with an average of ~ 7 meters and a 20% Gaussian deviation. The beat length of the PM fiber is ~ 3.1 mm at 1550 nm. Therefore, 15 sections of PM fiber generates ~ 40 ps of PMD. The total loss of the emulator is 6 – 10 dB and varies with the angles between the PM fiber sections. The loss can be made more uniform by careful consideration of the connectors themselves. The polarization dependent loss was measured to be less than 0.2 dB, and the DGD values were measured using the Jones matrix method.

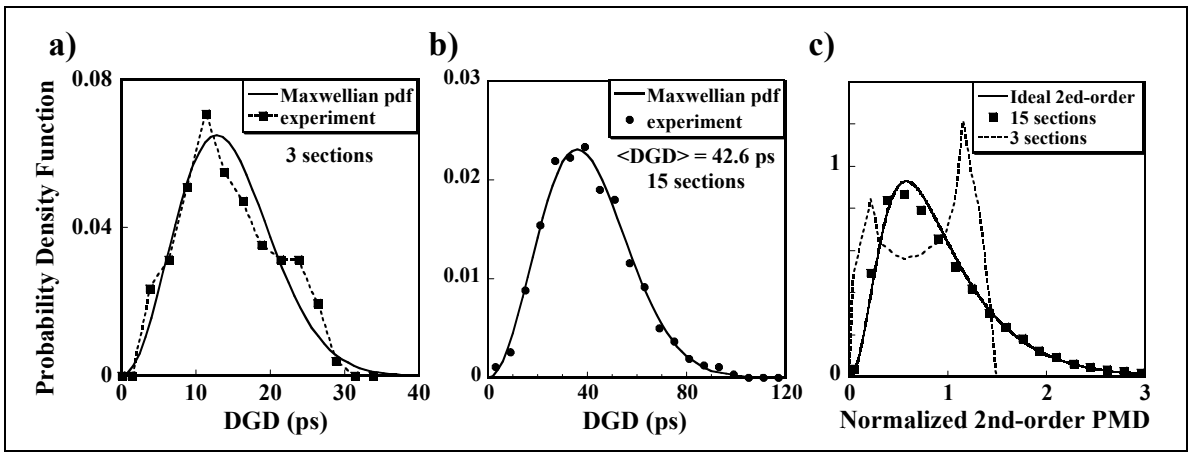

Figure 18. a), b) Experimental results of DGD distributions of 3- and 15-section PMD emulators with rotatable connectors at 1555 nm c) Simulation results of normalized second-order PMD magnitude for the 3- and 15-section emulators.

Figures 18(a) and (b) show the DGD density functions for 3- and a 15-section emulators at a **fixed** wavelength of 1555 nm. 1000 samples were taken by randomly rotating the angles between the fibers. The wavelength was swept over 1 nm with 0.02 nm steps for each set of angles to obtain a DGD pdf at 50 different wavelengths. Good distributions were obtained at other wavelengths as well, and the average DGD was very close to 40 ps at all wavelengths. As shown in figure 18(c), the 15-section emulator also exhibits good second-order PMD statistics that closely match the ideal theoretical distribution.

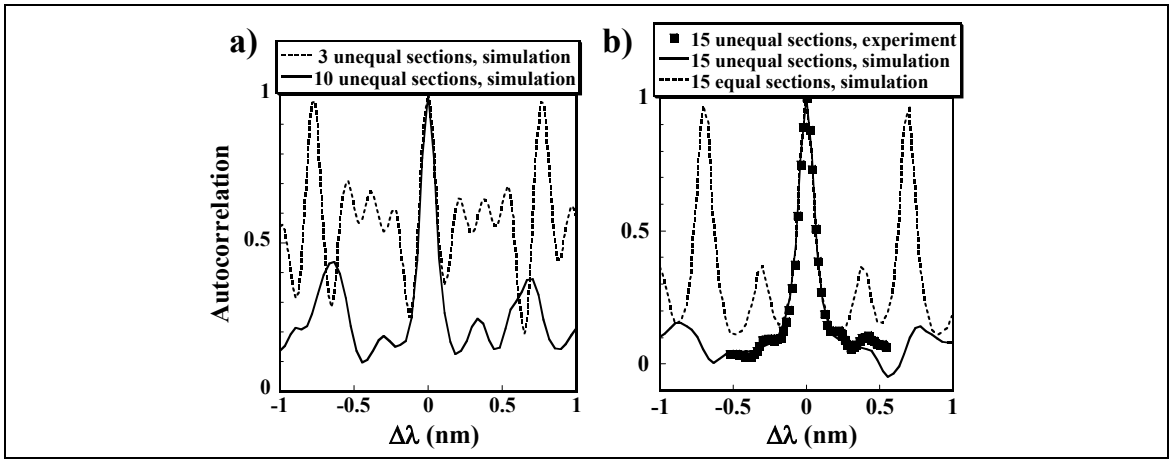

Figure 19. Frequency autocorrelation function of PMD vector for a) 3- and 10-section PMD emulators with unequal lengths of PM fibers (simulation), and b) a 15-section emulator with equal and unequal lengths of PM fibers (simulation and experiment). Note the undesired periodicity that results when equal-length sections are used.

In WDM systems, not only should the DGD pdf of each channel be Maxwellian, but the PMD characteristics of channels separated by large frequencies should also be statistically independent—i.e. the PMD vectors should be uncorrelated. For 40 ps of PMD, a real fiber shows negligible correlation between PMD vectors when the spacing is more than 0.2 nm. Figure 19 shows the autocorrelation function of the PMD vector for emulators with 3, 10, and 15 sections. For a 15-section, unequal-length PMD emulator, an average level of 10% correlation remains between well-spaced wavelengths. To avoid periodicity in the autocorrelation function and to decrease the residual correlation, it is preferable to employ unequal-length sections in PMD emulators. In addition, we theoretically determined that the use of polarization controllers rather than rotators only slightly reduces the residual correlation.

3.2 Emulator with Deposited Micro-Heaters for Thermally Tuned Birefringent Sections

The use of polarization controllers or rotatable connectors between sections of PM fiber proved to be cumbersome, lossy, and lacked automated control. To overcome these issues, we constructed a 30-section, compact, all-fiber PMD emulator that uses an integrated series of evaporated micro-heaters to thermally tune the birefringence of each DGD section to accurately reproduce PMD statistics. This all-fiber design combined with the use of a silicon V-groove array to mount the micro-heating elements enabled a

compact, low loss emulator that is electrically controllable, has no moving parts, negligible polarization-dependent loss (PDL), and no internal reflections.

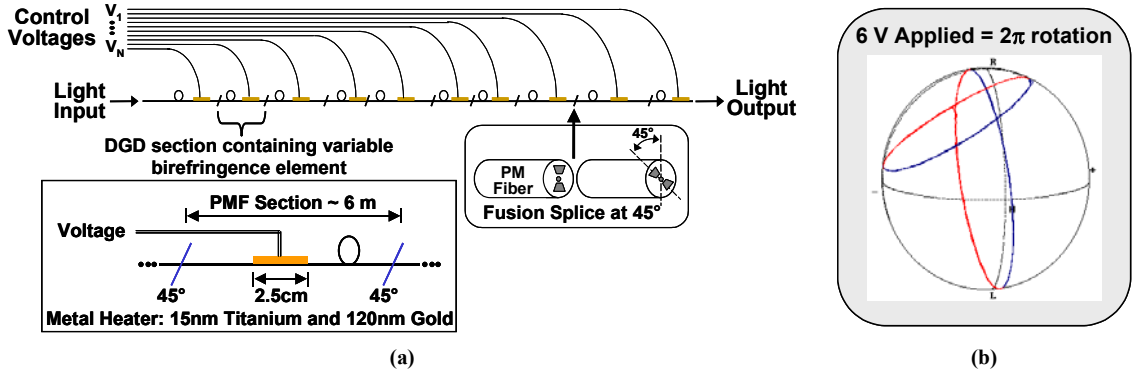

Figure 20. (a) Schematic diagram of the PMD emulator and (b) 2π rotation of the output state of polarization due to the temperature dependence of the birefringence as a single heater element is tuned from 0 to 6 V (two curves shown).

A schematic illustration of the emulator is shown in figure 20(a). Short sections of FiberCore HiBi polarization maintaining optical fiber are fusion spliced together at 45° angles as shown. The beat length of the fiber at 1550 nm is 4.1 mm. To produce an accurate PMD distribution, 30 sections of unequal lengths were used. The average length of each section was chosen to be ~6 meters with a 20% Gaussian deviation to obtain an average DGD of 42 ps. E-beam evaporation was used to deposit 2.5 cm long thin-film heaters near the center of each section.

Each heater is comprised of a 15 nm titanium layer for good adhesion to the glass and a 120 nm gold layer for good thermal conductivity. To achieve a compact emulator package, the fiber heaters were mounted on a 32-section silicon V-groove array with 1.25 mm spacing (see Figure 21(b)). The remaining two sections were used to build test elements to characterize the temperature dependence of the DGD and output polarization state of single PM fiber sections. A splice organizer tray houses the 171 meters of PM fiber and splices. A 40-conductor ribbon cable was used to make electrical contact to each of the 30 sections and the remaining 8 conductors were used as parallel return lines. The individual elements were computer controlled using a 32-channel analog output card. A photograph of the emulator is shown in figure 21. The measured loss of the emulator is 3.6 dB including the input connector and 33 splices (29 PM splices at 45°, 2 splices to SMF pigtails, and 2 PM splices to repair broken fibers). No PDL was seen using a conventional power meter, indicating that the PDL is < 0.05 dB.

Figure 20(b) shows the variation in the output state of polarization as the birefringence of one heater element is tuned to produce a 2π radian change. The temperature dependence of the birefringence of this PM fiber was measured to be 0.75 rad/°C/meter. This can be significantly increased by using a PM fiber with stronger temperature dependence or by using longer heater sections (4 - 6 cm).

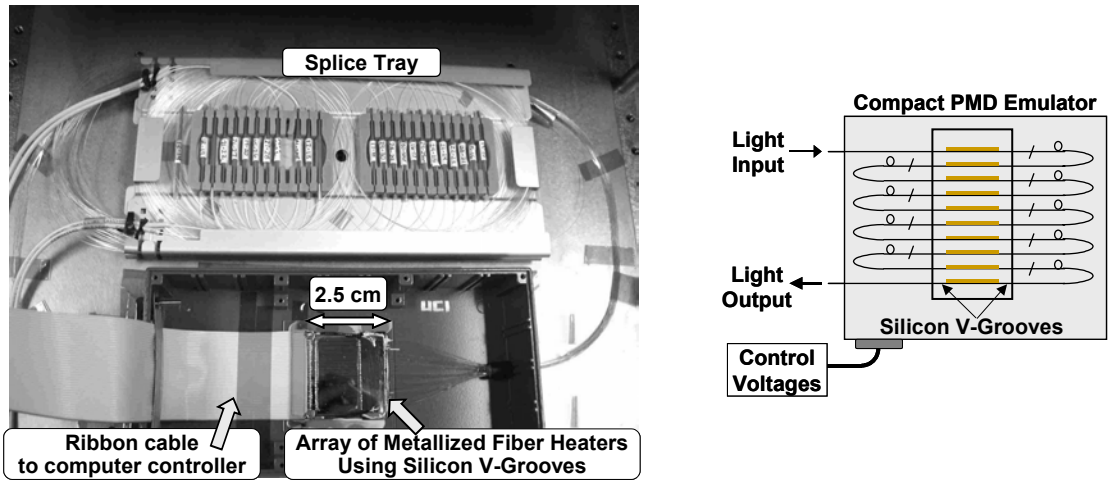

Figure 21. (a) Photograph of the PMD emulator showing heater array, fiber splice tray, and ribbon cable for control. (b) schematic illustration of the compact design with heaters mounted using a silicon v-groove array.

To cycle through the PMD states of the emulator, a simple software program was used to apply a set of 30 random voltages, chosen to achieve a uniform distribution of applied powers, to the heater elements between DGD samples. Figures 22(a) and (b) show the resulting first and second-order PMD distributions after taking 850 samples. It can be seen that the statistics of the PMD emulator closely match the theoretical curves. Figure 22(c) depicts the frequency autocorrelation function of the emulator showing that the PMD at different wavelengths has less than 20% correlation for channel spacings greater than ~0.3 nm.

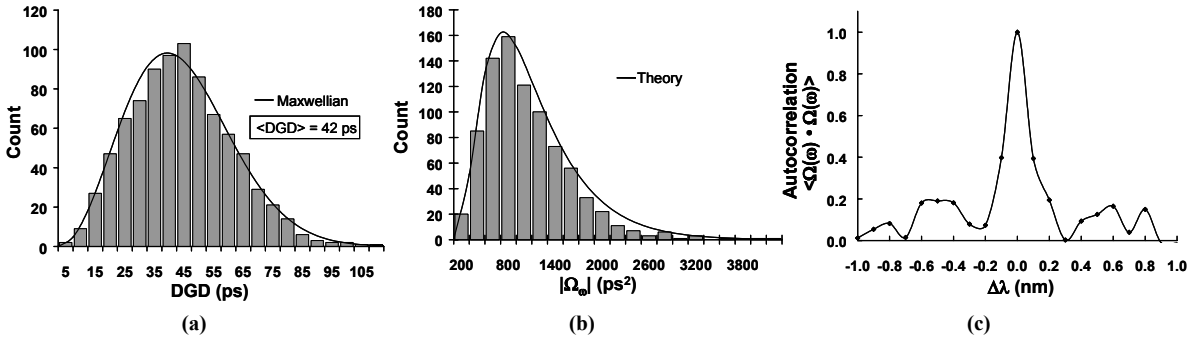

Figure 22. Experimental PMD statistics of the emulator versus theory. (a) DGD distribution, (b) 2nd-Order PMD distribution, (c) frequency autocorrelation function.

3.3 Accurate reproduction of Maxwellian PMD statistics in a short recirculating fiber loop

For the last decade, recirculating fiber loop testbeds have been powerful tools in the research and development of medium-to-long-haul optical transmission systems. Under most circumstances, these fiber loops are well behaved and can accurately replicate the characteristics of a point-to-point fiber link. However, in the presence of non-negligible polarization-dependent effects, specifically polarization mode dispersion (PMD), conventional recirculating loops are inadequate. PMD is unique because it is a stochastic process, whereas a recirculating loop exhibits some measure of deterministic behavior that artificially produces an unrealistic PMD distribution that is skewed towards higher differential group delays (DGD). Any testbed that does not accurately reproduce the tail of the distribution will give erroneous results.

A recirculating fiber loop testbed that is only ~100 km long and yet accurately replicates the true Maxwellian DGD distribution caused by PMD was demonstrated. A single section of polarization-maintaining (PM) fiber and a lithium-niobate ($LiNbO_3$) polarization controller was used which was synchronized to the electronic loop controller circuitry. The tail of the power penalty distribution after 650 km transmission with an average PMD of ~22 ps is close to that expected from a Maxwellian distribution of DGD. Therefore, the modified loop testbed provided an efficient tool for investigating the combined effects of fiber dispersion, nonlinearities, and PMD.

Figure 23 shows the experimental setup of a recirculating fiber loop that emulated PMD for long distance data transmission. An external-cavity laser at 1556.7 nm was externally NRZ-modulated with an electro-optic (EO) modulator at 10 Gbit/s.. The dispersion-managed recirculating fiber loop consisted of three in-line EDFAs, 84 km of single-mode fiber (SMF), and dispersion-compensating fiber (DCF) with dispersion of -1348 ps/nm. The input powers to the SMF and DCF were adjusted to 2.0 dBm and -1.0 dBm. The PMD of the loop was emulated by a single section, PM fiber (DGD ~8.3 ps) and a loop-synchronous $LiNbO_3$ polarization controller. The polarization transfer matrix of the scrambler was controlled by six input voltages and set to a random state during each loop period. These decorrelated polarization states were repeated after a certain number of loops as determined by the loop control signal. This provided a virtual increment of the length of the fiber loop in terms of the polarization state evolution along the transmission fiber. At the output of the loop, an pre-amplifier EDFA was used followed by a 1 nm bandwidth optical filter, for burst-mode bit-error-rate (BER) measurements.

Figure 24 shows measured optical power distributions at 10^{-9} BER using the recirculating PMD loop, both with and without inter-loop polarization decorrelation. Figure 24(a) shows the optical power distribution using 500 independent polarization samples taken by randomly changing the polarization states for 8-loop transmission. An alternative configuration for the PMD loop was also investigated. In this case, the PMD loop was replaced by a 15-section PMD emulator (average DGD ~8.9 ps) with three polarization controllers. The results are shown in Figure 24(b). The optical power distribution was taken by randomly changing the polarization coupling between 15-section PMD emulator inside of the loop after 6-loop transmission. Since the average

DGD of the emulator (~8.9 ps) was slightly larger than the average DGD of the a single section PM fiber, the expected average DGD value after 6-loop transmission in this case matched the expected DGD value after 8-loop transmission for the one-section PM fiber loop. Figure 24(c) shows the optical power distribution after 8-loop transmission for 1000 independent polarization samples. In this case, in addition to randomly changing the polarization states for each sample, the state-of-polarization was decorrelated after each loop circulation. It is clear that the power distributions without inter-loop polarization decorrelation have much longer tails than the distribution with inter-loop polarization decorrelation, even if a multi-section PMD emulator is used inside of the loop. To quantify the performance shown in Figure 24, the case of the loop without PMD was measured , followed by a lumped 44 ps average DGD. The worst case power penalties for 6-and 8-loop transmission are about 4.5 dB and 4.7 dB. Based on these results, the probability of a power penalty >4.5 dB (i.e., DGD >44 ps) would be about 32% for the case shown in Figure 24(b), and the probabilities of a power penalty >4.7 dB (i.e., DGD >44 ps) would be 31% and 0.5% for the cases shown in Figures. 24(a) and (c).

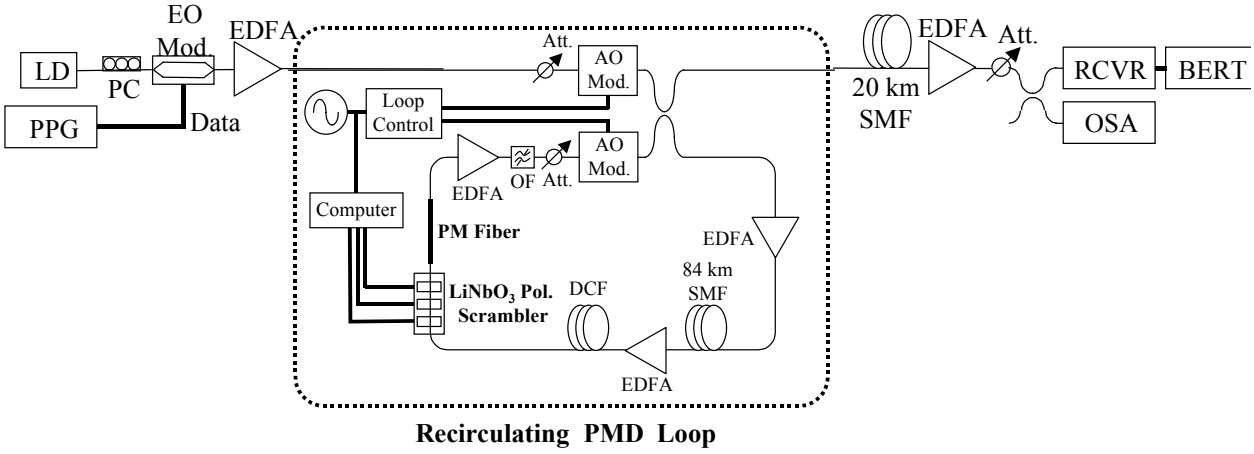

Figure 23. Experimental setup of recirculating PMD loop

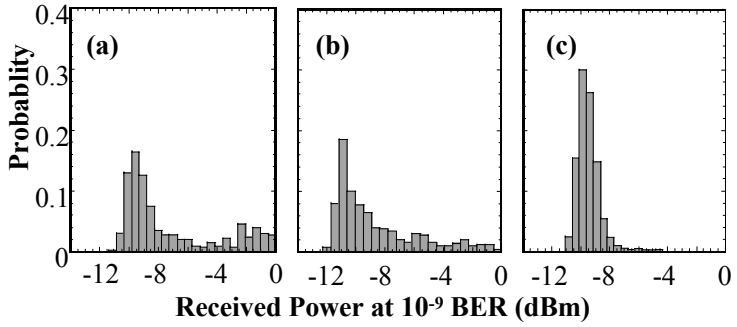

Figure 24. Received optical power distributions at 10^{-9} BER using our loop. (a) 500 independent samples using one-section PM fiber without inter-loop polarization decorrelation. (b) 500 independent samples using a 15-section PMD emulator without inter-loop polarization decorrelation. (c) 1000 independent samples using one-section PM fiber with inter-loop polarization decorrelation.

Figure 25(a) shows the simulated increase in average DGD with the number of loops. When there is no inter-loop decorrelation of polarization states, average DGD grows almost linearly (solid circles) because of a strong polarization correlation between loops. When inter-loop decorrelation of polarization is introduced by the loop-synchronous polarization controller, average DGD grows as the square root of the number of loops (open circles). The solid line shows the analytically expected growth of average DGD as the number of loops increases. Figure 25(b) shows the deviation of the DGD distribution from an ideal Maxwellian DGD distribution as the number of loops increases. The normalized deviation (Δ) from a Maxwellian is calculated as the integrated absolute difference between the simulated DGD probability density function (pdf) and a Maxwellian pdf for each loop number. For a PMD loop without inter-loop polarization decorrelation, the DGD distribution diverges significantly from a Maxwellian as the number of loops increases. However, for a PMD loop with inter-loop polarization decorrelation,

The DGD distribution converged to a Maxwellian as the number of loops increased. This is because each loop can be considered as a single section PMD emulator with random polarization coupling, and the DGD distribution will closely approximate a Maxwellian distribution as the number of sections in the PMD emulator is increased, or equivalently in our case, as the number of loops increased. Figure 25(c), (d), and (e) show numerical results for DGD distributions with the recirculating fiber loop configurations of Figure 24(a), (b), and (c). As shown in Figure 25(c) and (d), the distributions of DGD after loop transmission without inter-loop polarization decorrelation deviate significantly from a Maxwellian DGD distribution and had much longer tails, as was previously explained. In Figure 25(e), the DGD distribution with inter-loop polarization decorrelation closely approximated a Maxwellian DGD distribution. Also numerically the power penalty distributions for the cases in Figure 24 was calculated, taking into consideration the random distribution of the DGD and the power ratio between the two principal states of polarization. The simulation predicted that the probability for the power penalty to be greater than 4.5 dB for the case of Figure 24(b), and greater than 4.7 dB for the cases of Figure 24(a) and (c), are 20%, 21%, and 0.4%. These values agreed reasonably well with the experimental results.

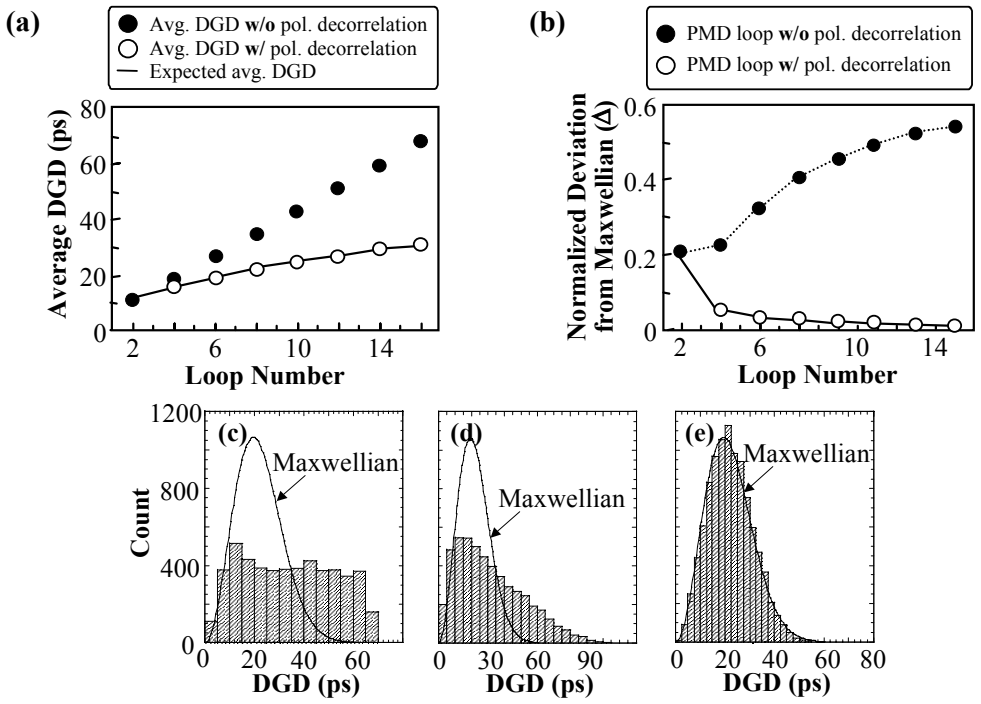

Figure 25. (a) The increase in average DGD with the number of loops, and (b) the normalized deviation from a Maxwellian DGD distribution as the number of loops increases (solid line shows expected average DGD), (c) Simulated DGD distribution of PMD loop without inter-loop polarization decorrelation (one-section PM fiber with pol. controller, 5000 independent pol. samples, 8 loop). (d) Simulated DGD distribution of PMD loop without inter-loop polarization decorrelation (15-section PMD emulator with three PCs, 5000 independent polarization samples, 6 loop) (e) Simulated DGD distribution of PMD loop with inter-loop polarization decorrelation (one-section PM fiber with pol. controller, 10000 independent pol. samples, 8 loop).

4. PMD Compensation

It is usually considered that the maximum tolerable PMD is between 10-20% of the bit duration. Typical PMD values of installed fibers are greater than 1.5ps/√km, which limits to a few 100km the transmission distance at 10Gb/s the maximum tolerable PMD value without compensation is rapidly reached. To be able to operate at higher bit rates or higher lengths, compensation or mitigation is required. The following projects were done with regards to PMD compensation. A summary of each approach will be explained but as the papers are attached to this report, only the WDM-PMD compensation using a single module will be explained in detail.

- Simultaneous PMD compensation of multiple WDM channels using a single compensator

Simultaneous PMD compensation for four 10 Gb/s WDM channels was demonstrated using only one single module. The technique optimized overall system performance by

reducing the channel fading probability. The 2% worst-case power penalty for the combined channels in a system with ~42 ps average DGD was improved by over 4 dB.

- Enhanced Higher-Order PMD Compensation Using a Variable Time Delay Between Polarizations

A simple model was introduced for a two-stage higher-order-PMD compensator that has one fixed and one variable differential-delay stage. The results compared the outage probability of the link with the two stage higher-order-PMD compensator and that of a first-order compensator. The results show the comparison for different amounts of PMD in the link and have shown that by using the two-stage higher-order-PMD compensator, achieved tolerable PMD is 50% greater than that of a first-order compensator.

- Enhanced PMD mitigation using forward-error-correction coding combined with a first-order PMD compensator

A significant increase in PMD tolerance using the combination of forward-error-correction (FEC) with a first-order PMD compensator was experimentally demonstrated and numerically verified. It was found that the PMD tolerance for 10 Gb/s systems can be increased to more than 40 ps of average PMD by combining FEC with first-order PMD compensation. Furthermore, it was shown that the system power margin for a transmission link with 43 ps of PMD can be improved by ~7.5 dB, compared with using only a first-order compensator.

- Intra-Bit Polarization Diversity Modulation (IPDM) for PMD Mitigation

A novel and straight forward intra-bit polarization diversity modulation (IPDM) technique was proposed and demonstrated to mitigate the effects of first-order PMD. The technique required only one feedback signal, was independent of the DGD of the optical fiber link, and could operate at >kHz speeds. A unique, but simple, polarization-based modulation format was used at the transmitter and a polarizer at the receiver to select the channel power from only one polarization direction. In the transmitter, each bit was split into two equal halves, with the first half transmitted at an orthogonal polarization to the second half. This modulation format guaranteed that the optical power in the two fiber PSPs be similar under almost all conditions. At the receiver, the first-order PMD effect could be completely removed by selecting only one polarization direction using a polarizer. This scheme had the same advantages of the published PST method, but its response time was orders of magnitude faster.

It was shown that the power penalty induced by first-order PMD was limited to 3 dB and independent of the DGD value of the fiber link. The 2% received optical power tail for the IPDM method had a 4 dB improvement when compared to NRZ signals in the presence of higher-order PMD.

- Demonstration of In-Line Monitoring and Dynamic Broadband Compensation of Polarization Dependent Loss

In-line monitoring and broadband compensation of PDL for four 10-Gbit/s WDM signals was demonstrated. Monitoring and dynamic compensation was performed every 100 km along the 800-km link. In order to avoid the influence of EDFA transients, monitoring was accomplished by using >20-kHz polarization scrambling on either: (i) the data wavelength, or (ii) an ancillary wavelength. Compensation was performed by gathering the monitored PDL and rotating two polarization controllers, each one preceding a fixed PDL component. Using this method, the dynamic PDL compensator reduced the 2% power penalty tail from 6.5 dB to < 2.0 dB in the presence of 14 ps average PMD. Given the 0.2-ps of PMD in the EDFAs, the compensator can correct for degradations over a wide 6-nm bandwidth. It should be emphasized that PDL compensation is easier to perform periodically along a link, whereas PMD compensation is easier to accomplish only once in a link, typically at the receiver.

Simultaneous PMD Compensation of Multiple WDM Channels Using a Single Compensator:

4.1 Simultaneous PMD compensation of multiple WDM channels using a single compensator

Simultaneous PMD compensation for four WDM channels using a single module that is designed to optimize the overall performance of a group of channels by reducing the highly-deleterious impact of the DGD distribution tails was demonstrated. We experimentally showed that this simple yet powerful compensation technique, which uses only a single photodetector and does not require demultiplexing of the individual channels, significantly reduces the probability of channel fading in a WDM system with four 10-Gb/s WDM channels and 42 ps of average DGD. For 1000 independent measurements, the 2% worst-case value of the power penalty for the combined WDM channels is reduced from 9.6 dB to 5.3 dB.

Several PMD compensators have previously been demonstrated for a single wavelength channel. One critical limitation in all previously reported compensation techniques is that each wavelength-division-multiplexed (WDM) channel would require its own separate PMD compensator module, increasing both system cost and complexity. An ideal multiple-channel first-order PMD compensator would generate PMD vectors opposite to the PMD vectors of the transmission fiber at each channel wavelength. In the high-PMD regime where PMD compensation becomes necessary, the correlation bandwidth of the PMD vectors is less than the WDM channel spacing and the PMD vectors are independent from each other. In this case, a single PMD compensator with a fixed PMD vector cannot fully compensate for all WDM channels. However, as we show, a single compensator can significantly decrease both the worst case power penalty and the channel fading probability by optimizing over the entire group of WDM channels.

The effectiveness of our technique is based on the fact that it is highly unlikely that two or more channels will be severely degraded at any given time. Figure 26 shows simulation results of the power penalty corresponding to different DGD values. Note that the power penalty for small DGD is negligible and only high DGD values generate

significant power penalties. Additionally, from the Maxwellian distribution, it is apparent that the probability of a large DGD value is very small. Moreover, even if the situation does occur in which two channels both have a large DGD, the channels will be severely degraded only if the state-of-polarization of each channel is somewhat orthogonal to its own PMD vector. Therefore, it is highly unlikely that more than one channel will be severely degraded at any given time.

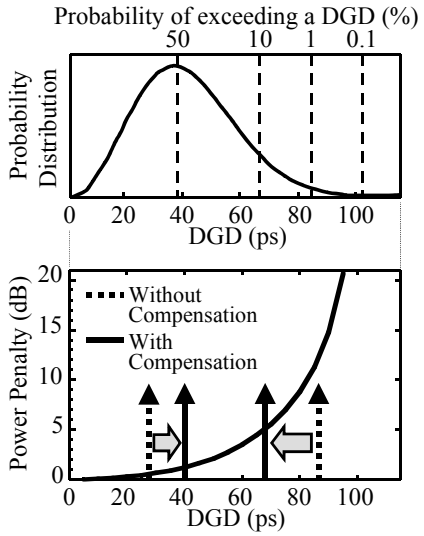

Figure 26. (Top) Due to the Maxwellian distribution of DGD, the probability is low that more than one channel is degraded at any given time. (Bottom) The simulation results show the exponential increase in power penalty with increasing DGD. Using our technique, the DGD of the worst channel is significantly decreased, with a slight change in other channels.

Our compensation module is shown in Figure 27. The input to our module consists of four equal-power 4-nm-spaced WDM channels. We used a multi-section PMD emulator with rotatable connectors to provide a realistic 42 ps of PMD; the emulator produces Maxwellian-distributed DGD with a PMD-vector autocorrelation function that closely resembles that of real fiber. Compensation is provided by an electrically-controlled polarization controller followed by a short length of polarization-maintaining (PM) fiber that provides 30 ps of DGD. Following the PM fiber, a small portion of the WDM data stream is tapped off and fed to a single photodetector.

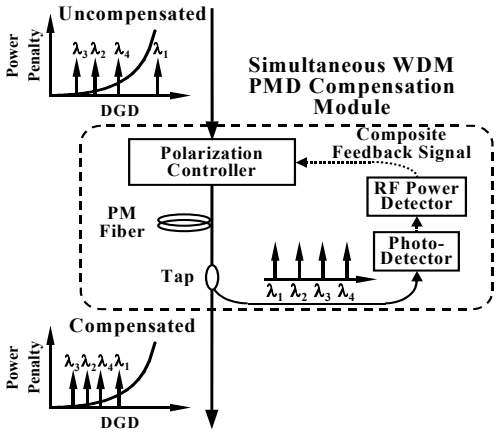

Figure 27. Our compensator uses a feedback signal derived from the combined channels in a WDM data stream to simultaneously optimize system performance.

A portion of the high-frequency components of the combined WDM signal from the photodetector is then mixed with itself to generate a signal that is proportional to the overall RF power. This signal is then fed back to the polarization controller to increase the detected RF power by optimizing the overall system performance, resulting in increased eye openings for the WDM data streams.

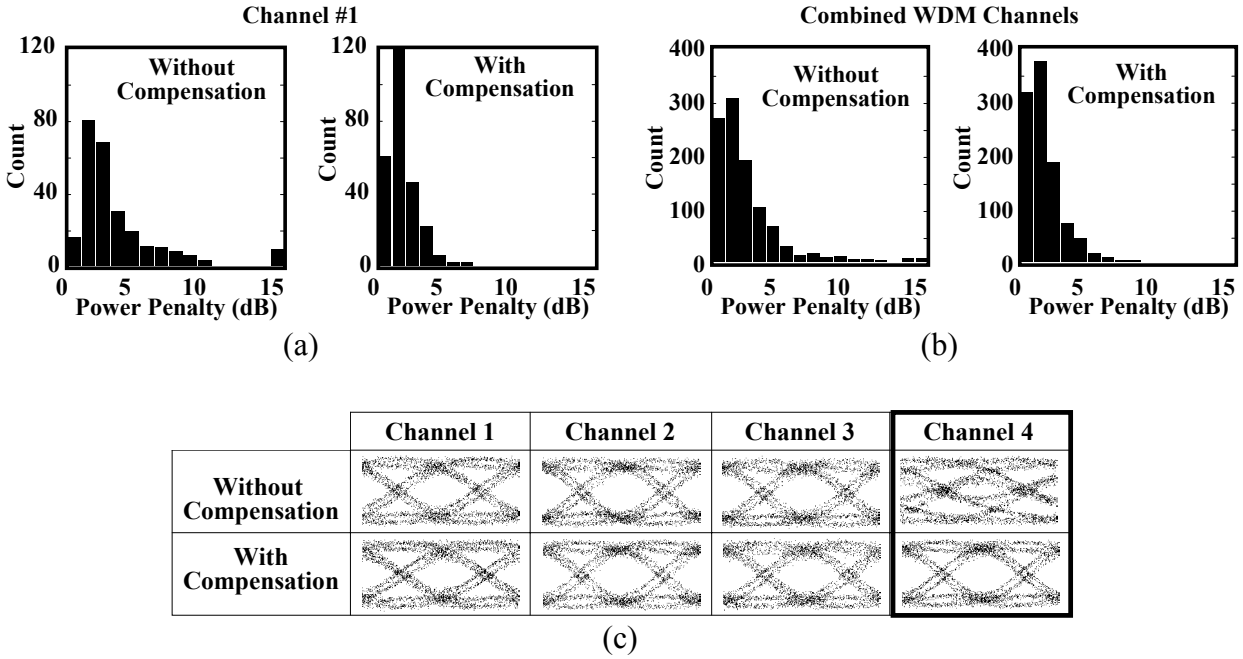

Figure 28. (a) Power penalty histogram for a typical WDM channel (channel #1) without and with compensation. (b) Combined power penalty histogram for a four-channel WDM system without and with compensation. (c) Eye diagram of each channel without and with compensation.

Figure 28 shows the results of our power penalty measurements (1000 independent measurements—250 per channel) for a typical channel (Figure 28(a)) and the combined four WDM channels (Figure 28(b)). Each independent measurement corresponds to a different emulator state. Note that simultaneous compensation of all WDM channels reduces the probability of the highly-degraded tail events and decreases the worst case power penalty by more than 4 dB. For the combined WDM channels, the 2% worst case of the power penalty distribution tail for the channels is reduced from 9.6 dB to 5.3 dB. Figure 28(c) shows one measurement of the eye diagram of the four channels before and after compensation. Channel 4 has been improved significantly after compensation without impacting the other channels. Although we reported the 2% worst case, we emphasize that these results show definite trends for more demanding link outage scenarios.

By using additional polarization controllers and PM fiber sections in series within the compensator, additional degrees of freedom would allow generation of frequency dependent PMD vectors, providing even more complete compensation of even greater numbers of WDM channels.

5. PMD Monitoring

Since the birefringence of a fiber changes randomly along a fiber link and the state-of-polarization of an optical signal changes with environmental conditions, PMD effects on the data signal are stochastic and time varying. Therefore, any PMD compensator at a receiver must track the degrading effects of PMD and dynamically adjust the amount of compensation. Such tracking requires accurate monitoring of these ≥ms-time-scale effects. The following several techniques have been proposed and tested under this grant to monitor the PMD of the system and to be able to either electrically or optically compensate for PMD. Each approach has it's own advantages and disadvantages, but since the papers explaining all the methods are attached in appendix A, only the Degree of Polarization Method (DOP) (method 4) which seems to be the most promising approach will be explained in more detail.

- Simultaneous PMD monitoring of several WDM channels using subcarrier tones

A novel and simple technique for simultaneous and independent PMD monitoring of WDM channels in 10 Gbit/s systems was presented. A subcarrier tone was added to each of the WDM channels using a 10% modulation depth (power penalty <0.3 dB). The subcarriers had the same power but slightly different frequencies. It was shown through statistical measurements that the subcarrier power fading due to PMD was strongly correlated to the PMD-induced degradation on that channel. In the demonstration a single module was used to monitor the PMD of two channels by tracking each channel's subcarrier tone power. This technique did not require any optical demultiplexing of the WDM channels.

- Simple bit-rate-independent PMD Monitoring for WDM Systems using a PDL element

A simple bit-rate independent technique for PMD monitoring was proposed using a PDL element which operated within a few milliseconds for a single channel, and could accommodate many WDM channels by sweeping the optical filter across all channels. This method utilized: (i) a polarization scrambler at the transmitter, and (ii) a combination of a polarization scrambler, optical filter, and polarization-dependent-loss (PDL) element at the receiver.

For a fixed position of the optical filter, the instantaneous differential group delay (DGD) was measured for an individual channel. This monitor signal was generated by the root-mean-square (RMS) value of the optical power that was fluctuating due to the scrambling and subsequent passing through a PDL element. The instantaneous DGD value of 0 to 70 ps was monitored for NRZ and RZ formats, and the monitor output was used as a feedback signal for PMD compensation of a 10-Gb/s NRZ channel. For first-order PMD compensators, this scheme can readily be adapted for much higher bit rates, reduces the feedback control complexity, and significantly improves stability.

- PMD monitoring in WDM systems for NRZ data using a chromatic-dispersion-regenerated clock

A dispersive element can be used at the receiver to regenerate a clock component for NRZ data, and it was shown that this regenerated clock is very sensitive to PMD and can be extracted to monitor PMD of an optical transmission link. Successful PMD compensation at 10 Gbit/s using this regenerated clock power as a control signal was also demonstrated.

- Wide-dynamic-range DGD monitoring by partial optical signal spectrum DOP measurement

Degree of Polarization measurement to monitor PMD is already a well known technique but in this project it is shown that by filtering the signal before the receiver and then measuring the DOP (partial-optical-spectrum DOP measurement), the pulse-width dependent DGD monitoring range is increased for 10, 20, and 40-Gbit/s RZ and the sensitivity is increased for 10-Gbit/s NRZ signals. The monitoring range for 20 and 40-Gbit/s RZ signals is extended to one bit time.

5.1 Wide-dynamic-range DGD monitoring by partial optical signal spectrum DOP measurement

Several types of PMD monitors have been reported that measure PMD or data integrity. However, the technique of measuring the signal's degree-of-polarization (DOP) has the advantage of not requiring high speed circuit and is independent of the bit-rate. Unfortunately, DOP measurements as a function of instantaneous DGD suffer from the following crucial systems disadvantages: (i) there is a small DGD monitoring window when measuring a short pulse return-to-zero (RZ) signal, and (ii) there is a lack of

sensitivity when measuring a non-return-to-zero (NRZ) signal, and iii) the higher-order PMD affects the DOP measurement for DGD. It would be highly desirable to have a PMD monitor for which the DOP can be measured to obtain wide monitoring windows and high sensitivity for both RZ and NRZ signals and low sensitivity to higher order PMD.

We demonstrate a technique for measuring the signal's DOP as a function of DGD for RZ signals such that the DGD monitoring range is dramatically enhanced. Using a narrowband optical filter that is either centered at the carrier or on one of the signal's sidebands, we change the detected DOP to get wider monitoring range or higher sensitivity. For different pulse-widths at bit rates of 10, 20, and 40 Gbit/s, using our technique, the monitoring range for 12.5-ps pulse 10, 20, and 40 Gbit/s RZ signals are increased by 32, 33, and 12 ps, respectively. Moreover, the monitoring range of 25-ps pulse 20 Gbit/s RZ signals is extended from 26 ps to 45 ps.

Pulse width modification for DOP-based PMD monitoring

While a signal's DOP has been shown to be related to the PMD of an optical link, making it a convenient monitoring tool, the usefulness of this technique when applied to varied pulse-width RZ systems is not well understood. The DOP of a signal at the receiver depends on the DGD of the system, the polarization splitting ratio, and the signal pulse width. As the width of an RZ pulse decreases, the DGD monitoring range provided by DOP monitoring decreases as well. The case when the polarization splitting ratio is equal to 50% (equal optical power in each polarization state, or polarization scrambling at the transmitter), is shown in Figure 29(a) for varying pulse widths. This figure shows that the DOP reaches its first minimum value when the DGD is equal to the pulse width. Thus, a DGD monitor utilizing DOP measurement suffers a reduction in its DGD monitoring window as the pulse width decreases (for example, in a short-pulse RZ system).

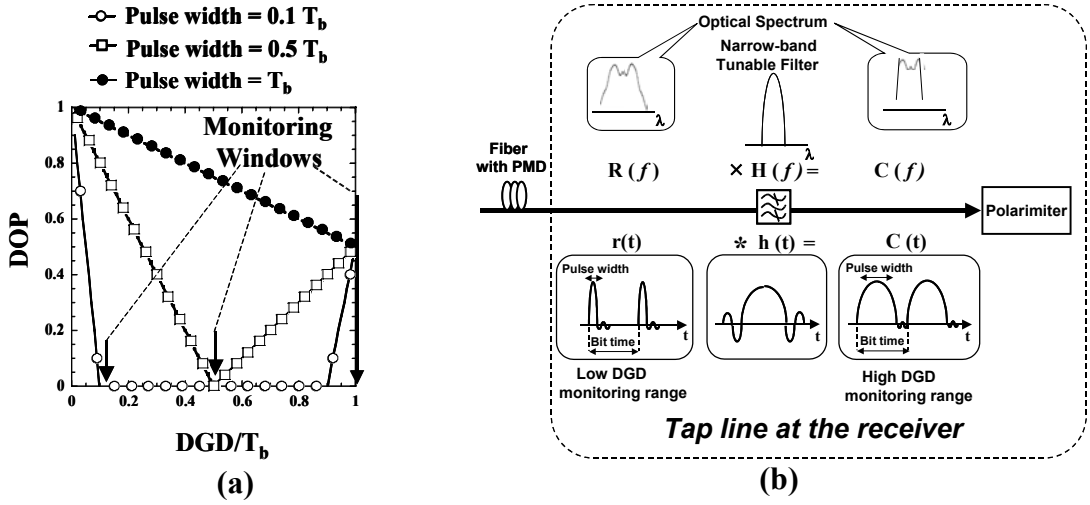

Figure 29. (a) The effective DGD monitoring window is limited to the pulse width of the RZ signal. (b) Narrowband optical filtering can increase the DGD monitoring window by broadening the pulse in the time domain.

One solution that can enhance the DGD monitoring windows in short-pulse systems is broadening the optical pulse in the time domain, which moves the first DOP minimum to a higher DGD value. This concept is illustrated in Figure 29(b). This is achieved through the use of a narrowband optical filter that can be centered on either the carrier or the first optical clock component. As multiplication in the wavelength domain corresponds to convolution in the time domain, a sufficiently narrowband optical filter (with a broad time domain response) can be used to broaden a pulse in time via convolution. Simulation results for this system are shown in Figure 30 for varying bit rates and pulse widths. The width of the filter is an important parameter when utilizing this technique - too narrow a filter results in too little optical power and lower sensitivity, while too wide a filter (with a shorter time response) reduces the pulse broadening that is key to this technique. Our simulations show the ideal filter bandwidth to be $0.8*R_b$, where R_b is the bit rate of the system. As seen in Figure 30(a) and (b), side band filtering, i.e., by centering the narrowband optical filter at the first optical clock sidebands (either upper or lower), results in a near-doubling of the DOP sensitivity for PMD monitoring in 40 and 10 Gbit/s NRZ systems without affecting the monitoring windows. Figure 30(c) and (d) show that center and sideband filtering results in 25 and 50 ps increases in the monitoring windows in 40 and 10 Gbit/s RZ systems, respectively, corresponding to bit-time-length DGD monitoring windows.

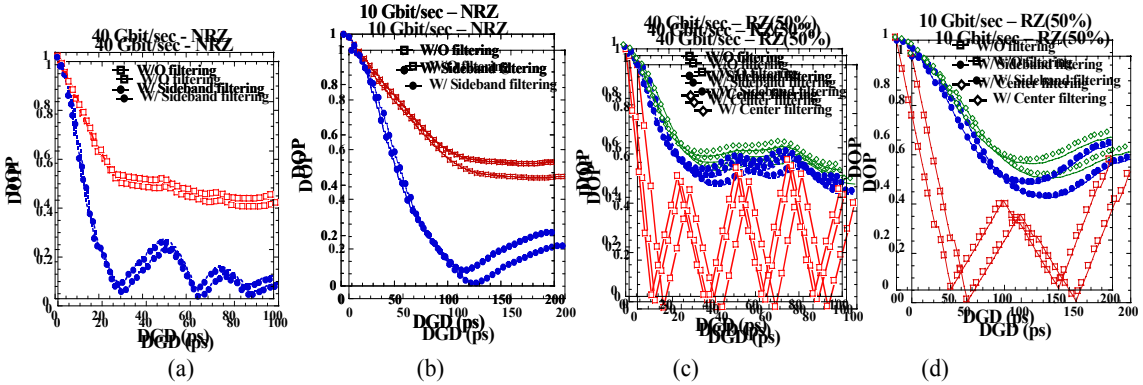

Figure 30. (a),(b) Sideband filtering results in a near-doubling of the DOP sensitivity for PMD monitoring in 40 and 10 Gbit/s NRZ systems without affecting the monitoring windows. (c),(d) Center and sideband filtering results in 25 and 50 ps increases in the monitoring windows in 40 and 10 Gbit/s RZ systems, respectively, corresponding to bit-time-length DGD monitoring windows.

In addition, when the narrowband optical filter is centered on the RZ carrier, the resulting DOP values are much less sensitive to higher-order PMD, as the filtered signal includes only optical frequency components that experience similar PMD vectors.

40, 20, 10-Gbit/s Systems Experiments

Figure 31(a) shows the experimental setup of a 10, 20, and 40-Gb/s system with varying pulse widths. The 10 Gbit/s RZ data (2^{23}-1 PRBS) with 50% duty cycle is first generated using two cascaded electro-optic modulators. The pulse width is then compressed to 12.5 ps and 25 ps by adjusting the amplitude of a phase

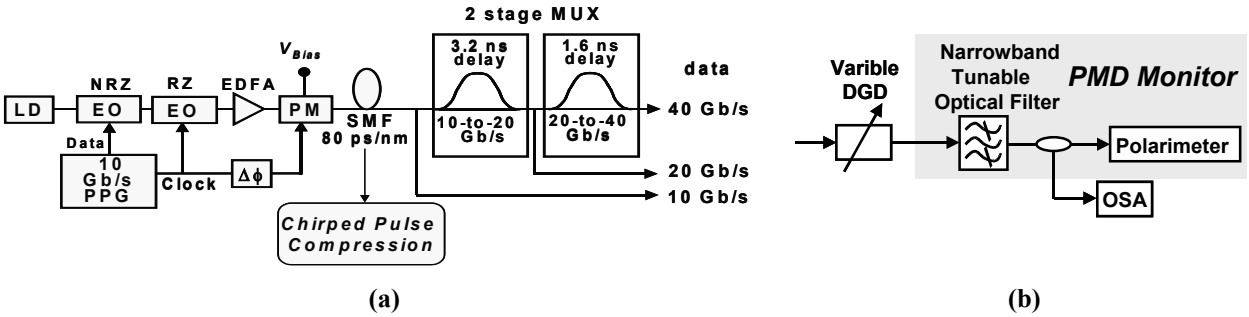

Figure 31. (a) Experimental setup of a 10, 20, and 40 Gbit/s OTDM system with 12.5 and 25 ps RZ pulse widths obtained by changing the bias voltage on the phase modulator. (b) The DGD monitoring system setup using the narrowband optical filter and polarimeter.

modulator followed by a spool of single-mode-fiber (SMF) with a dispersion value of 80 ps/nm. A two-stage optical multiplexer is used to generate 20 Gbit/s and 40 Gbit/s data stream. After the transmitter, a variable DGD element is used to generate varying amounts of first-order PMD by aligning the input polarization state to provide equal power to the fast and slow axes of the DGD element. The PMD monitoring configuration is shown in Figure 31(b). A narrowband tunable optical filter is used to filter out a partial optical spectrum from the signal. The bandwidth of the filter depends on the data rate, e.g. 0.28 nm, 0.12 nm and 0.28 nm for 10, 20, and 40 Gbit/s, respectively. A polarimeter is used to gather the DOP information of the monitoring signal, and an the optical spectrum analyzer (OSA) is used for spectrum analysis.

The measurement results for different pulse widths in different bit rate systems are shown in Figure 32 (a)-(d). As we can see that, for 12.5-ps pulse widths, the narrowband optical filtering technique increases the DGD monitoring windows by at least 12 ps, 33 ps, and 32 ps for 40, 20 and 10 Gbit/sec signals. For 25-ps pulse widths, the dynamic range increases by 20 ps for 20-Gbit/s signals.

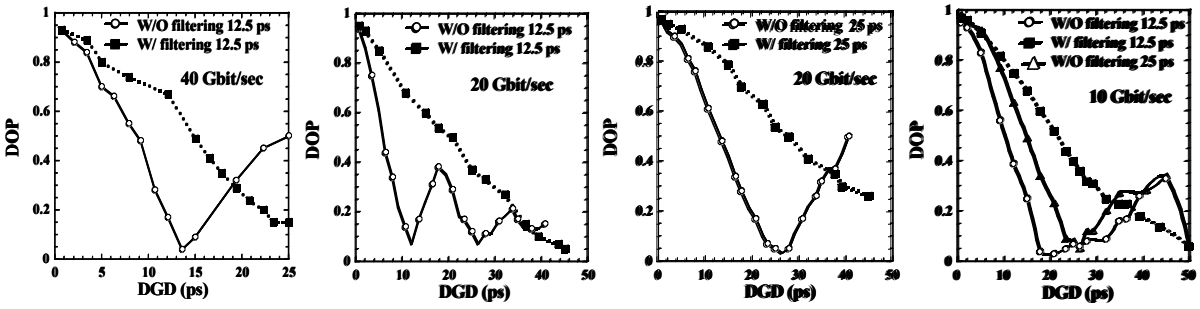

Figure 32. The narrowband optical filtering technique increases the DGD monitoring windows in (a) 40 Gbit/sec 12.5 ps pulse RZ systems by at least 12 ps, in (b) 20 Gbit/sec 12.5 ps pulse RZ systems by 33 ps, (c) 20 Gbit/s 25 ps pulse RZ systems by 20 ps, and (d) 10 Gbit/sec 12.5 ps pulse RZ systems by 32 ps.

Cumulative Journal Publications:

1. S. Lee, R. Khosravani, J. Peng, V. Grubsky, D.S. Starodubov, A.E. Willner, and J. Feinberg, "*Adjustable Compensation of Polarization Mode Dispersion Using a High-Birefringence, Nonlinearly-Chirped Fiber Bragg Grating,*" **IEEE Photonics Technology Letters**, vol. **11**, pp. 1277-1279, 1999.

2. R. Khosravani, I.T. Lima Jr., P. Ebrahimi, E. Ibragimov, A.E. Willner, and C.R. Menyuk, "*Time and Frequency Domain Characteristics of Polarization Mode Dispersion Emulators,*" **IEEE Photonics Technology Letters**, vol. **13**, 2001.

3. S. Lee, P. Ebrahimi and A.E. Willner, "*All-optical remote location of high polarization mode dispersion fiber spans using stimulated Brillouin Scattering,*" submitted to **IEEE Photonics Technology Letters.**

4. R Khosravani and A. E. Willner, "*System performance evaluation in terrestrial systems with high polarization mode dispersion and the effect of chirping*,", **IEEE Photonics Technology Letters,** vol 13, April 2001.

5. Reza Khosravani, Steven A. Havstad, Y. W. Song, P. Ebrahimi, Alan E. Willner, " *Polarization-mode dispersion compensation in wdm systems* ", **IEEE Photonics Technology Letters**, vol 13, Dec 2001.

6. Y. Xie, Q. Yu, L.-S. Yan, O. H. Adamczyk, Z. Pan, S. Lee, A. E. Willner, and C. R. Menyuk, "*Enhanced PMD mitigation using forward-error-correction coding and a first-order compensator*," to be submitted to **IEEE Photonics Technology Letters.**

7. S. Lee, Q. Yu, L.-S. Yan, Y. Xie, O. H. Adamczyk, and A. E. Willner, "*A short recirculating fiber loop testbed with accurate reproduction of Maxwellian PMD statistics*", to be submitted to **IEEE Photonics Technology Letters.**

8. Q. Yu, L. S. Yan, Y. Xie, M. Hauer, A. E. Willner, "*Higher order polarization mode dispersion compensation using a fixed time delay followed by a variable time delay",* **IEEE Photonics Technology Letters**, vol 13, Aug 2001.

9. P. Ebrahimi, M. C. Hauer, Q. Yu, R. Khosravani and A. E. Willner, *"The effect of PMD on the Polarization Dependant Gain of Raman Fiber Amplifiers***",** to be submitted to **IEEE Photonics Technology Letters.**

10. Z. Pan, Y. Wang, C. Yu, T. Luo, A. B. Sahin, Q. Yu, and A. E. Willner, "*A Novel PMD Compensation Technique by Using Intra-Bit Polarization Diversity Modulation Format",* to be submitted to **IEEE Photonics Technology Letters.**

11. S. M. R Motaghian Nezam, Y. Wang, M. Hauer and A. E Willner, " *Simultaneous PMD Monitoring of Multiple WDM Channels Using subcarrier*", to be submitted to **IEEE Photonics Technology Letters.**

12. L.-S. Yan, Q. Yu, A. E. Willner, "*Demonstration of In-line Monitoring and Compensation of Polarization Dependent loss for multiple channelss*", **IEEE Photonics Technology Letters,** vol 14, June 2002

13. L.-S. Yan, Q. Yu, A.B. Sahin, A. E. Willner, "*Differential Group Delay (DGD) Monitoring Used as Feed Forward Information for Polarization Mode Dispersion Compensation*", to be published in **IEEE Photonics Technology Letters**

14. M.C. Hauer, Q. Yu, E.R. Lyons[+], C. H. Lin[+], A. A. Au[+], H.P. Lee[+], A.E. Willner , "*Electrically controllable all-fiber PMD emulator using a compact array of thin-film micro-heaters*", to be published in **IEEE Photonics Technology Letters**

15. S. M. R. Motaghian Nezam,Y. W. Song , A. B. Sahin, Z. Pan, and A. E. Willner**, "**PMD monitoring in WDM systems for NRZ data using a chromatic-dispersion-regenerated clock," to be submitted to **IEEE Photonics Technology Letters.**

16. Z. Pan, Q. Yu, Y. Arieli[+], and A. E. Willner, "*Fast XPM-induced polarization-state fluctuations in WDM systems and their mitigation,"* to be submitted to **IEEE Photonics Technology Letters.**

17. C. Yu, Q. Yu, Z. Pan, A. B. Sahin, and A. E. Willner, "*Optical compensation of PMD-induced power fading for single sideband subcarrier-multiplexed systems"* to be submitted to **IEEE Photonics Technology Letters.**

the two PDL elements. In such a loop this randomization could be easily achieved with a number of commercially available devices.

Conclusion

In conclusion, the measured and modeled Q factor distribution in a 107 km recirculating loop was significantly different from that of the long straight-line systems where the fibers environment is not static. We show that by randomizing the polarization between multiple PDL elements one can achieve a Q distribution that is more like that of a straight-line system.

References

1. F. Bruyere, O. Auduin, V. letellier, G. Bassier, and P. Marmier, "Demonstration of an optimal polarization scrambler for long haul optical amplifier systems," IEEE Photon Technol. Lett., vol.6, no. 9, pp. 1153–pp. 1155, Sep. 1994.
2. Yu Sun, Ding Wang, Pranay Sinha, Gary M. Carter, Curtis Menyuk, "Polarization evolution in a 107 km dispersion-managed recirculating loop," CLEO 2000, pp 59, May, 2000.
3. D. Wang and C.R. Menyuk, "Reduced model of the evolution of the polarization states in wavelength-division-multiplexed channels," Opt. Lett., pp. 1677–1679, November, 1998.
4. C.R. Menyuk, D. Wang and A.N. Pilipetskii, "Repolarization of polarization-scrambled optical signals due to polarization dependent loss," *IEEE Photon. Technol. Lett.*, vol. 9, pp 1247–1249, September 1997.
5. J. Jacob, E.A. Golovchenko, A.N. Pilipetskii, G.M. Carter and C.R. Menyuk, "10 Gb/s transmission of NRZ over 10,000 km and solitons over 13,500 km error-free in the same dispersion-managed system," *IEEE Photon. Technol. Lett.*, vol. 9, pp. 1412–1414, Oct. 1997.
6. Dietrich Marcuse, "Derivation of analytical expressions for the bit-error probability in lightwave systems with optical amplifiers," J. Lightwave Technol., vol. 8, no. 12, pp. 1816–1823, Dec. 1990.

CFE5 **11:30 am**

10-Gb/s PMD Compensation Following a Recirculating Fiber Loop

Q. Yu, L.-S. Yan, and A.E. Willner, *Department of Electrical Engineering-Systems, EEB-500, University of Southern California, Los Angeles, CA 90089; Email: qiany@usc.edu*

1. Introduction

Polarization mode dispersion (PMD) has emerged as a critical issue for the deployment of high bit-rate systems over the installed fiber infrastructure. PMD is unique because it is a stochastic, dynamically changing process.[1] Extensive research efforts have been made on PMD compensation in recent years. Reported experiments of PMD compensation are using either PMD emulators or in-ground fiber links to generate PMD.[2–7] However, lumped PMD emulators cannot correctly taken into account the combined effect of fiber nonlinearity and PMD, while field trials lack flexibility for research. Because the stochastic behavior of PMD can vary from fiber to fiber, ensuring that a specific field-trial result will be applicable for different links is problematic.

Recirculating fiber-loop testbeds have been powerful tools in the research and development of optical transmission systems. Conventional recirculating loops, however, are inadequate in the presence of non-negligible PMD, because a recirculating loop exhibits some measure of periodic behavior that artificially produces an unrealistic PMD distribution that is skewed towards higher differential group delays (DGD). Our solution to this problem is to employ loop-synchronous polarization scrambling.[8] However, the effectiveness of this technique for the investigation of PMD compensation is yet to be verified.

In this paper, PMD compensation following a 10-Gb/s, 8 × 82-km recirculating fiber loop is demonstrated. We use a simple PMD compensator comprised of a polarization controller followed by a polarization-maintaining (PM) fiber with 42-ps DGD. For this system, with an average PMD of 27 ps, the bit-error-rate (BER) distribution tail at 5% probability can be reduced from 10^{-6} to 10^{-8} after PMD compensation, with the received power fixed at the level corresponding to a 10^{-9} BER without PMD.

2. Experimental Setup

Fig. 1 shows the experimental setup. An external cavity laser at 1557 nm is NRZ-modulated at 10 Gb/s ($2^{15}-1$ PRBS). The dispersion-managed recirculating loop consists of three EDFAs operating in the saturated regime, 82 km of single-mode fiber (SMF), and 12 km of dispersion-compensating fiber (DCF) with a chromatic dispersion of −1348 ps/nm. The input powers to the SMF and DCF are fixed at 3.0 dBm and −1.0 dBm, respectively. In order to replicate the Maxwellian PMD statistics, a loop-synchronous $LiNbO_3$ polarization controller (PC) and a section of PM-fiber are used inside the loop. The polarization transfer matrix of the $LiNbO_3$ PC is controlled by six input voltages and can be set to a random state during each loop period. These decorrelated polarization states are repeated after a certain number of loops as determined by the loop control circuitry. We use 8 passes through the loop, corresponding to about 650-km transmission. The PM-fiber inside the loop has a DGD of 10.2 ps, so the average DGD after 8 loops is about 27 ps. The PMD compensator can be automatically adjusted by maximizing the RF power of the photo-detected signal within a limited bandwidth (4.5~8.5 GHz).

3. Results and Discussion

Fig. 2 shows the histograms of the BER measured for 300 statistically independent samples with the received optical power fixed at −16.5 dBm, which is the receiver sensitivity at 10^{-9} BER after 650-km transmission without the 10.2-ps PM-fiber inside the loop. The BER tail of 300 samples extends to 10^{-3} without PMD compensation,

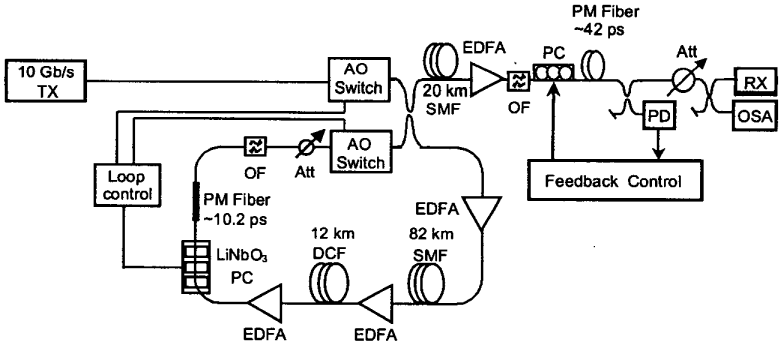

CFE5 **Fig. 1.** Setup of PMD compensation experiment using recirculating fiber loop with loop-synchronous polarization scrambling.

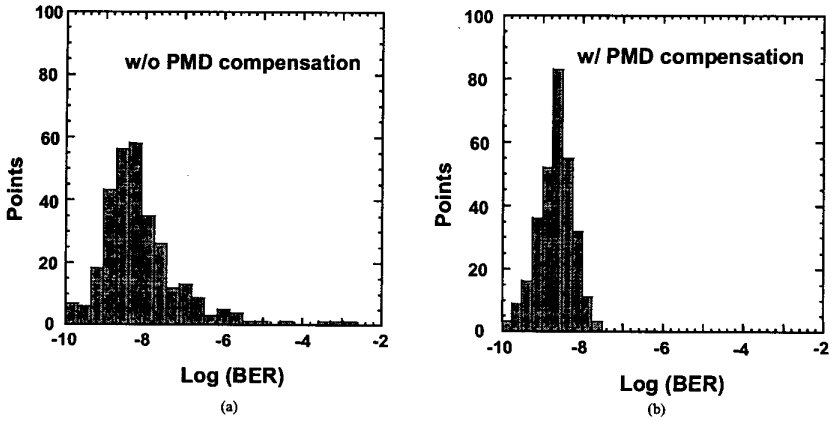

CFE5 **Fig. 2.** Histograms of BER for 300 statistically independent samples. (a) without PMD compensation, (b) with PMD compensation.

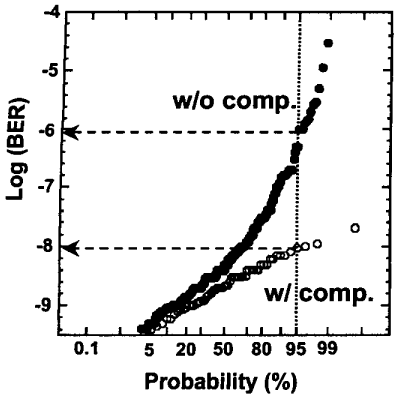

CFE5 Fig. 3. Cumulative probability distribution of BER.

whereas the BER after automatic PMD compensation is reduced to less than 10^{-7}.

Furthermore, the cumulative probability distributions of the above BER results are shown in Fig. 3. For an average PMD of 27 ps, the BER distribution tail at 5% probability decreases from 10^{-6} to 10^{-8} using PMD compensation. The corresponding power penalty can be reduced from about 3 dB to 1 dB.

Although our experiment is done for a typical compensator, the recirculating fiber loop can be a flexible tool for the research and development of other PMD mitigation technologies. We may also use the fiber loop to emulate the fast, stochastic variation of PMD, so as to evaluate the dynamic tracking performance of an adaptive PMD compensator. We expect our fiber-loop testbed to be an effective tool for investigating the combined effects of dispersion, nonlinearity, and PMD on high-bit-rate systems.

4. References

1. C.D. Poole, J. Nagel, "Polarization Effects in Lightwave Systems," Optical Fiber Telecommunications IIIA, 114–161, Academic Press (1997).
2. T. Takahashi, T. Imai and M. Aki, "Automatic compensation technique for timewise fluctuating polarisation mode dispersion in inline amplifier systems," Electronics Letters, 30, 348–349, (1994).
3. F. Heismann, D.A. Fishman, and D.L. Wilson, "Automatic compensation of first-order polarization mode dispersion in a 10 Gb/s transmission system," Proc. ECOC'98, Madrid, Spain, 529–530, (1998).
4. M.W. Chbat, J.P. Soigné, T. Fuerst, J.T. Anthony, S. Lanne, H. Février, B.M. Desthieux, A.H. Bush, and D. Penninckx, "Long Term Field Demonstration of Optical PMD compensation on an Installed OC-192 Link," OFC'99, postdeadline paper PD12, (1999).
5. D.A. Watley, K.S. Farley, W.S. Lee, G. Bordogna, B.J. Shaw, A.P. Hadjifotiou, "Field evaluation of an optical PMD compensator using an installed 10 Gb/s system," paper ThB6, OFC'2000.
6. J.A. Nagel, M.W. Chbat, L.D. Garrett, J.P. Soigné, N.A. Weaver, B.M. Desthieux, H. Bülow, A.R. McCormick, and R.M. Derosier, "Long-term PMD mitigation at 10 Gb/s and time dynamics over high-PMD installed fiber," paper 4.2.1, ECOC'2000.
7. S. Lanne, J.P. Thiéry, D. Penninckx, J-P. Hamaide, J-P. Soigné, B. Desthieux, J. Le Briand, L. Macé, P. Gavignet, "Field optical PMD compensation at 10 Gb/s over installed fibre totaling 35 ps of PMD," paper P.3.9, ECOC'2000.
8. S. Lee, Q. Yu, L.-S. Yan, Y. Xie, O.H. Adamczyk, and A.E. Willner, "A Short Recirculating Fiber Loop Testbed with Accurate Reproduction of Maxwellian PMD Statistics," submitted to OFC'2001.

CFE6 **11:45 am**

Influence of polarization-mode dispersion on soliton interaction in dispersion-managed soliton transmission systems

Yuichi Takushima, Tomohiro Douke, and Kazuro Kikuchi, *Research Center for Advanced Science and Technology, University of Tokyo, 4-6-1 Komaba, Meguro-ku, Tokyo 153-8904, Japan; Email: ytaku@ginjo.rcast.u-tokyo.ac.jp*

Recent studies of dispersion-managed (DM) solitons have shown that the DM soliton pulse can withstand the pulse broadening due to the polarization-mode dispersion (PMD), and that the single pulse can propagate stably even under the influence of the PMD.[1,2] In most of DM soliton systems, however, the transmission distance is limited by the soliton interaction, and hence the behavior of the soliton interaction under the influence of the PMD seems to be rather important. In this paper, we numerically investigate the influence of the PMD on the soliton interaction. We show that the PMD could either enhance or reduce the soliton interaction depending on the distribution of the fiber birefringence, and that the transmission performance is improved by the PMD in certain cases.

One period of the DM link used in the numerical simulation consists of a 50-km dispersion-shifted fiber and a 3-km single-mode fiber, whose dispersion values are –0.9 and 15.7 ps/nm/km, respectively. The average dispersion is 0.07 ps/nm/km. A 7-ps DM soliton pulse can be transmitted stably when the pulse energy is 0.12-0.25 pJ in this DM link. These parameters are the identical to those used in the 40-Gbps DM soliton transmission experiment.[3]

We assume that the transmission fiber has a linear birefringence with the group-delay difference of polarization components, $\Delta\beta$, and the birefringence axes are rotated at every correlation length, L_{cor}. If the rotation angle is chosen randomly, this model follows the standard technique used in previous studies.[1,2,4]

To grasp the influence of the PMD on the soliton interaction, we calculate the pulse propagation in two ideal conditions: (A) the case when the rotation angle of the birefringence axes is zero, i.e., the completely linear birefringent fiber link, and (B) the case when the rotation angle is 90 degrees, i.e., the birefringence axes alternate at interval of L_{cor}. In both cases, the launched pulse is a 7-ps Gaussian pulse with the energy of 0.175 pJ/pulse, and has a linear polarization oriented by 45 degrees with respect to the principle axis.

Figure 1(a) shows that the evolution of the waveform when a single pulse is launched into the link with $\Delta\beta$ = 0.032 ps/km in case (A). It is clearly seen that the DM soliton can maintain the single peak pulse though the differential group delay accumulates as the pulse propagates.

Although the single DM soliton pulse can overcome the accumulation of the DGD, the fiber birefringence significantly modifies the behavior of the soliton interaction between pulses. Figures 1(b) and (c) show the evolution of two pulses with separation of 25 ps when $\Delta\beta$ = 0 and 0.032 ps/km, respectively. When $\Delta\beta$ = 0, the two pulses attract each other as the pulse propagates, and the pulse separation narrows down to 18 ps at the distance of 1590 km. (We call the distance at which the pulse separation becomes narrower than 70% of the bit interval *the collision distance.* It roughly corresponds to the transmission distance for bit error rate = 10^{-9}.[3]) On the contrary, when $\Delta\beta$ = 0.032 ps/km, the collision distance is reduced to 1378 km. This is because the pulse separation between the slow axis component of the front pulse and the fast axis component of the backward pulse is always kept narrower than

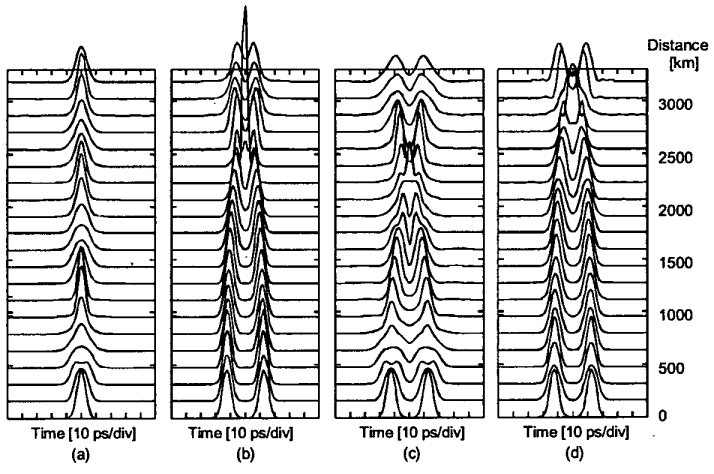

CFE6 Fig. 1. Evolutions of the waveform in ideal DM transmission links. Figures (a) shows the propagation of the solitary pulse in the linear birefringent fiber link with $\Delta\beta$ = 0.032 ps/km. Figures (b)–(d) show the propagation of a pulse pair (b) in zero PMD fiber link, (c) in the linearly birefirengent fiber link and (d) in the linearly birefringent fiber link whose polarization axis is periodically rotated by 90 degree, respectively.

All-optical remote location of high polarization mode dispersion fiber spans using stimulated Brillouin Scattering

S. Lee and A. E. Willner
Dept. of Electrical Engineering- Systems
University of Southern California
Los Angeles, CA 90089-2565
(213) 740-1488, fax: (213) 740-8729 sanggeon@scf.usc.edu

Polarization mode dispersion (PMD) has emerged as a key limitation in high-speed and long-distance fiber communication systems. This is particularly true due to the unusually high PMD values of many sections of fiber installed prior to the mid 1990's. Although present-day fibers have PMD values ~0.1 ps/km$^{1/2}$, isolated spans of older installed fiber can have values ranging from 1 to as high as 10 ps/km$^{1/2}$. These older fibers were never tested for their PMD values, and system integrators must locate them in order to design around such high-PMD fiber spans since their location within a much longer link is unknown. Therefore, it would be highly advantageous to have an all-optical technique that can remotely determine the location and magnitude of a high-PMD fiber span.

One method that has been reported for determining the location and magnitude of high PMD fiber is to launch a high-power pulse at different wavelengths into a long-distance fiber link and analyze Rayleigh back-scattering [1]. This technique uses a tunable laser, a MHz optical modulator, an OTDR, and a PMD analyzer or inline polarizer to examine the Rayleigh back-scattered pulse. Although the results are accurate, the optical hardware required is fairly complex and expensive, making it difficult to implement for field use.

We report a method for an all-optical remote locator of high PMD fiber spans using stimulated Brillouin scattering (SBS). Both the length of the high PMD fiber span and the magnitude of PMD itself can be inferred from the slope change of the reflected SBS pulse. The optical hardware required in the field to measure the reflected SBS pulse is much simpler than what was previously reported and includes only an oscilloscope, a kHz optical modulator, and a standard DFB laser. Our results show sufficiently accurate readings for spans as short as 5 km and having PMD values as low as ~1 ps/km$^{1/2}$. Advantages of our method include: (a) simpler hardware field requirements and (b) lower required laser power due to SBS amplification versus Rayleigh attenuation.

Stimulated Brillouin scattering has been used as an all-optical sensor for environmental perturbations (i.e. temperature[2], strain[2], and stress[3]) in optical fiber. And, SBS gain changes due to fiber nonuniformites [4]. Since PMD is closely related to all of these changes, SBS can be used to monitor and locate an installed fiber span with high PMD values. Fig. 1 shows the conceptual diagram for SBS gain spectrum changes due to PMD. Fiber spans 1 and 3 have low PMD values and have almost uniform SBS gain spectra if fiber losses are not considered. But, fiber span 2 has a perturbed SBS gain spectrum due to PMD induced by external perturbation; such as stress change. To emulate controllable high PMD conditions, ~ 4.5 km of single mode fiber (SMF) is laid in adjacent non overlapping layers on a 1.2 m long plate and external stress is applied. Using a PMD analyzer (3 Stokes parameter method), changes in PMD and loss due to stress are monitored. Without stress, the average PMD is about 0.061 ps, which changes to 0.93 ps when stress is applied. Loss due to external stress is maintained less than 0.15 dB through out the entire process.

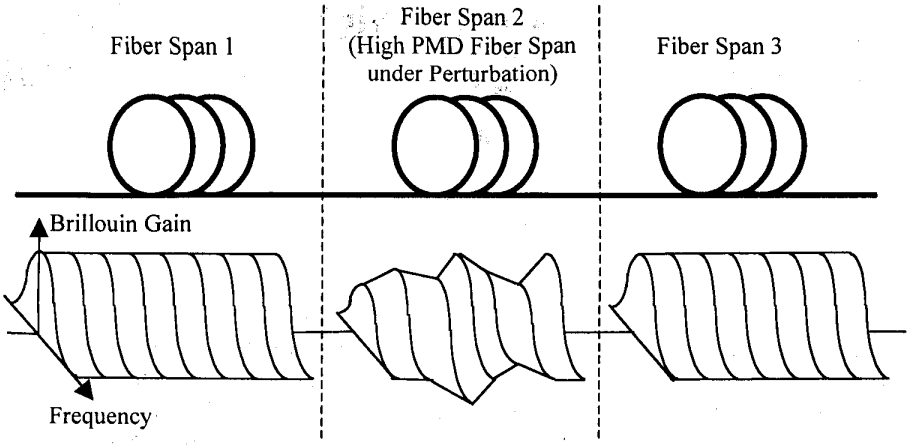

Fig. 1. Conceptual diagram of SBS gain changes within a high PMD fiber span.

Our experimental setup for location of high PMD fiber spans is shown in Fig. 2. The external cavity tunable laser is amplified using an EDFA and modulated using an acousto-optic modulator to get ~ 530 μs square pulses. These pulses are slightly longer than round trip delay of the of fiber span, to provide amplification of the SBS which is generated at the end of the fiber span. These square pulses are input to the 51.5 km SMF fiber span that consists of 29 km SMF, 4.5 km SMF with controllable stress, and 18 km SMF. The reflected SBS is tapped using a 90/10 coupler and monitored using a low-speed photodetector and an oscilloscope. PMD values over both entire 51.5 km SMF span and the 4.5 km isolated span under stress are measured with a PMD analyzer and a tunable laser by scanning the wavelength from 1500 nm to 1580 nm.

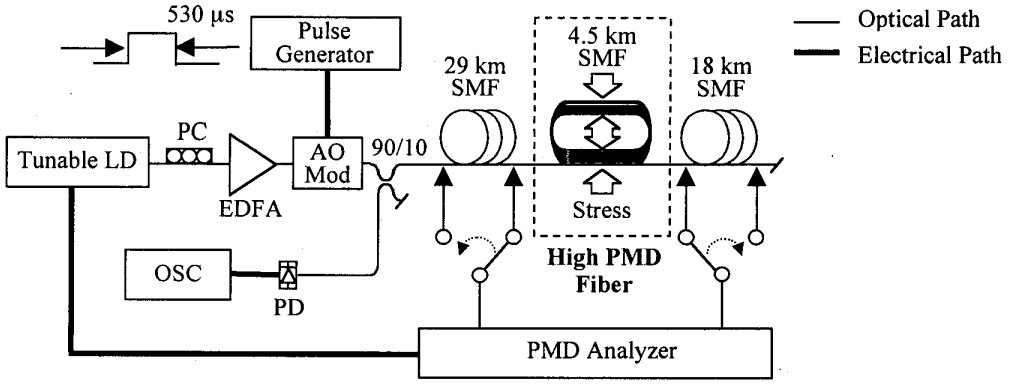

Fig. 2. Experimental setup for high PMD location using SBS.

Fig. 3 shows measurements of the average value of PMD of the 51.5 km span and the 4.5 km span under variable stress. Without stress or with very small stress, the overall PMD value is around 0.36 ps which is mostly determined by the 29 km and 18 km SMF spans. By applying more stress, the overall PMD values goes up to 1.0 ps (278 % change from original value) and this value is dominated by the 4.5 km SMF span under stress. The dotted line shows the expected PMD values, calculated as the square root of the sum of the squared PMD values. The measured data matches well the expected values.

Fig. 4(a) shows the oscilloscope trace of the reflected SBS from the entire SMF span at an input wavelength of 1549.59 nm and average optical power of 7.59 dBm. The input optical power is adjusted so as not to saturate SBS through the whole fiber span, and to give a gradual increment in SBS pulse power over time. The trace is shown with 64 times averaging using an oscilloscope. SBS is generated and

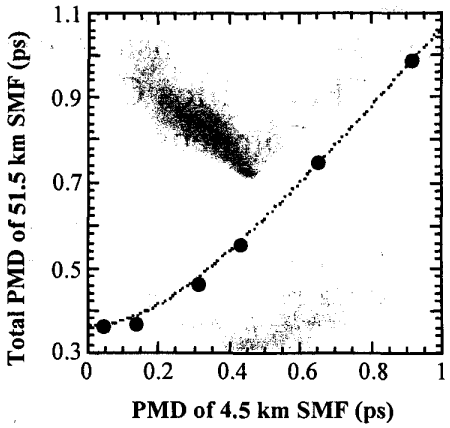

Fig. 3. Total PMD of 51.5 km span vs. average PMD of 4.5 km span under different stress (dotted line shows the expected PMD calculated as the square root of the sum of the squares of the PMD values).

amplified in the backward direction by the forward optical pump. Thus, SBS power increases as more of the input pulse enters the fiber and then decreases abruptly as the tail of the pulse leaves the input of the fiber. The slope of the SBS pulse changes at the 4.5 km span corresponding to the different PMD values (0.43 ps and 0.91 ps in our case) in that span caused by different stress. The position and the magnitude of the slope change gives information about the location of a high PMD fiber span and the related PMD value. The slope of the scope trace in a time interval of 10 μs is calculated and shown in Fig. 4(b). A 10 μs time interval corresponds to about 1 km of fiber because the roundtrip propagation time (sum of propagation time of the input optical pump and propagation time of reflected SBS) is needed. In this figure, it is very clear to see the slope change due to PMD changes. After the high PMD fiber span, the slopes return to almost the same values as before the high PMD fiber span. The dip is roughly proportional to the PMD values and the location is clearly indicated.

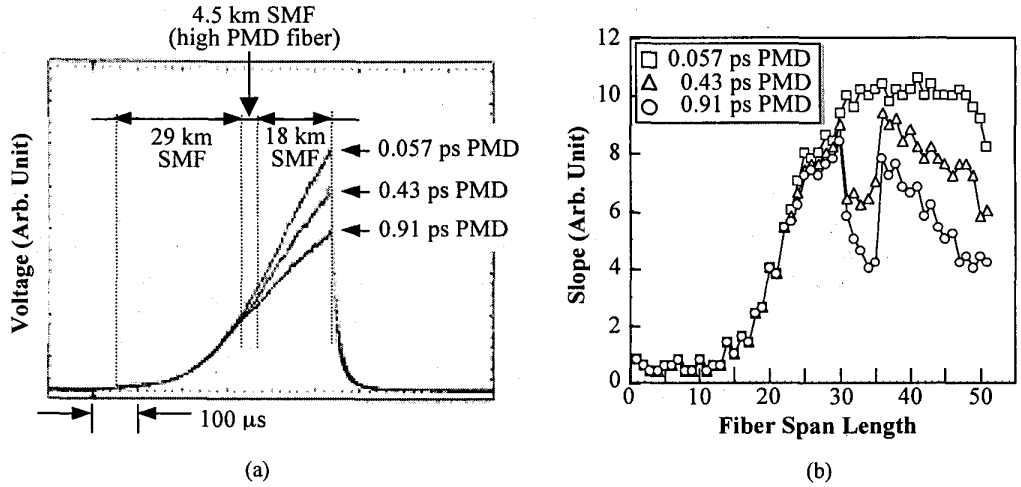

Fig. 4. (a) Oscilloscope trace of reflected SBS at input wavelength of 1549.59 nm and optical power of 7.59 dBm, and (b) Calculated slope change of reflected SBS for different PMD values in a 4.5 km SMF span.

References

1. H. Sunnerud, B.-E. Olsson, and P.A. Andrekson, *Electron. Lett.*, vol. 34, pp. 397-398, 1998.
2. T. R. Parker, M. Farhadiroushan, V. A. Handerek, and A. J. Rogers, *IEEE Photon. Technol.Lett.*, vol. 9, pp. 979-981, 1997.
3. T. Saida and K. Hotate, *IEEE Photon. Technol. Lett.*, vol.9, pp. 484-486, 1997.
4. X. P. Mao, R. W. Takach, A. R. Chraplyvy, R. M. Jopson, and R. M. Derosier, *IEEE Photon. Tech. Lett.*, vol. 4, pp. 66-69, 1992.

Appendix C

A short recirculating fiber loop testbed with accurate reproduction of Maxwellian PMD statistics

S. Lee, Q. Yu, L.-S. Yan, Y. Xie, O. H. Adamczyk, and A. E. Willner

Dept. of EE-Systems, EEB-500, University of Southern California, Los Angeles, CA 90089-2565, USA.

Tel: 213-740-1488, Fax: 213-740-8729, E-mail: sanggeon@usc.edu

Abstract: A short recirculating fiber loop (~100 km) that can emulate PMD with Maxwellian statistics is realized by loop-synchronous polarization scrambling inside the loop. The performance of our distribution-correct PMD loop is compared both experimentally and numerically to that of a distribution-incorrect PMD loop.

OCIS codes: (060.2330) Fiber optics communications; (060.2360) Fiber optics links and subsystems

1. Introduction

For the last decade, recirculating fiber loop testbeds have been powerful tools in the research and development of medium-to-long-haul optical transmission systems [1]. Under most circumstances, these fiber loops are well behaved and can accurately replicate the characteristics of a point-to-point fiber link. However, in the presence of non-negligible polarization-dependent effects, specifically polarization mode dispersion (PMD), conventional recirculating loops are inadequate. PMD is unique because it is a stochastic process, whereas a recirculating loop exhibits some measure of deterministic behavior that artificially produces an unrealistic PMD distribution that is skewed towards higher differential group delays (DGD) [2].

PMD has emerged as a critical challenge for deploying high bit-rate systems (>10 Gbit/s/channel). To first order, PMD can be represented by a DGD between the two principal states of polarization. For a fixed PMD, the DGD is a random variable that has a Maxwellian probability density function. A critical aspect of investigating PMD induced penalties is to account for the low probability but high degradation tail of this distribution. Any testbed that does not accurately reproduce the tail of the distribution will give erroneous results.

We demonstrate a recirculating fiber loop testbed that is only ~100 km long and yet accurately replicates the true Maxwellian DGD distribution caused by PMD. Our straightforward method uses a single section of polarization-maintaining (PM) fiber and a lithium-niobate ($LiNbO_3$) polarization controller that is synchronized to the electronic loop controller circuitry. The tail of the power penalty distribution after 650 km transmission with an average PMD of ~22 ps is close to that expected from a Maxwellian distribution of DGD. Therefore, our modified loop testbed provides an efficient tool for investigating the combined effects of fiber dispersion, nonlinearities, and PMD.

2. Experimental Setup

Fig. 1 shows the experimental setup of a recirculating fiber loop that emulates PMD for long distance data transmission. An external-cavity laser at 1556.7 nm is externally NRZ-modulated with an electro-optic (EO) modulator at 10 Gbit/s. Our dispersion-managed recirculating fiber loop consists of three in-line EDFAs, 84 km of single-mode fiber (SMF), and dispersion-compensating fiber (DCF) with dispersion of -1348 ps/nm. The input powers to the SMF and DCF are adjusted to 2.0 dBm and -1.0 dBm. The PMD of the loop is emulated by a single section, PM fiber (DGD ~8.3 ps) and a loop-synchronous $LiNbO_3$ polarization controller. The polarization transfer matrix of the scrambler is controlled by six input voltages and set to a random state during each loop period. These decorrelated polarization states are repeated after a certain number of loops as determined by the loop control signal. This provides a virtual increment of the length of the fiber loop in terms of the polarization state evolution along the transmission fiber. At the output of the loop, we use an EDFA pre-amplifier followed by a 1 nm bandwidth optical filter, for burst-mode bit-error-rate (BER) measurements.

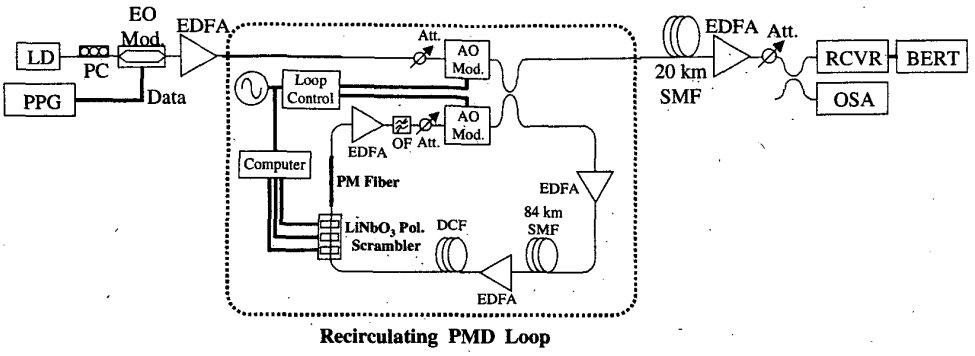

Fig. 1. Experimental setup of recirculating PMD loop

3. Experimental Results

Fig. 2 shows measured optical power distributions at 10^{-9} BER using our recirculating PMD loop, both with and without inter-loop polarization decorrelation. Fig. 2(a) shows the optical power distribution using 500 independent polarization samples taken by randomly changing the polarization states for 8-loop transmission. An alternative configuration for the PMD loop is also investigated. In this case, the PMD loop is replaced by a 15-section PMD emulator (average DGD ~8.9 ps) with three polarization controllers and the results are shown in Fig. 2(b). The optical power distribution is taken by randomly changing the polarization coupling between 15-section PMD emulator inside of the loop after 6-loop transmission. Since the average DGD of the emulator (~8.9 ps) is slightly larger than the average DGD of the a single section PM fiber, the expected average DGD value after 6-loop transmission in this case matches the expected DGD value after 8-loop transmission for the one-section PM fiber loop. Fig. 2(c) shows the optical power distribution after 8-loop transmission for 1000 independent polarization samples. In this case, in addition to randomly changing the polarization states for each sample, the state-of-polarization is decorrelated after each loop circulation. It is clear that the power distributions without inter-loop polarization decorrelation have much longer tails than the distribution with inter-loop polarization decorrelation, even if a multi-section PMD emulator is used inside of the loop. To quantify the performance shown in Fig. 2, we measured the case of the loop without PMD, followed by a lumped 44 ps average DGD. The worst case power penalties for 6-and 8-loop transmission are about 4.5 dB and 4.7 dB. Based on these results, the probability of a power penalty >4.5 dB (i.e., DGD >44 ps) is about 32% for the case shown in Fig. 2(b), and the probabilities of a power penalty >4.7 dB (i.e., DGD >44 ps) are 31% and 0.5% for the cases shown in Figs. 2(a) and (c).

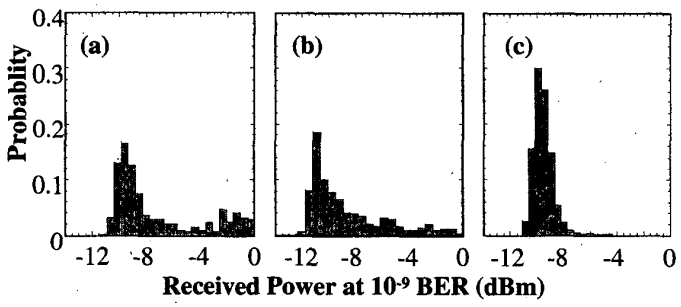

Fig. 2. Received optical power distributions at 10^{-9} BER using our loop. (a) 500 independent samples using one-section PM fiber without inter-loop polarization decorrelation. (b) 500 independent samples using a 15-section PMD emulator without inter-loop polarization decorrelation. (c) 1000 independent samples using one-section PM fiber with inter-loop polarization decorrelation.

4. Numerical Simulations and Discussion

Fig. 3(a) shows the simulated increase in average DGD with the number of loops. When there is no inter-loop decorrelation of polarization states, average DGD grows almost linearly (solid circles) because of a strong polarization correlation between loops. When inter-loop decorrelation of polarization is introduced by the loop-synchronous polarization controller, average DGD grows as the square root of the number of loops (open circles).

The solid line shows the analytically expected growth of average DGD [3] as the number of loops increases. Fig. 3 (b) shows the deviation of the DGD distribution from an ideal Maxwellian DGD distribution as the number of loops increases. The normalized deviation (Δ) from a Maxwellian is calculated as the integrated absolute difference between the simulated DGD probability density function (pdf) and a Maxwellian pdf for each loop number. For a PMD loop without inter-loop polarization decorrelation, the DGD distribution diverges significantly from a Maxwellian as the number of loops increases. However, for a PMD loop with inter-loop polarization decorrelation, the DGD distribution converges to a Maxwellian as the number of loops increases. This is because each loop can be considered as a single section PMD emulator with random polarization coupling, and the DGD distribution will closely approximate a Maxwellian distribution as the number of sections in the PMD emulator is increased [4], or equivalently in our case, as the number of loops increases. Fig. 3(c), (d), and (e) show numerical results for DGD distributions with the recirculating fiber loop configurations of Fig. 2(a), (b), and (c). As shown in Fig. 3(c) and (d), the distributions of DGD after loop transmission without inter-loop polarization decorrelation deviate significantly from a Maxwellian DGD distribution and have much longer tails, as was previously explained. In Fig. 3(e), the DGD distribution with inter-loop polarization decorrelation closely approximates a Maxwellian DGD distribution. We also numerically calculate the power penalty distributions for the cases in Fig. 2, taking into consideration the random distribution of the DGD and the power ratio between the two principal states of polarization. Our simulation predicts that the probability for the power penalty to be greater than 4.5 dB for the case of Fig. 2(b), and greater than 4.7 dB for the cases of Fig. 2(a) and (c), are 20%, 21%, and 0.4%. These values agree reasonably well with our experimental results.

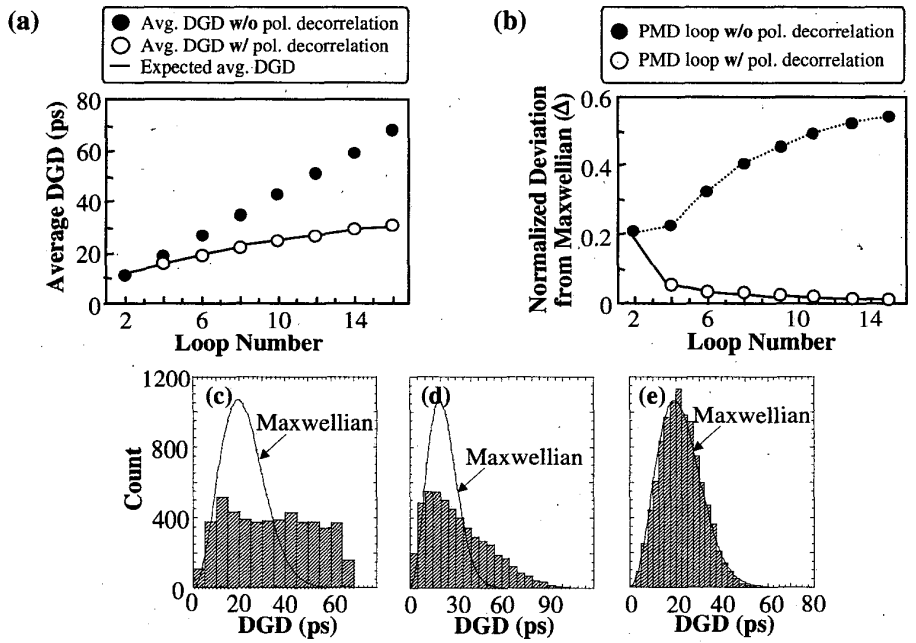

Fig. 3. (a) The increase in average DGD with the number of loops, and (b) the normalized deviation from a Maxwellian DGD distribution as the number of loops increases (solid line shows expected average DGD), (c) Simulated DGD distribution of PMD loop without inter-loop polarization decorrelation (one-section PM fiber with pol. controller, 5000 independent pol. samples, 8 loop). (d) Simulated DGD distribution of PMD loop without inter-loop polarization decorrelation (15-section PMD emulator with three PCs, 5000 independent polarization samples, 6 loop) (e) Simulated DGD distribution of PMD loop with inter-loop polarization decorrelation (one-section PM fiber with pol. controller, 10000 independent pol. samples, 8 loop).

5. References

[1] N. S. Bergano, and C. R. Davidson, "Circulating loop transmission experiments for the study of long-haul transmission systems using erbium-doped fiber amplifiers," IEEE J. of Light. Tech., vol. 13, pp. 879-888, (1995).

[2] Workshops on Conference on Optical Fiber Communications OFC 2000, W207, (2000).

[3] C. D. Poole, and D. L. Favin, "Polarization-mode dispersion measurement based on transmission spectra through a polarizer," IEEE J. of Light. Tech., vol. 12, pp. 917-929, (1994).

[4] I. Lima, R. Khosravani, P. Ebrahimi, E. Ibragimov, A. E. Willner, and C. R. Menyuk, "Polarization mode dispersion emulator," Conference on Optical Fiber Communications OFC 2000, paper ThB4, (2000).

Chirp-Free Tunable PMD Compensation using Hi-Bi Nonlinearly-Chirped FBGs in a Dual-Pass Configuration

Z. Pan, Y. Xie, S. Lee, and A.E. Willner
Dept. of Electrical Engineering-Systems
University of Southern California, Los Angeles, California, 90089-2565
Tel: (213)740-1488, Fax: (213)740-8729, Email: zpan@usc.edu
V. Grubsky*+, D.S.Starodubov+, and J.Feinberg*+
**Dept. of Physics*
University of Southern California
Los Angeles, CA 90089
+ D-STAR technologies, Inc.
Manhatten Beach, CA 90226
web site: www.d-startech.com

1. Introduction

Polarization-mode-dispersion (PMD) is considered a key limitation in ≥10-Gbit/s/channel transmission systems due to the high PMD fiber (1-100 ps/km$^{0.5}$) that had been deployed throughout the 1980's and early 1990's. In general, PMD is caused by the different speeds of the two states-of-polarization (SOPs) as they propagate along a fiber having a slow and fast axis. Since the state-of-polarization of a signal changes randomly along a fiber link, PMD is a random quantity. To the first order, PMD can be compensated by delaying one state-of-polarization with respect to the other; this is more accurately known as differential group delay although we will refer to it as PMD for this paper. Because PMD can change for both dynamically reconfigurable networks in which the paths change and also for a point-to-point link in which the polarization states vary due to temperature fluctuations, it would be quite beneficial to have an adjustable PMD compensator.

All-optical PMD compensation techniques that allow for periodic in-line use of PMD compensation in a long distance link include: (a) splitting the signal into two orthogonal polarization directions and delaying one of the polarization components relative to the other using free-space optics[1], a technique that may be cumbersome, and (b) temperature tuning short lengths of highly-birefringent polarization maintaining (PM) fiber [2], a method that may have limitations in speed, tunability and flexibility. Previously, we reported using a tunable nonlinearly-chirped fiber Bragg grating (FBG) [3] written into a high-birefringence fiber to compensate for varying amounts of PMD [4, 5]. The high-birefringence fiber provides a different time delay for different states-of-polarization, and the nonlinear chirp of the grating provides the selectability of varying amounts of differential polarization time delay when the FBG is stretched. This all-fiber method showed good performance for a 10 Gb/s signal with 175 ps of adjustability. Unfortunately, the nonlinearly-chirped FBG, by its very nature, induces a chirp into the PMD-compensated signal. This chirp may limit the distance of transmission after the compensator due to the fiber chromatic dispersion.

We demonstrate **chirp-free tunable PMD compensation** for a 10-Gbit/s signal by using an adjustable high-birefringence nonlinearly-chirped (HN) FBG in a novel **dual-pass configuration** that significantly reduces the induced chirp of the FBG. In order to eliminate the chirp of the FBG, the signal passes through the high-reflectivity grating from one direction and then passes again through the same grating from the opposite direction, with the second pass negating the induced chirp of the first pass. We show PMD compensation with tunability from 250-600 ps in which the power penalty due to fiber dispersion in a 45-km link interacting with the FBG induced chirp is reduced from 4.0 to 0.5dB. Additionally, this configuration provides twice amount of the PMD compensation and the tunability because the signal passes twice through the same high-reflectivity grating.

2. Dual-Pass Configuration

As described in [3], when the input optical signal is reflected by an HN-FBG, this grating can give a time delay $\Delta t = 2n\Delta L_{eff}/c$ between the two polarization directions. However, this method also induces some chromatic dispersion because of the chirp of the HN-FBG. Figure 1(a) shows the arrangement of our

dispersionless PMD compensator. By using a symmetric structure, the incoming signal is reflected twice by the same HN-FBG. Figure 1(b) shows the operational principle. After the first reflection from the HN-FBG, the optical signal passes through a polarization rotator, which is used to rotate the polarization state by $\pi/2$ and then switch the propagation axis of the second reflection in the FBG. The fast axis polarization state has smaller time delay than the slow axis polarization state when the signal enters the FBG from the long-λ port, but the slow axis polarization state will have smaller time delay when the signal enters from the short-λ port. Consequently, by properly controlling the polarization states, the dual-pass scheme can double the time delay between the two polarization states. This time delay can be used to realize the PMD compensation. Moreover, due to the fact that the chromatic dispersion depends upon the incident port of the FBG, when the optical signal enters into long-λ port (or short-λ), and then is reflected, the dispersion is negative (or positive), so any chirp that the signal acquires due to the first reflection off the grating is canceled by the second reflection off the grating(see Fig.1 (b)). As a result, the undesired chromatic dispersion induced by the chirped grating is significantly reduced.

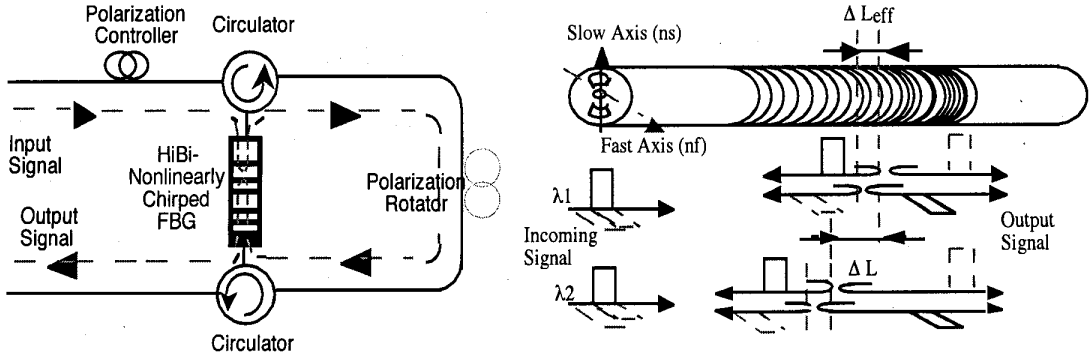

Fig. 1. Diagram of chirp-free tunable PMD compensator

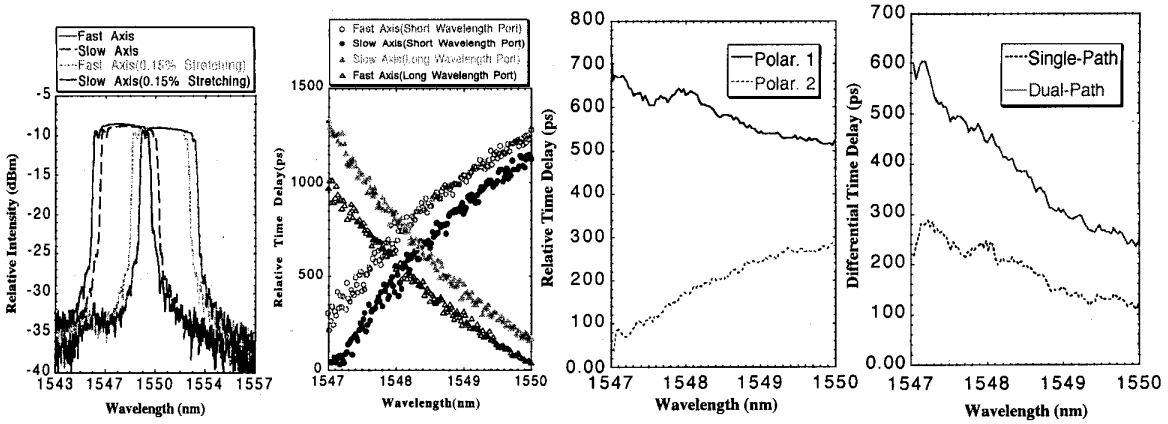

Fig. 2. (a) Reflection spectrum of two polarization states. (b) Reflected time delay of two polarization states for single path (enter into different ports of FBG). (c) The time delay for dual-path setup. (d) DGD of single and dual path.

We write the HN-FBG through a nonlinearly chirped phase mask. The bandwidth of this grating is 1547-1550nm. Figure 2(a) is the reflection spectrum. Figure 2 (b) shows the time delay of fast and slow axis after only one reflection (single path), (c) is the time delay curve of dual path, and (d) is the measured DGD curve of single and dual paths. These figures indicate that the time delay between the two

polarization states ranges from 120ps to 300ps for single-path, but for the dual-path scheme the time delay (also the tuning range) is from 250ps to 600ps (see Fig.2 (d)). Meanwhile, the dual-path method also has much lower chromatic dispersion (< 100ps/nm) (see Fig. 2 (c)), while the single-path method gives larger dispersion (600ps/nm)(see Fig. 2(b)). From these results, it was verified that the dual-path setup provides both much lower chromatic dispersion and larger PMD compensation ability.

3. Results and Discussion

We have completed an experiment to assess the compensation effects of the dual-path method. The experimental setup is shown in Figure 3. A tunable laser was externally modulated with a 10 Gbit/s PRBS in a Mach-Zehnder modulator. A free-space variable time delay device, which can provide 250-500 ps DGD, was used as the PMD source. After PMD compensation, the signal was launched into 45km of SMF. We have compared the performance of single and dual-path compensation methods before and after 45km of SMF transmission. Figure 4 shows the BER measurement results and received eye diagram. For the dual-path case, because the optical signal passed through the grating twice, the reflectivity of the grating should be very high in order to minimize the interferometrical effect between two arms. Otherwise, coherent noise will limit the compensation performance. Since the transmitted power is just 23-25dB lower than the reflected power of the grating, the dual-path method has more power penalty than the single-path technique right after PMD compensation. But after transmission, compared to the 4dB power penalty of the single-path method, the dual-path compensation method has just 0.5dB power penalty and the eye diagram shows that the signal is not degraded. With a better quality FBG, the dual-path method should have even better performance.

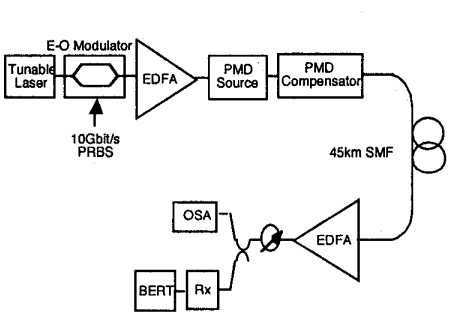

Fig. 3. Experimental configuration of dispersionless PMD compensation by an HN-FBG

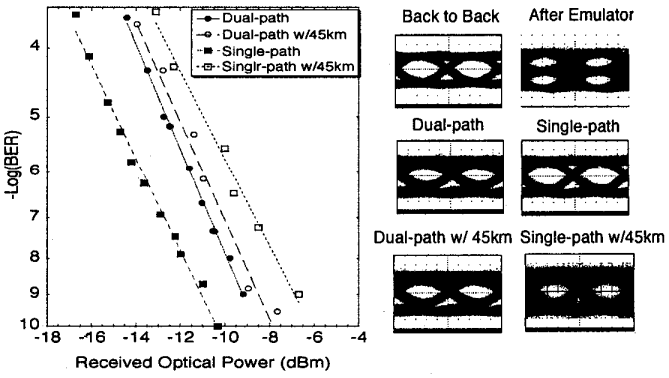

Fig. 4. BER measurement results and eye diagrams

In conclusion, a new PMD compensation method using an HN-FBG was proposed and demonstrated. This method provides a large amount of PMD compensation ability (250-600ps). Furthermore, the induced chirp of the HN-FBG is significantly reduced. As a consequence, the 45km SMF transmission power penalty for the single and dual path method is improved from 4dB to 0.5dB. So the dual-path method is a promising in-line PMD compensation technique which also has the advantage of being widely tunable, fiber compatible and compact.

4. References

[1] H.Bülow, "Limitation of Optical First-Order PMD Compensation", WE1, OFC, San Diego, 1999.

[2] Takeshi Ozeki, Masato Yoshimura, Teruhiko Kudo, Hiroshi Ibe, "Polarization-mode-dispersion equalization experiment using a variable equalizing optical circuit controlled by a pulse-waveform-comparison algorithm," Conference on Optical Fiber Communication, 1994, Technical Digest Series, Paper TuN4 (Optical Society of America, Washington, D.C., 1994).

[3] S.Lee, R.Khosravani, J.Peng, A.E.Willner, V.Grubsky, D.S.Starodubov, J.Feinberg, " High-birefringence nonlinearly-chirped fiber Bragg grating for tunable compensation of polarization mode dispersion ", TuS3, OFC, San Diego, 1999.

[4] Bahsoun. S, J. Nagel, C. Poole, "Measurement of temporal variations in fiber transfer characteristics to 20GHz due to polarization-mode dispersion", ECOC'90, Amsterdam,1003. Postdeadline paper.

[5] C. Poole, J.H.Winters, J.A.Nagel, " Dynamic equation for polarization dispersion", Optics Letters 16: 372-374,1991.

taneous and independent PMD monitoring, we consider the simple case of a 2-channel system. Fig. 3(c) shows the subcarrier tone power on channel #2 as a function of the subcarrier tone power on channel #1 (500 independent measurements). It is clearly seen that the subcarrier tone powers are independent, as expected. Fig. 3(d) shows the eye diagrams and the corresponding subcarrier tone powers and BERs (bit-error-rate) for typical cases for each channel and qualitatively represents the independence of the performance degradation between WDM channels.

In summary, we demonstrated a simple technique for simultaneous and independent PMD monitoring by adding subcarrier tones at slightly different frequencies to the different WDM channels. Our statistical investigation shows a close correlation between the measured power penalty and the subcarrier power fading of each channel. This technique could be very useful for in-line monitoring of several optical channels without the need for optical demultiplexing and multiple detectors.

References

1. H. Sunnerud, J. Hansryd, P.A. Andrekson and M. Karlsson, "Impact of PMD on FWM Crosstalk in WDM Systems", Tech. Dig. OFC'00, ThB1, (2000).
2. F. Heismann, D.A. Fishman, D.L. Wilson, "Automatic compensation of first order polarization mode dispersion in a 10 Gbit/s transmission system", 24th European Conference on Optical Communication ECOC'98, vol. 1, pp 529–530, (1998).
3. H. Bülow et al., "Adaptive PMD mitigation at 10 Gbit/s using an electronic SiGe equaliser IC", proc. ECOC'99, We C3.4, (1999).
4. M.W. Chbat, J.P. Soigne, T. Fuerst, J.T. Anthony, S. Lanne, H. Fevrier, B.M. Desthieux, A.H. Bush, and D. Penninckx, "Long Term Field Demonstration of Optical PMD Compensation on an Installed OC-192 Link", post deadline paper, OFC/IOOC'99, PD12, (1999).
5. M. Karlsson and J. Brentel, "Autocorrelation function of the polarization-mode dispersion vector," Opt. Lett., vol. 24, pp. 939–941, (1999).
6. H. Schmuck, "Effect of polarization-mode-dispersion in fiber-optic millimeter-wave systems," Electron. Lett. 30, pp. 1503–1504, (1994).
7. I.T. Lima, R. Khosravani, P. Ebrahimi, E. Ibragimov, A.E. Willner, and C.R. Menyuk, "Polarization Mode Dispersion Emulator", Techn. Dig. OFC'00, ThB4, (2000).

CFE2 **10:30 am**

Clock Regenerating Effect for NRZ Data due to Higher-Order Polarization Mode Dispersion

Z. Pan, Q. Yu, Y. Xie, Y.W. Song, A.E. Willner, *Department of Electrical Engineering-Systems, University of Southern California, Los Angeles, California, 90089-2565; Email: zpan@usc.edu*

1. Introduction

Polarization mode dispersion (PMD) is considered to be the next critical hurdle in ≥ 10-Gbit/s/channel transmission systems. Since PMD is a stochastic, dynamically varying process, compensation of the channel degradation induced by PMD is extremely challenging. Several automatic PMD compensation technologies have been reported.[1-3] Most of these methods use one section of differential group delay (DGD) as the main first-order compensator element. Consequently, the system performance is limited by higher-order PMD and achieved PMD tolerance is around 30 ps for 10-Gbit/s systems.[4]

In order to enhance the higher-order PMD compensation and hence increase the PMD tolerance, a compensator with multiple DGD sections has been proposed.[5,6] Since multi-section compensators have more degrees of freedom, the feedback control is an open problem. Previous work on one-section PMD compensators uses one feedback signal, such as the degree of polarization, the signal's spectral component, and the eye opening parameter. However, multi-section compensators may require other feedback signals that can distinguish higher-order PMD from first-order PMD.

We have demonstrated that the clock component corresponding to the data rate can be used for chromatic dispersion monitoring.[7] Because higher-order PMD can induce polarization-dependent chromatic dispersion, the data clock is also expected to be an indicator of higher-order PMD. In this paper, we verify that the extracted clock power from the received non-return-to-zero (NRZ) data is correlated with higher-order PMD. After first-order compensation, higher clock power corresponds to a higher power penalty. Therefore, the clock power may be used for multi-section PMD compensator as an auxiliary feedback signal. It is important to note that, when considering only first-order PMD, the clock component would not be extracted at the receiver. In contrast, the clock can be used as first-order PMD monitor for return-to-zero (RZ) data.[8]

2. Clock regenerating effect for NRZ data due to PMD

We simulated the 10 Gbit/s NRZ transmission system with first and higher-order PMD, neglecting chromatic dispersion and fiber nonlinearities. The clock power was measured after a PMD emulator, which consists of one-section DGD or two-section DGD. Fig. 1 (a) shows the RF spectra and eye diagrams for 50 ps of DGD. Fig. 1 (b) shows the clock power versus mean value of DGD. It is interesting that there is no clock signal

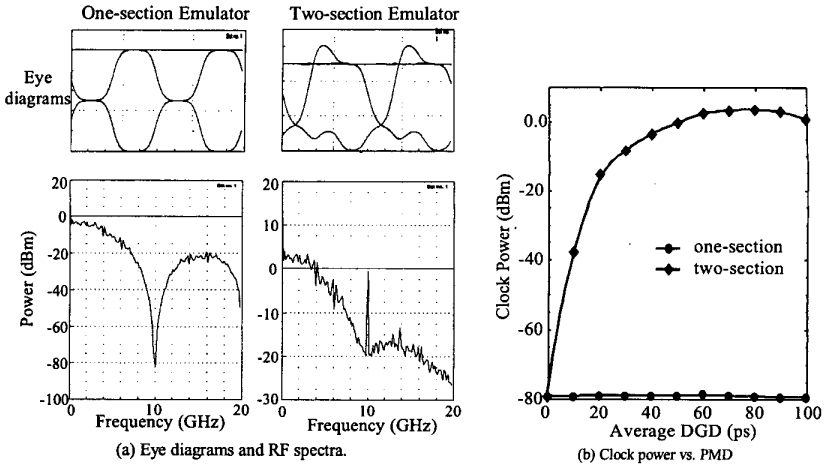

(a) Eye diagrams and RF spectra. (b) Clock power vs. PMD

CFE2 Fig. 1. Clock signal of 10 Gbit/s due to one-section, two-section PMD emulators.

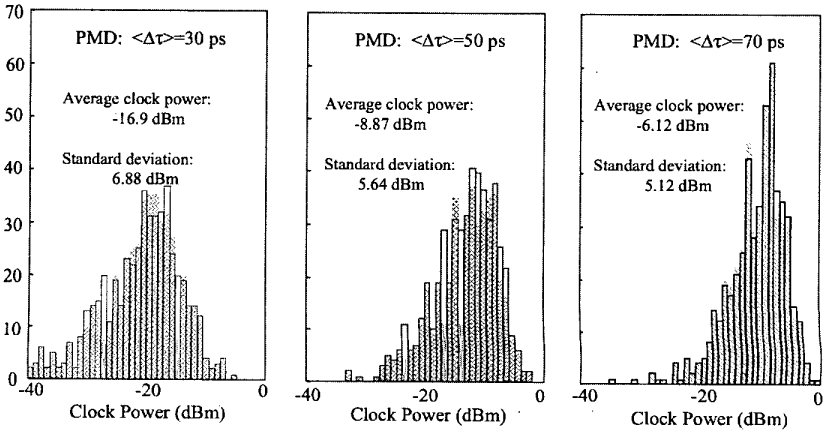

CFE2 Fig. 2. 10 GHz clock power distribution at different average PMD values.

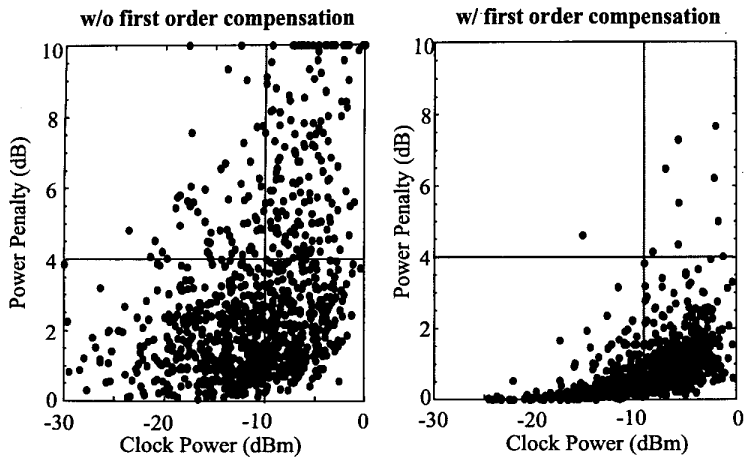

CFE2 **Fig. 3.** System power penalty vs. clock power without and with first order PMD compensation. Before first-order compensation, there is still significant possibility of higher penalty (>4dB) with lower clock power (<–10 dB). But after first-order compensation, almost all higher penalty points (>4dB) occurred in the higher clock power region (>–10 dB).

being regenerated for a one-section emulator, i.e., only the DGD, or first-order PMD, does not affect the clock power. However, when the PMD emulator has more than one section, the clock power will vary significantly due to the fact that any emulators with more than one section have higher-order PMD in addition to DGD. First-order PMD is a linear transform of the optical power. Therefore, the received optical pulse is the superposition of two undistorted polarization states. But higher-order PMD is a function of optical frequency, and is nonlinear with optical power, so the pulse shape of each polarization state is also distorted. Consequently, once there is higher-order PMD, the distortion of the optical pulses will generate the clock signal.

3. Results and discussion

For real fiber, the pulse broadening induced by PMD is not deterministic and is unstable in time. Therefore the regenerated clock power is also a random variable. Fig. 2 shows the calculated clock power in a fiber with 30 ps, 50 ps, and 70 ps of average DGD. In each case we collected 500 samples. The average clock power and the standard deviation are –16.92, –8.867, –6.12 dBm and 6.88, 5.64, 5.12 dBm respectively. Higher PMD has a higher average clock power and a narrower distribution, i.e., there is more probability to have a higher clock power in high PMD systems. This result verifies that when the average DGD is higher, higher-order PMD become more important.

We compared the system penalty versus clock power with and without first-order PMD compensation to examine the correlation between higher-order PMD and clock power. Fig. 3 shows the simulation results for a 50 ps PMD system. Without the compensation, we find that even when the clock power is very low, the system still has a high outage probability. The system power penalty and clock power are uncorrelated. However, after first-order compensation, we find that the lower clock power corresponds to a lower power penalty and higher clock power corresponds to a higher power penalty.

4. References

1. T. Takahashi, T. Imai, and M. Aiki, "Automatic compensation technique for timewise fluctuating polarization mode dispersion in in-line amplifier systems," *Electron. Lett.* vol. 30, pp. 348–349 (1994).
2. F. Heismann, D.A. Fishman, and D.L. Wilson, "Automatic compensation of first-order polarization mode dispersion in a 10-Gb/s transmission system," in *Proc. ECOC'98*, vol. I, Madrid, Spain, pp. 529–530 (1998).
3. Z. Haas, C.D. Poole, M.A. Santoro, and J.H. Winters, "Fiber-optic transmission polarization-dependent distortion compensation," U.S. Patent 5 311346, (1994).
4. H. Bülow, "Limitation of Optical First-Order PMD Compensation," WE1, OFC'99, San Diego, (1999).
5. R. Noé, D. Sandel, M. Yoshida-Dierolf, S. Hinz, V. Mirvoda, A. Schöp in, C. Glingener, E. Gottwald, C. Scheerer, G. Fischer, T. Weyrauch, and W. Haase, "Polarization Mode Dispersion Compensation at 10, 20, and 40 Gb/s with Various Optical Equalizers," JLT, Vol. 17, No. 9, pp. 1602–1616, (1999).
6. Q. Yu, L. Yan, S. Lee, Y. Xie, M. Hauer, Z. Pan and A. E. Willner, "Enhanced Higher-Order PMD Compensation using a Variable time delay between Polarizations," ECOC'2000, pp47–pp48, Munich, Germany, (2000).
7. Z. Pan, Q. Yu, Y. Xie, S. A. Havstad, A. E. Willner, D. S. Starodubov, and J. Feinberg, "Chromatic dispersion monitoring and automated compensation for NRZ and RZ data using clock regeneration and fading without adding signaling," Submitted to OFC'2001.
8. G. Ishikawa, H. Ooi, "Polarization-mode dispersion sensitivity and monitoring in 40-Gbit/s OTDM and 10-Gbit/s NRZ transmission experiments," WC5, OFC'98, San Jose (1998).

CFE3 **(Invited)** **10:45 am**

Optimization of a PMD compensator with constant differential group delay using importance sampling

I.T. Lima, Jr.,[1] G. Biondini,[2] B. Marks,[1,2] W.L. Kath,[2] and C.R. Menyuk,[1,3] *1) Department of Computer Sciences and Electrical Engineering, University of Maryland Baltimore County, Baltimore, MD, 21250; Email: lima@engr.umbc.edu; 2) Engineering Sciences and Applied Mathematics, McCormick School of Engineering and Applied Sciences, Northwestern University, 2145 Sheridan Rd., Evanston, IL, 60208-3125; 3) Laboratory for Telecommunication Sciences, c/o USARL, Bldg. 601, Rm. 131, 2800 Powder Mill Road, Adelphi, MD 20783-1197*

Polarization-mode dispersion (PMD) is a significant barrier to achieving single-channel data rates at 10 Gbit/s and beyond in optical communication systems. There have been numerous proposals to use optical PMD compensators to mitigate this problem,[1–7] and much of this work has focused on first-order compensators because they are the simplest to build, to control, and to analyze. Theoretical[1–3] and experimental[4–7] work has shown that first-order PMD compensators can significantly reduce the average pulse spreading and hence the average power penalty due to PMD. However, this average reduction does not address the issue of greatest practical importance. Designers specify a power margin for PMD, and they want to ensure that the probability that the power penalty due to PMD exceeds this margin, the outage probability, is very low. Typical parameters are a power penalty of 2 dB with an outage probability of 10^{-6}.[2]

Work to date on first-order PMD compensators has focused on two types. The first type cancels out the differential group delay (DGD) at the central frequency of the channel and requires a variable DGD element as well as a polarization controller.[1] The second type attempts to eliminate the component of the principal state that is orthogonal to the output polarization state and only requires an element with fixed DGD as well as a polarization controller.[3] Here we focus on the second type.

It is not practical to calculate outage probabilities on the order of 10^{-6} using standard Monte Carlo simulations. To do so would require on the order of 10^{10} realizations. For this reason, we use importance sampling to calculate the outage probabilities.[8] The optimum DGD for minimizing the average PMD penalty approximately equals $\langle\Delta\tau\rangle$, the expected DGD. By contrast, we find that the optimal DGD for minimizing the outage probability is a factor of 2–3 higher for a 10 Gbit/s channel with $\langle\Delta\tau\rangle$ = 25 ps or 35 ps.

To apply the importance sampling technique, we first recall that P_I the probability of an event defined by the indicator function $I(\mathrm{x})$, can be written as,[8]

$$P_I = \frac{1}{N}\sum_{i=1}^{N} I(\mathrm{x}_i)\left[\frac{p(\mathrm{x}_i)}{p^*(\mathrm{x}_i)}\right], \qquad (1)$$

where $p(\mathrm{x})$ and $p^*(\mathrm{x})$ are the unbiased and biased distribution functions of the random vector x so that $p(\mathrm{x})/p^*(\mathrm{x})$ is the importance weight. The key difficulty in applying importance sampling is to properly choose $p^*(\mathrm{x})$. We have found that the appropriate parameters to control are the angles

Comparison of different modulation formats in terrestrial systems with high polarization mode dispersion

R. Khosravani and A. E. Willner
Dept. of Electrical Engineering- Systems
University of Southern California
Los Angeles, CA 90089-2565
(213) 740-1488, fax: (213) 740-8729, khosrava@usc.edu

1. Introduction

Polarization mode dispersion has emerged as one of the next critical hurdles for next-generation high bit rate transmission systems. PMD is caused by different transmission speeds along the two principal states of polarization in a fiber with random birefringence. Since the birefringence of a fiber changes randomly along a fiber link, PMD's effects are stochastically random and time varying [1]. Specifically, the cases of high PMD values are of intense interest since a fair amount of the fiber installed throughout the 1980's had PMD values that were 10-100 times that of the current state-of-the-art.

Systems designers have typically struggled to determine the relative merits of the several possible data formats for future deployed systems using the embedded fiber base. The formats considered are non-return-to-zero (NRZ), return-to-zero (RZ), solitons (and specifically dispersion-managed solitons (DMS)), and pre-chirped RZ (CRZ). Many signal degrading effects evolve quite differently in the regime of high accumulated PMD (>20 ps) as compared to the regime of low accumulated PMD (<10 ps) at 10 Gb/s. In particular, although solitons are not affected much at low PMD due to the pulse stability and trapping in one state-of-polarization [2], they tend to become unstable under high PMD conditions. Previously published analyses of different modulation formats have generally been limited to the statistical average time evolution of optical pulses as they propagate along a fiber link. However, there has been very little systems study of the relative limitations placed on terrestrial systems by high PMD fiber.

We compare the performance of NRZ, RZ, DMS, and CRZ formats in the presence of high PMD for 10-Gbit/s terrestrial systems through numerical simulations. We consider system Q-factors and power penalties for the case of an integrate-and-dump receiver. Fiber nonlinearities and signal chirp interact with PMD-induced pulse distortion to generate clear trends in system power penalties. We show that CRZ pulses are even more tolerant to high PMD values than dispersion-managed solitons because of pulse compression, and NRZ exhibits the worst performance. The electrical eye diagrams demonstrate that: (a) the "0" level of NRZ is raised due to intersymbol interference, (b) RZ pulses tend to split apart, (c) dispersion-managed solitons lose the integrity of their shape, and (d) chirped-RZ pulses are relatively unaffected.

2. System Model

We have concentrated on terrestrial systems operating at 10 Gbit/s. Fig. 1 shows the setup of our model. 80 km of single-mode fiber (SMF) along with 15 km of dispersion compensation fiber (DCF) and 2 gain stages are considered for each dispersion map. This is a commonly used map for terrestrial systems. The average input power is set to 5 dBm and −1 dBm for SMF and DCF fibers respectively. Six stages of dispersion map (totaling 570 km) transmission are considered. We assume zero average dispersion for NRZ and RZ pulses, and approximately 0.4 ps/nm/km DMS pulses. For each PMD value, 10,000 ensembles of fibers have been evaluated using the coarse step method [3]. An ideal integrate-and-dump receiver with optimized sampling time and decision threshold is considered to make a fair

comparison for all formats. Amplified spontaneous emission noise is assumed as the dominant noise source.

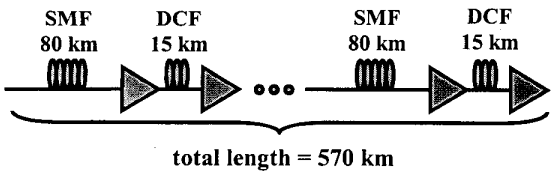

Fig. 1. Model used for terrestrial system.

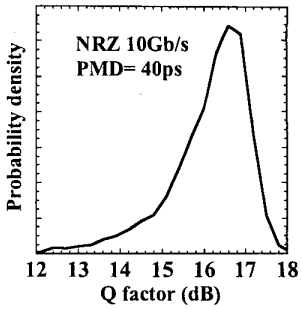

Fig. 2. Q factor distribution for 10,000 ensembles of fibers. PMD value is 40 ps.

3. Results

Fig. 2 shows the Q-factor probability distribution function for a 10 Gb/s NRZ system with 40 ps of total accumulating PMD. As is apparent from the figure, the Q-factor can vary over a wide range depending on the birefringence of different segments of transmission fiber. To avoid fading [4], systems need to take into account the worst case Q-factor which appears in the tail of the distribution. We have considered the tails with probability of 0.001 to represent the worst case Q-factor, though even more stringent criteria may be needed to further limit fading.

Figs. 3(a) and (b) show average and the worst case (with probability 0.001) power penalties at BER=10^{-9} for different total accumulated PMD values and different modulation formats at 10Gb/s,. It is clear that worst case scenarios can cause more severe power penalties. In general, pulses with shorter duty cycles (including RZ, DMS and CRZ) perform better because they have a wider margin which allows them to retain their pulse power during a bit time, especially for small PMD values. Another reason for the fast growing power penalty in the NRZ case is the increased zero level caused by PMD pulse broadening and intersymbol interference. Higher zero levels generate higher noise on zeros and increase the power penalty. DMS performs slightly better than RZ because of narrower pulse widths. However soliton trapping can not prevent PMD-induced distortion as PMD values considered here are much higher than trapping limit. For CRZ pulses that undergo an initial compression in the dispersive fiber [5], the average dispersion is adjusted to give the maximum compression at the end of the transmission. This leads to a better performance for CRZ pulses, especially at higher PMD values. Fig. 4 shows an example of the worst case (with probability 0.001) bit pattern and eye diagram for different modulation formats at 0 and 40 ps total accumulated PMD. NRZ pulses are severely distorted and the eye is completely closed. For RZ pulses, pulses split and the eye is distorted, but it is open wider than in the NRZ case. Dispersion-managed solitons are completely distorted and adjacent pulses merge together. However the eye is still open, since pulse energy is mainly maintained during a bit time. For the CRZ format, compression helps the pulses cancel out part of the broadening caused by PMD. Therefore a wide-open eye is observed.

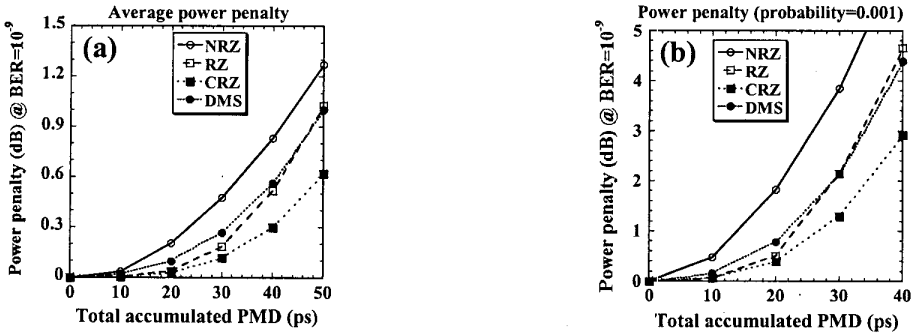

Fig. 3. Power penalty (@ BER 10^{-9}) for different PMD values in 10,000 ensembles of fiber after 580km transmission. a) average power penalty, b) worst case power penalty (probability 0.001).

Fig. 5 shows the influence of chirp on power penalty for RZ pulses at 40 ps total accumulated PMD. Again, the average dispersion is adjusted to give maximum compression at the end of the transmission. It is shown that pre-chirping can reduce the power penalty caused by PMD. For chirp=1, ~ 1.7dB improvement is obtained. By increasing the chirp, performance still improves more but at a slower rate.

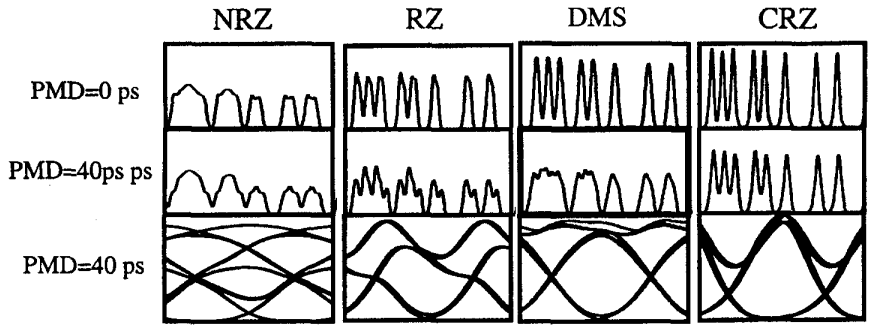

Fig. 4. Output bit pattern after 570 km transmission with no PMD (upper), with 40 ps total accumulated PMD (middle), and output eye opening with 40 ps total accumulated PMD (lower) at 10 Gb/s and worst case (probability 0.001).

Fig. 6 shows the total power penalty, caused mainly by fiber nonlinearities and PMD (PMD=1 ps/km$^{1/2}$). Since PMD accumulates along the fiber, different lengths represent different total accumulated PMD values. RZ, DMS and CRZ are more robust in short distance where the total accumulated PMD is small but degrade over longer distances. CRZ format (with chirp=1) overtakes the other formats as maximum compression occurs at the end of the transmission. It is seen that for <3 dB power penalty, CRZ format can be transmitted over more than three times the distance of NRZ format.

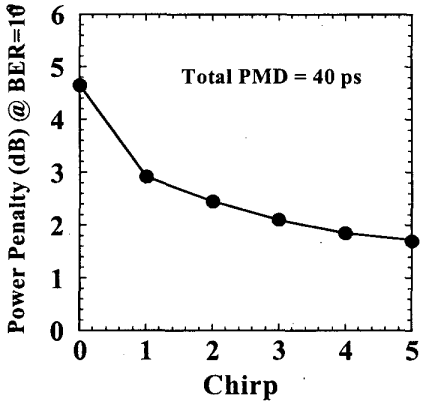

Fig. 5. Chirp effect on RZ transmission for 40 ps total accumulated PMD, 10 Gb/s, 570 km.

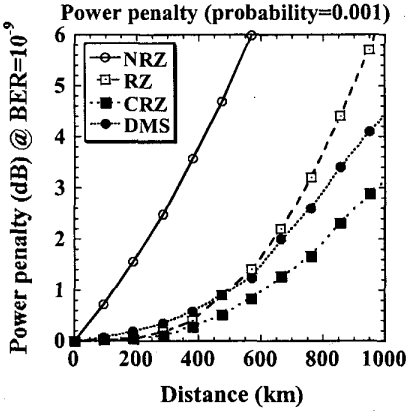

Fig. 6. Total power penalty versus transmission length, PMD=1 ps/km$^{1/2}$.

References:

[1] N. Gisin, R. Passy, J. C. Bishoff, and B. Perny, "Experimental Investigations of the Statistical Properties of Polarization Mode Dispersion in Single Mode Fibers," *IEEE Photonics Tech. Letters*, Vol. 5, No. 7, pp. 819-821, July 1993

[2] C. R. Menyuk, "Stability of solitons in birefringent optical fibers. I: Equal propagation amplitudes," *Optics Letters,* Vol. 12, No. 8, pp. 614 - 616, August 1987

[3] D. Marcuse, C.R. Menyuk, and P.K.A. Wai, "Application of the Manakov-PMD equation to studies of signal propagation in optical fibers with randomly varying birefringence", *Journal of Lightwave Technology*, Vol. 15, No. 9, pp. 1735-46, Sep. 97

[4] C. D. Poole, R. W. Tkach, A. R. Chraplyvy, and D.A. Fishman, "Fading in Lightwave Systems Due to Polarization – Mode Dispersion," *IEEE Photonics Tech. Letters*, Vol. 3, No. 1, pp. 68-70, Jan. 1991

[5] G. P. Agrawal and M. J. Potasek, "Effect of frequency chirping on the performance of optical communication systems," *Optics Letters,* Vol. 11, No. 5, pp. 318 – 320, May 1986

TuB2
9:30 am – 9:45 am

Deleterious systems effects due to polarization scrambling in the presence of polarization dependent loss

L.-S. Yan, Q. Yu, T. Luo, and A.E. Willner
Department of Electrical Engineering-Systems, EEB-500, University of Southern California, Los Angeles, CA 90089
Tel: 213-740-1488, Fax: 213-740-8729, E-mail: lianshay@usc.edu

High-performance optical transmission systems may be degraded by several types of polarization-dependent effects [1], including polarization-mode-dispersion (PMD) from optical fiber and in-line components, polarization-dependent gain (PDG) in optical amplifiers, and polarization-dependent loss (PDL) from many types of in-line devices [2]. Polarization scrambling of the signal at the transmitter has been shown: (i) as a valuable facilitator for generating the monitoring feedback signal in a PMD compensator [3-5], and (ii) to significantly reduce signal fluctuations due to PDG [6-9].

In general, polarization scrambling modulates the signal's state-of-polarization (SOP) at certain frequencies. Both experimental and simulation results have shown the effectiveness of this technique for ultra-long undersea transmission systems using either low frequency (~10 kHz) or bit-synchronous polarization scrambling. It has been noted in previous publications that the PDL-induced intensity modulation caused by polarization scrambling is a potential system degrading effect [2]. However, the modeling surprisingly shows that this effect can be dramatically suppressed by PDG in ultra-long undersea transmission systems using low frequency scrambling.

Recently, polarization scrambling has become an important technique for PMD monitoring and compensation in terrestrial transmission links because it provides a means of monitoring the instantaneous differential group delay (DGD) values and thus reduces the feedback tracking complexity [3-5]. Instead of modulating the SOP along a great circle on the Poincarè sphere, polarization scrambling that moves the input SOP to many random points along the whole Poincarè sphere on millisecond time scales is desired for the purpose of PMD monitoring. In this case, the polarization scrambling frequency is defined as the SOP update frequency, typically, tens of kHz. However, no published work has appeared that describes any measurements on the impact of this kind of low-frequency polarization scrambling in terrestrial systems, where the instantaneous PDL may be high but the PDG effect is fairly small as to be considered negligible, and hence, the PDL-induced intensity modulation can be a deleterious effect.

We experimentally verify that this low-frequency polarization scrambling at the transmitter will produce significant system performance degradation for a link with non-negligible values of instantaneous PDL. We also measure the system BER fluctuation using a recirculating loop testbed that can emulate distributed PDL along an 800-km NRZ transmission link at a 10-Gb/s data rate. We emphasize that network designers might determine that polarization scrambling will be necessary for PMD monitoring, but this could require either the reduction of PDL in all in-line components or the use of a PDL compensator [10].

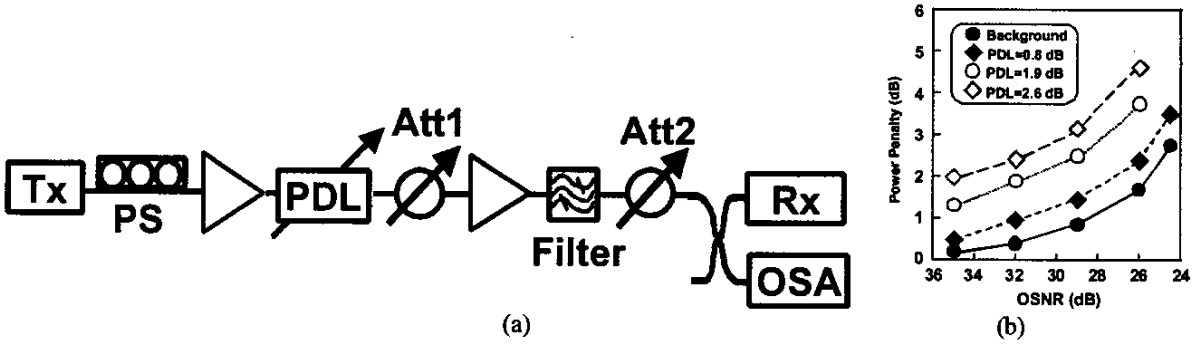

Fig.1 (a) Experimental setup for investigating the system impact of polarization scrambling in the presence of PDL. (b) Power penalty as a function of received OSNR for a group of PDL values with a scrambling frequency of 20 kHz.

First we use a variable lumped PDL element to investigate the system impact of PDL-induced intensity modulation due to polarization scrambling. The experimental setup for 10-Gb/s NRZ data (2^{23}-1 PRBS) transmission is shown in Fig.1 (a). The use of a polarization scrambler right after the transmitter can generate fast polarization scrambling over a series of uncorrelated SOPs. The first optical attenuator is used to adjust the OSNR of the received signal.

0-7803-7378-2/02/$17.00©2002 IEEE

The power penalty is compared with the back-to-back sensitivity measured at 10^{-9} bit-error-rate (BER) for different OSNR and different PDL values at a 20-kHz scrambling frequency as shown in Fig. 1(b). Significant performance degradation occurs when a link has non-negligible values of PDL. For example, a 2.6-dB instantaneous PDL gives ~3 dB power penalty at a 26-dB OSNR. We find that, when the scrambling frequency is less than 1 kHz, the scrambling effect is negligible since the EDFA operating in the saturated regime is able to alleviate low speed power fluctuation due to PDL, and the optical receivers usually cut off all fluctuations at a frequency lower than their cut-off frequencies (kHz range). In contrast, if the scrambling frequency is beyond tens of kHz, the optical intensity modulation will be detected at the receiver and cause eye closure.

Although the use of a lumped PDL element can somewhat illustrate the effects of polarization scrambling, it would be more interesting to investigate the effect in a real long distance transmission link with distributed PDL statistics. In order to emulate these statistics, we use a recirculating loop testbed that closely reproduces the PDL statistics in a typical terrestrial long distance system, as shown in Fig. 2 (a). A single channel at 1555 nm is NRZ modulated at 10 Gbit/s (2^{23}-1 PRBS). A polarization scrambler with 20-kHz scrambling frequency is placed right after the transmitter. The dispersion-managed loop consists of three EDFAs operating in the saturated regime, 82 km of SMF, and 12 km of dispersion-compensating fiber (DCF). In order to emulate the statistical distribution of PDL, the loop contains a loop-synchronized polarization controller (PC) and a variable PDL element. The Jones matrix of the PC is updated after each round-trip interval of the loop to generate a series of random, uncorrelated polarization states during the entire loop running period (a particular number of loops), which is determined by the loop control circuitry. The background PDL of our loop is ~ 0.25 dB. The PDL element can be changed from 0.05 dB to 0.9 dB. Here we use 8 passes that emulate an 800-km transmission link with the average PDL growing according to the square root law [10]. The received optical SNR without PDL inside the loop is ~27 dB.

For a given PDL value inside the loop, we fix the input power into the receiver and measure the BER fluctuation as the link instantaneous PDL varies, i.e. different measurement samples according to PDL statistics. The two cases of with polarization scrambling and without scrambling are compared in Fig. 2 (b). With 0.45 dB and 0.9 dB PDL inside loop, which correspond to ~1.3 dB and 2.5 dB average PDL along the whole link, respectively, the 5% tails of BER without scrambling are 1.3×10^{-7} and 4.0×10^{-7}, which are extended to 4.0×10^{-6} and 5.0×10^{-5} with polarization scrambling. As the PDL increases, serious BER fluctuations (higher standard deviation) occur (Fig. 2c).

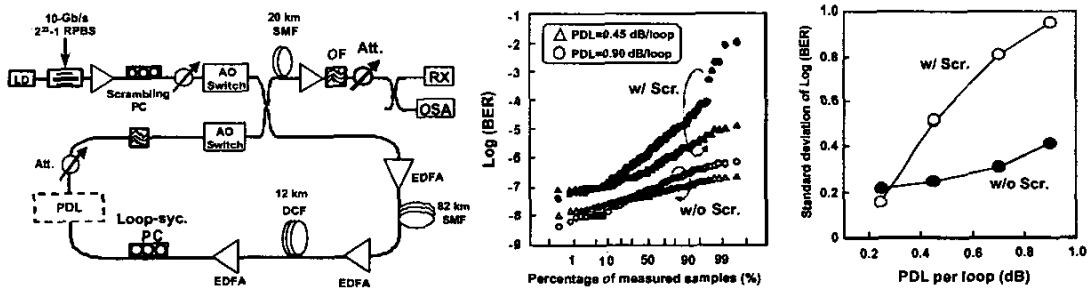

(a) (b) (c)

Fig.2 (a). Recirculating loop testbed that can emulate the distributed PDL along an 8×100-km link. (b) Statistics of BER fluctuation with different PDL values (open symbols indicate the case without scrambling while solid symbols indicates with scrambling case), each curve obtained from 200 sample. (c). Standard deviation of Log(BER) as a function of PDL per loop with each point obtained from 200 measurement samples.

References

[1] C. D. Poole, and J. Nagel, *Optical Fiber Telecommunications*, San Diego: Academic, vol. III-A, chapter 6, pp. 114-161, (1997).
[2] E. Lichtman, J. of Lightwave Technol., vol. 13, pp. 906-913, (1995).
[3] H.Y. Pua, et. al., J. of Lightwave Technol., vol. 18, pp. 832-841, (2000).
[4] H. Rosenfeldt, et. al., paper PD27, OFC'2001, (2001).
[5] P. C. Chou, et. al., *IEEE Photon. Technol. Lett.*, vol. 13, no.6, pp. 568-570, (2001).
[6] F. Bruyère, et. al., IEEE Photonics Technol. Lett., vol. 6, pp. 1153-1155, (1994).
[7] N.S. Bergano, et. al., Elect. Lett., vol. 32, pp. 52-54, (1996).
[8] M.G. Taylor, IEEE Photonics Technol. Lett., vol. 6, pp. 860-862, (1994).
[9] F. Heismann, et. al., IEEE Photonics Technol. Lett., vol. 6, pp.1156-1158, (1994).
[10] L.-S. Yan, et. al., paper We.P.38, ECOC'2001, (2001).

Demonstration of In-Line Monitoring and Dynamic Broadband Compensation of Polarization Dependent Loss

L.-S. Yan, Q. Yu, and A. E. Willner
Dept. of Electrical Engineering-Systems, EEB-500, University of Southern California, Los Angeles, CA, 90089
Tel: 213-740-1488, Fax: 213-740-8729, E-mail: lianshay@usc.edu

Abstract: We demonstrate in-line monitoring and dynamic broadband compensation of PDL for an 800-km optical link with 2.4-dB average PDL and 14-ps average PMD. The 2% power penalty tail of 10-Gb/s, WDM signals is reduced from 6.5 dB < 2 dB within a 6-nm PDL compensation bandwidth.

Introduction

For the past few years, there has been much interest in the limitations of high-speed optical systems caused by the stochastic nature of polarization mode dispersion (PMD) /1/. Additionally, it has recently become clear that even polarization dependent loss (PDL) produces more complex systems effects than originally assumed and can be a key limiting factor in high-capacity WDM systems /2-5/. This issue becomes especially pronounced because many optical in-line components, such as EDFAs, produce non-negligible PDL in optical systems.

Some of the deleterious systems effects induced by PDL include: (i) variation in the optical power and signal-to-noise ratio (SNR) of each WDM channel, (ii) degradation enhanced by the combined effect of PMD and PDL which broadens the distribution of system penalties /3/, /4/, (iii) for non-negligible amounts of PMD, the effects of PDL for many WDM channels will not be correlated with each other, (iv) similar to PMD, the effects of PDL are random and vary dynamically in an optical system due to the environment, and (v) PMD compensation becomes much more difficult in the presence of PDL due to their mutual interaction /5/.

Given the above effects, it is clear that a PDL compensator would be of enormous value for high-performance systems. To date, a functional dynamic PDL compensator has not been demonstrated. Furthermore, given that PDL interacts with PMD along a fiber link, it becomes imperative that PDL compensation be performed periodically along the transmission line. Moreover, a practical scheme of fast PDL monitoring will be critically necessary for dynamic PDL compensation. We note that a specific challenge for designing a PDL monitor is that EDFA gain transients may disrupt the measurement.

We demonstrate in-line monitoring and broadband compensation of PDL for four 10-Gbit/s WDM signals. Monitoring and dynamic compensation is performed every 100 km along the 800-km link. In order to avoid the influence of EDFA transients, monitoring is accomplished by using >20-kHz polarization scrambling on either: (i) the data wavelength, or (ii) an ancillary wavelength. Compensation is performed by gathering the monitored PDL and rotating two polarization controllers, each one preceding a fixed PDL component. In our experiment, the dynamic PDL compensator **reduces the 2% power penalty tail from 6.5 dB to < 2.0 dB** in the presence of 14 ps average PMD. Given the 0.2-ps of PMD in our EDFAs, our compensator can correct for degradations over a wide 6-nm bandwidth. We emphasize that PDL compensation is easier to perform periodically along a link, whereas PMD compensation is easier to accomplish only once along a link, typically at the receiver.

In-line PDL monitoring and compensation

In order to monitor the PDL along a cascaded EDFA link and avoid the influence of EDFA transients, we use fast polarization scrambling, or repeated scanning, over a series (typically, 100) of uncorrelated states of polarization (SOP) at the starting point of the link as shown in Fig. 1(a). The PDL value is obtained from the root-mean-square variation of the photo-detected signal power induced by PDL. PDL compensation is performed at each optical node between transmission fibers by adjusting the in-line compensators to minimize the monitored optical power variation. Broadband compensation for wavelength independent PDL can be realized by scrambling a continuous-wave, ancillary wavelength without affecting the data. The PMD of the transmission fiber will not influence the PDL monitoring and compensation. On the other hand, for the case when the PDL is not wavelength independent, polarization scrambling of the modulated data may be used for channel-by-channel compensation. We note that only one scrambler, regardless of the input SOP, is required for multi-wavelength scrambling for the entire link.

Experimental Setup

Fig. 1(b) shows the experimental setup which includes a recirculating loop testbed that closely reproduces a Maxwellian PMD distribution /6/. Four channels (1552 nm, 1554 nm, 1556 nm and 1558 nm) are modulated at 10 Gbit/s and decorrelated through 7 km of conventional single-mode fiber (CSMF). An ancillary wavelength at 1555 nm is used for broadband PDL monitoring and compensation. The dispersion-managed loop consists of four EDFAs operating in the saturated regime, 82 km of CSMF, and 12 km of dispersion-compensating fiber (DCF). In order to emulate the statistical distribution of PMD and PDL in real systems, the loop contains two loop-synchronized polarization controllers (PC), a polarization-maintaining (PM) fiber with ~5.4 ps DGD, and a PDL emulator. The Jones matrix of each PC is updated after each round-trip interval of the loop to generate a series of random, uncorrelated polarization states during the whole loop running period (a particular number of loops), which is determined by the loop control circuitry. The PDL per loop, including the PDL emulator, is about 0.85 dB. By tapping off part of the signals and filtering out the desired

wavelength, we can monitor the PDL value along the link and adjust a variable PDL compensator automatically. The testbed emulates an 800-km transmission link with ~14-ps average PMD and 2.4-dB average PDL. The received optical SNR without PDL inside the loop is ~27 dB.

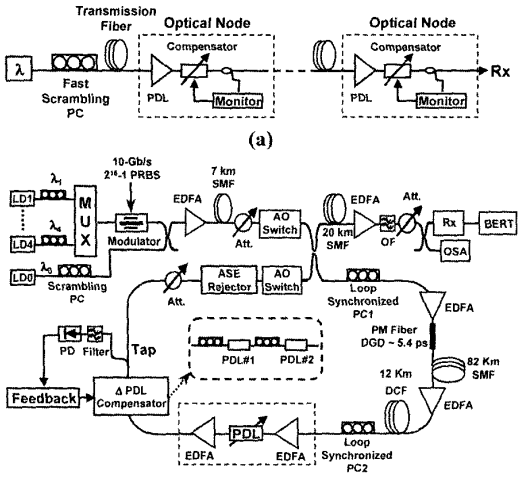

Fig. 1. (a) Schematic diagram of PDL in-line monitoring and compensation. (b) Broadband PDL compensation using a loop testbed with close reproduction of Maxweillian PMD (For single-channel compensation, the scrambling PC is put after the modulator).

Results and Discussion

Fig. 2(a) shows the RMS power variation of the monitored signal after passing through only one loop as a function of the polarization scrambling frequency (SOP update frequency). At a frequency higher than 2kHz, the influence of EDFA transients is suppressed and the results agree well with measurements taken for a passive PDL emulator (i.e., without EDFAs). The limited high frequency response is due to the photodiode bandwidth (~200 kHz). Fig. 2(b) shows the measured PDL versus transmission distance with inter-loop polarization decorrelation. Similar to PMD, the average PDL accumulates according to the square-root law. Fig. 2(c) shows the cumulative probability of measured power penalty at a 10^{-9} bit-error-rate for the testbed with (i) only 14-ps average PMD (5.4 ps/loop), (ii) only 2.4-dB average PDL (0.85 dB/loop), and (iii) both PMD and PDL. In the latter case, the 2% penalty dramatically increases from about 1.5 dB to 6.5 dB after introducing 2.4-dB PDL to the 14-ps PMD, and **even error floors (≥ 9 dB penalty) occurred for 5 out of 500 samples**. As comparison, 43-ps DGD after the same 800-km transmission without PDL will induce ~4.0-dB power penalty.

The resulting 500-sample power penalty histograms for in-line PDL compensation in the presence of 14-ps average PMD are shown in Fig. 3. We use a scrambling frequency of 200 kHz. The average PDL without compensation is still 2.4 dB. Using a dummy wavelength for PDL monitoring located at the center of the wavelength band (1555nm), the 2% power penalty is reduced to 1.4 dB (Fig. 3a) and 1.9 dB (Fig. 3b) for the channels 1-nm and 3-nm apart from the dummy wavelength, respectively. The residual penalties are induced mostly by the PMD. A major limitation of broadband PDL compensation is the PMD of the PDL components, which can induce wavelength dependent PDL.

Given the 0.2-ps of PMD in our EDFAs, our PDL compensator can correct for degradations over a wide 6-nm bandwidth. Compensation of wavelength dependent PDL can be implemented on a per channel basis by scrambling the SOP of the modulated data signals. In this case, the 2% power penalty can be reduced to 2.0 dB (Fig. 3c). We note that, after in-line compensation of PDL, traditional PMD compensation may still be applied before the receiver.

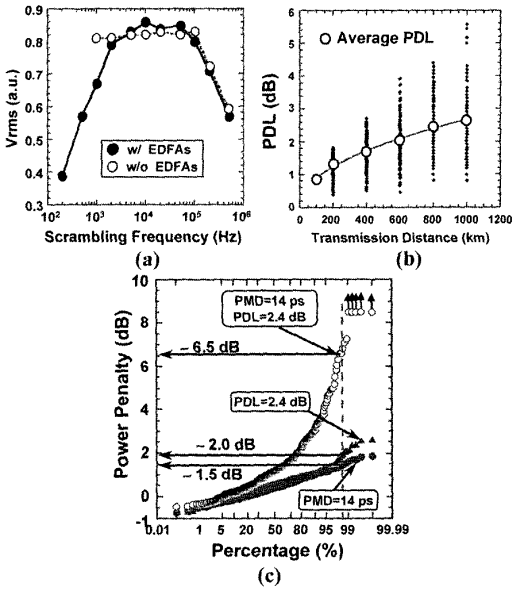

Fig. 2. (a) RMS power variation due to fast polarization scrambling and PDL. (b) PDL distribution at different transmission distances (100 samples for each distance). (c) Cumulative probability distributions of the power penalty at 10^{-9} BER for three different cases: (i) 14-ps average PMD only, (ii) 2.4-dB average PDL only, and (iii) combined PMD and PDL. Each case 500 samples.

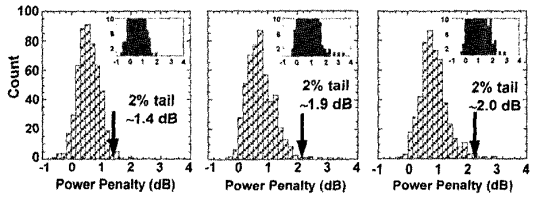

Fig. 3. Histograms of the power penalty at 10^{-9} BER: Broadband PDL compensation for (a) the 1556-nm channel and (b) the 1558-nm channel, with the PDL monitored at 1555 nm, and (c) compensation of a single data channel with the PDL monitored by scrambling the data itself.

References

/1/ C. D. Poole, and J. Nagel, Optical Fiber Telecommunications, vol. III-A (1997), pp. 114-161.

/2/ D. Wang, et al., CLEO'99, paper CMH2, 1999

/3/ B. Huttner, et al., IEEE J. Selected Topics in Quantum Electron, (2000), vol. 6, pp. 317-329

/4/ L.-S. Yan, et al., OFC'2001, paper WT5

/5/ Na Young Kim, et al., OFC'2001, paper WT6

/6/ Q. Yu, et al., OFC'2001, paper WT2

crease the efficiency of a given PMD compensator by insertion of a narrow band optical filter prior to the compensator. For NRZ signal the optimum filter is a vestigial sideband filter (VSB) having a bandwidth of less than the bitrate and a position for left or right sideband extraction. The concept of pre-filtering was confirmed by experiment at 40 Gb/s using a 30 GHz FBG filter and analyzed theoretically showing that the measured reduction of the probability (10^{-2}) for a PMD induced BER degradation also holds for a more system relevant lower value of less than 10^{-3}.

1. S. Lanne, W. Idler, J.-P. Thiéry, J.-P. Hamaide, "Demonstration of adaptive PMD compensation at 40 Gb/s", Techn. Dig. OFC 2001, Anaheim, 2001, TuP3.
2. L. Möller, "Broadband PMD Compensation in WDM Systems", proc. ECOC 2000, Sep 3–7, Munich, Germany, 2000, P 1.15.
3. R. Noé, D. Sandel, M. Yoshida-Dierolf, S. Hinz, et al., "Polarization Mode Disp . . . ", J. if Lightw. Technol., v. 17, n. 9, 1999, pp. 1602–1615.
4. T. Kudou, M. Iguchi, M. Masuda, T. Ozeki, "Theoretical Basis of Polarization Mode Dispersion Equualization up to the Second Order", J. of Lightw. Technol., vol. 18, no. 4, 2000, pp. 614–617.
5. D. Penninckx, S. Lanne, "Influence of the statistics on polarization-mode dispersion compensator", Techn. Dig. OFC 2000, Mar 2000, Baltimore, USA, WL6.
6. F. Buchali, S. Lanne, J.-P. Thiéry, W. Baumert, H. Bülow, "Fast Eye Monitor for 10 Gbit/s and its Application for Optical PMD Compensation", Techn. Dig. OFC 2001, Anaheim, 2001, TuP5.
7. I.T. Lima et al., 'Analysis of polarization-mode dispersion compensators using importance sampling', OFC '01, Anaheim, CA, MO4-1.
8. S. Bigo et al., "10.2 Tbit/s (256 × 42.7 Gbit/s PDM/WDM) transmission over 100 km TeraLight™ fiber with 1.28 bit/s/Hz spectral efficiency", OFC 2001, Anaheim, 2001, PD 25.
9. S. Lanne, D. Penninckx, J-P. Thiéry, J-P. Hamaide, "Extension of polarization-mode dispersion limit using optical mitigation and phase-shaped binary transmission", Techn. Dig. OFC 2000, Mar 2000, Baltimore, USA, ThH3.
10. H. Sunnerud, M. Karlsson, P.A. Andrekson, "A Comparison Between NRZ and RZ Data Formats with Respect to PMD-induced System Degradation", Tech. Dig. OFC 2001, Anaheim, 2001, WT3.

ThA7 **10:15 am**

Fast XPM-induced polarization-state fluctuations in WDM systems and their mitigation

Z. Pan, Q. Yu, and A.E. Willner, *Department of Electrical Engineering—Systems, University of Southern California, Los Angeles, California, 90089–2565, Email: zpan@usc.edu*

Y. Arieli, *Jerusalem College of Technology, Jerusalem, Israel*

1. Introduction

Polarization mode dispersion (PMD) has emerged as a key limitation in: (i) 10-Gb/s systems that use older legacy fiber, and (ii) 40-Gb/s systems that use even the newest types of fiber due to the non-zero PMD that appears in most in-line components. For such systems, PMD compensators would be needed to reduce the probability of network outage. Typically, PMD compensators attempt to correct a single WDM channel and are composed of a polarization controller, a differential-group-delay element, and a monitoring feedback loop.[1,2] The feedback loop is necessary to rotate the state-of-polarization (SOP) of the incoming signal for optimal alignment to the DGD element. Almost all PMD compensators have assumed that the system is linear and that the effects of PMD do not change much faster than on a millisecond time scale.

Unfortunately, optical fiber has nonlinear birefringence, thereby causing the signal SOP to wander depending on the local total optical power. This nonlinear effect can occur on nanosecond time scales and has serious implications for WDM systems. In a WDM link, the presence of other channels will rapidly alter a signal's SOP and dramatically reduce the instantaneous effectiveness of a PMD compensator. Recently, there were some reports of this effect,[3,4,5] but without much quantifiable systems results or proposing a possible method of mitigating this issue. These reports include: (i) an evolution of the channel polarization in dense WDM systems caused by cross-phase modulation (XPM),[3] and (ii) the general limitation of the effectiveness of PMD compensation in the presence of fiber nonlinear effects.[4,5] Note that since this effect occurs on the time scale of individual bits, it is highly unlikely that present optical PMD compensators can be modified to mitigate this effect.

In this paper, we show numerically and experimentally the degradation caused by XPM in systems that use PMD compensators, as well as demonstrate a modulation scheme for mitigating this problem. We use a simple and effective model to evaluate this problem. We show the quantity of XPM-induced polarization-state fluctuations and induced system penalty for different conditions. In order to overcome this problem, we propose and demonstrate a novel intra-bit polarization modulation (IPDM) format.[6] Unlike conventional NRZ or RZ signals, for which the polarization state does not change within a bit time, the IPDM format contains two orthogonal polarization states per bit interval. These two orthogonal signals are staggered so that they do not overlap in the time domain. This modulation format guarantees that the optical power is constant in any given polarization direction. Therefore, the XPM-induced phase difference for a signal's two polarization states is constant. Thus, polarization fluctuations can be depressed to a large extent. The results show a 7 dB improvement using the IPDM format over NRZ and RZ formats in a 40 ps DGD compensation system.

2. Nonlinear Transformation of the SOP due to XPM

In practical communication fiber with rapidly varying birefringence, signal propagation can be described by the Manakov-PMD equation *without* the nonlinear PMD term.[7] Consider the two-channel case with a probe signal at channel 1 and a pump signal at channel 2. Assume fiber PMD is small enough so that there is no polarization coupling (power exchange) between the parallel ($\parallel$) and perpendicular ($\perp$) components of the probe with respect to the pump polarization. Neglecting pump waveform distortion, the pump-induced phase change for the two probe components can be expressed as:

$$\phi_{\perp}(t) = \gamma \int_0^L P_2(t + d_{12}\, z) e^{-\alpha z}\, dz$$

$$\text{and} \quad \phi_{\parallel}(t) = 2\phi_{\perp}(t) \tag{1}$$

where γ is the nonlinear coefficient, $P_2(t)$ is the input pump intensity, $d_{12} = D(\lambda_1 - \lambda_2)$ is the walk-off parameter with D the chromatic dispersion coefficient. On the Poincare sphere, the probe SOP sphere will rotate an angle $\phi_{NL} = \phi_{\parallel} - \phi_{\perp}$ around the axis in the direction of the pump SOP. The probe will have the maximum modulation of SOP when the pump is polarized at a 45° angle relative to the probe. In this worst case, if $P_2(t)$ is sinusoidally-modulated at an angular frequency Ω, the peak-to-peak rotation angle of the probe SOP is given by:

$$\Delta\phi_{pp} = \gamma(\Delta P_{2,pp}) \left| 1 - e^{-(\alpha - i\Omega d_{12})L} \right| / \left| \alpha - i\Omega d_{12} \right| \tag{2}$$

In WDM systems, this effect induces bit-pattern-dependent polarization fluctuations in an optical signal whenever there is optical power present at other wavelengths. Fig. 1 illustrates this concept for a simple 2-channel (pump-probe) system. Channel 2 experiences changes of SOP due to XPM effects in the fiber caused by the bit "1" at channel 1. This effect becomes significant when the relative SOPs of the channels are preserved over distances long enough for nonlinear interactions to accumulate, implying that nonlinear changes in SOPs are more prevalent in fibers with low PMD, in which the relative polarization states of the channels remain correlated over long distances. If the PMD is not uniformly distributed along the transmission fiber, for example, lumped high DGD components are followed by low PMD transmission fibers, the overall link will still require compensation. However, the nonlinear change of the SOPs in the low PMD fiber can seriously reduce the effectiveness of PMD compensators, due to the fact that the overall PSP is dependent on the power of the other optical channels and their SOPs. Since first-order PMD compensation depends on applying the appropriate amount of DGD, aligned with the PSPs of the signal, it follows that if the PSP is bit-pattern-dependent, PMD compensation cannot be effectively realized.

3. System Model and Experimental Evaluation Setup

Based on the above theory, we investigate the performance of an ideal first-order PMD compensation system using this pump-probe model. Figure 2 shows our simulation and experimental setup. λ_1 is the pump channel with high launched optical power, representing all other WDM channels. λ_2 is the probe channel, suffering the XPM-induced polarization fluctuation. The probe channel goes through a variable DGD element and co-propagates with the pump channel in a low PMD transmission fiber. At the receiver end, another DGD element is used to compensate the first DGD section. In the absence of nonlinear effects,

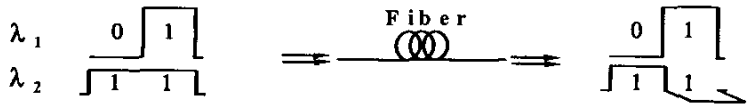

ThA7 Fig. 1. Concept of XPM induced bit-dependent polarization state change.

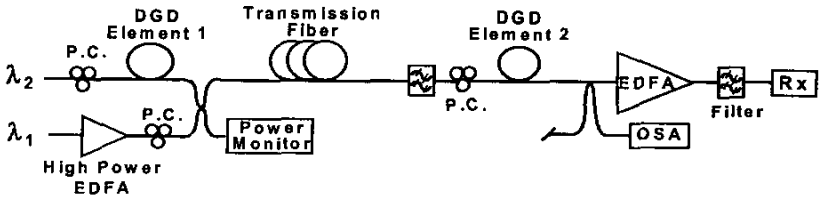

ThA7 Fig. 2. System model and experimental setup. λ_1: pump, λ_2: probe.

e.g., without the pump channel, the DGD is perfectly compensated in the system. With increasing pump power, the system will no longer be compensated and degradations will arise. We calculate and measure this degradation under different circumstances, e.g., by varying pump power and DGD values, by changing the pump modulation format, and by varying the channel spacing between pump and probe.

4. Proposed IPDM Format for the Mitigation of Nonlinear Effects

In general, methods to reduce nonlinear effects in fibers include: decreasing launched optical power, and destroying phase matching conditions. We propose a novel modulation format, IPDM, to decrease signal's degree of polarization, as shown in Fig. 3(a). The generation of this format is shown in Fig. 3(b). In the transmitter, each bit is split into two equal halves, with the first half transmitted at an orthogonal polarization to the second half. This modulation format guarantees that the optical power is constant in any given polarization direction. Therefore, if launched power for all WDM channels are bi-polarized, the two polarization components of the probe channel will not see any nonlinearly-induced phase difference. Thus XPM-induced polarization fluctuations can be supressed to a large extent. Fast polarization scrambling (on the scale of a bit time) may also reduce this problem, but will require fast polarization tracking for PMD compensation.

5. Results

To evaluate the XPM interaction with PMD for NRZ and RZ formats, we first use a continuous wave (CW) signal as the pump and normalize the XPM effect to the nonlinear phase difference between the two polarization states, denoted by $\phi_{NL} = \gamma P_1 L_{eff}$, which represents the magnitude of the XPM effect. PMD is represented by the DGD value. Fig. 4(a) shows system degradation vs. ϕ_{NL} in the XPM-inducing channel with a DGD value of 40 ps. Fig. 4(b) shows the power penalty vs. DGD value of the system with the nonlinear phase of 1. These results show that although in a single channel system without XPM the initial DGD can be fully compensated after transmission, in a WDM system with XPM, the probe SOP will rotate an angle ϕ_{NL}, causing system degradations. We note here that the worst case occurs at $\phi_{NL} = \pi$ when a slow PMD compensator is used for first-order PMD compensation. For 40 ps DGD, this corresponds to a 10 dB penalty for NRZ signals and an 8 dB penalty for RZ signals.

We also use a sinusoidally-modulated pump to investigate the effect of different channel spacing (the walk-off effect). Fig. 4(c) shows power penalty vs. pump-probe channel spacing. Negligible phase or polarization fluctuations occur when the channel spacing is greater than 3 nm.

For the IPDM format, experimental results are also shown in Fig. 4. Under all these conditions, both the pump and probe are in IPDM format. We find very low XPM induced polarization state

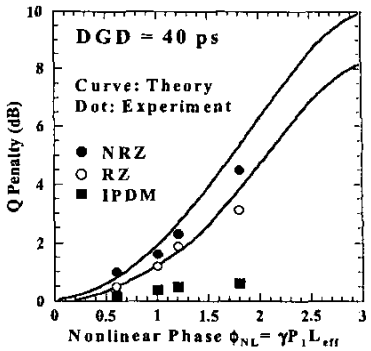

(a) Penalty vs. nonlinear phase

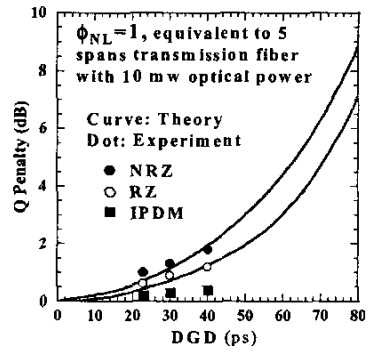

(b) Penalty vs. DGD value

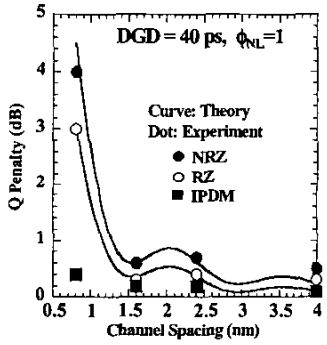

(c). Penalty vs. channel spacing

ThA7 Fig. 4. System degradations caused by XPM induced polarization fluctuation for different formats. $\phi_{NL} = \gamma P_1 L_{eff}$: nonlinearity induced phase change.

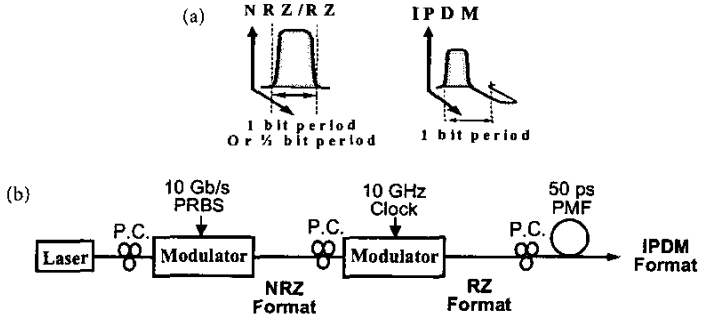

ThA7 Fig. 3. (a). Uni-polarization format (NRZ/RZ) and bi-polarization format (IPDM). (b). Setup for the generation of 10-Gb/s intra-bit polarization diversity modulation (IPDM) format.

fluctuations in this case. The performance is greatly enhanced when considering the system penalty (<0.5 dB). Note the one drawback of IPDM is that only half the optical power is used at the receiver causing a 3 dB back-to-back penalty.[6]

References

1. F. Heismann, D.A. Fishman, and D.L. Wilson, "Automatic compensation of first-order polarization-mode-dispersion in a 10 Gb/s transmission system", Proc. ECOC '98, Madrid, Vol. I, pp. 529–530, 1998.
2. D. Penninckx, S. Lanne, "Reducing PMD impairments", in Proc. of OFC, Vol. 2, paper TuP1, 2001.
3. B.C. Collings, and L. Boivin, "Nonlinear polarization evolution induced by cross-phase

modulation and its impact on transmission systems", *IEEE Photonics Technol. Lett.*, Vol., No. 12, pp. 1582–1584, 2000.
4. L. Möller, L. Boivin, S. Chandrasekhar, and L.L. Buhl, "Setup for demonstration of cross channel-induced nonlinear PMD in WDM system," Electron. Lett. Vol. 37, No. 5, 306–308 (2001).
5. R. Khosravani, Y. Xie, L. Yan, Y.W. Song, A.E. Willner and C.R. Menyuk, "Limitations to first-order PMD compensation in WDM systems due to XPM-induced PSP changes," in Proc. of OFC, Vol. 3, paper WAA5, 2001.
6. Z. Pan, Y. Wang, C. Yu, T. Luo, A.B. Sahin, Q. Yu, and A.E. Willner, "Intra-Bit Polarization Diversity Modulation for PMD Mitigation", in Proc. of ECOC, paper We.P.37, 2001.
7. G.P. Agrawal, *Nonlinear Fiber Optics*, (Academic Press, 2nd edition, 1995).

ThB 8:30 am–10:30 am Ballroom B

Raman 3

Andrew J. Stentz, *Photuris Inc., USA, Presider*

ThB1 8:30 am

Quantitative analysis of second order distributed Raman amplification

Y. Hadjar and N.J. Traynor, *Corning Fontainebleau Research Center, 7 bis Avenue de Valvins, 77210 Avon,, France, Email: traynorn@corning.com*

1. Introduction

The benefits of distributed Raman amplification in telecommunications networks have been widely reported.[1,2] The main limitations of this technique arise from the phenomena of single and double pass Rayleigh back-scattering of amplified spontaneous emission (ASE) and optical signals in the transmission fiber.[3] These impairments grow super-linearly with increasing distributed gain, imposing limits on the maximum allowable distributed gain in a system. One can improve the equivalent noise figure (NF) associated with this maximum allowed gain by use of a second Raman pump with a photon energy two Stoke's shift above the signal photon energy (so called second order Raman pumping). This technique was first proposed with the second order pump co-propagating with the signals, in order to provide Raman gain at the beginning of a fiber link without the noise transfer problems associated with first order co-propagating Raman pumps.[4] Subsequently a second technique of second order Raman pumping was proposed whereby both the first and second order pumps counter-propagate with respect to the signal.[5] There is a certain interaction length associated with the transfer of power from the second to first order pump which pushes the distributed gain further back into the fiber, thus improving the effective noise figure. Such a scheme is more appropriate than forward propagating second order pumping when span lengths are long, or when long distance unrepeatered transmission is sought. In addition, this configuration implements Raman amplification in the unsaturated gain regime, and as such will be more immune to transient effects.

In this paper we present a detailed experimental analysis of the performance benefits and pump power trade-offs associated with second order Raman pumping in the backward pumping regime.

2. Experimental method

The experimental configuration used is shown in figure 1. The pump lasers used in the experiment were a fixed wavelength Raman fiber laser at 1410 nm, which served as a second order pump source, and a tunable Raman fiber laser whose wavelength was set to 1495 nm and which was used as the first order pump. Maximum output powers of 3W and 1W were available from the respective pumps. The signal source was an external cavity tuned semiconductor diode laser tunable from 1520–1620 nm. The signal and pumps were counter-propagated in 100 km of Corning SMF-28 fiber, and the on/off Raman gain and ASE spectral density at the output were measured on an optical spectrum analyzer (OSA). To provide a reference for the second order pumping results the gain and effective NF were experimentally determined from 1580–1615 nm for a simple first order pump with 400 mW of power launched into the fiber at 1495 nm. The effective NF is defined by equation 1:

$$\rho_{ASE}(\upsilon) = h\upsilon(G_R F - 1) \qquad (1)$$

where $\rho_{ASE}(\upsilon)$ is the ASE spectral density, h is Planck's constant, υ is the optical frequency, G_R is the on/off Raman gain and F is the effective NF in linear units.

Subsequently, the power in the first order pump was decreased to 200 mW and the power in the second order pump increased to achieve the same gain as in the reference case, and again the gain and NFs were measured from 1580–1615 nm. The process was iterated with first order pump powers of 100, 50 and 25 mW.

3. Experimental results

Figure 2 shows the gain and NF comparison between the reference case (400 mW first order pump) and a configuration with 630 mW of second order pump and 100 mW of first order.

The curves in figure 2 represent steady state numerical solutions of the Raman equations for the given pump and fiber configuration. These simulations use measured Raman gain spectra, fiber loss spectra and Rayleigh scattering coefficients and calculate all pump-signal, pump-pump, and signal-signal interactions in the fiber link, giving the gain and noise figure at the output for each signal wavelength. We can see from the data that there is good agreement with the simulation results. For the pumping configurations considered in figure 2 we see around 0.8 dB improvement in the effective NF for second order pumping over the whole gain band. Figure 3 summarizes the results for all the configurations of first and second order pumping considered, showing the average NF achieved over the 1580–1615 nm band for the same nominal gain (13 dB) in each case, and the second order power required to achieve this gain as the first order

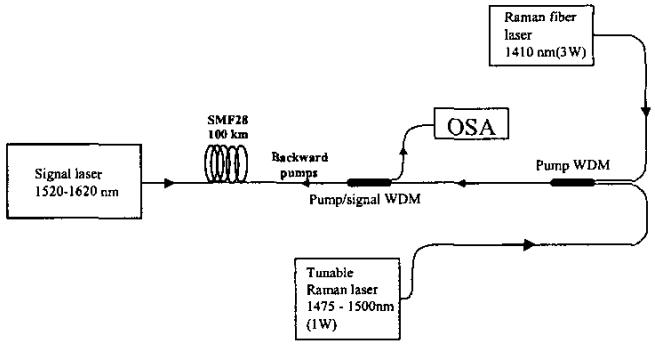

ThB1 Fig. 1. Experimental set-up.

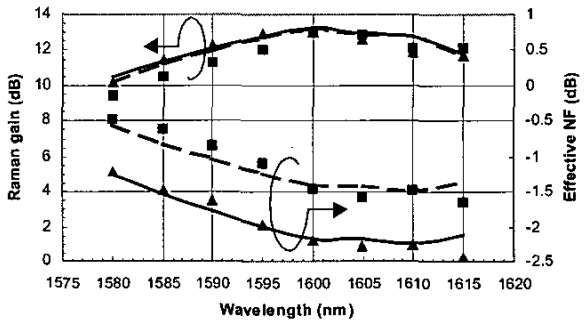

ThB1 Fig. 2. Gain and noise figure measurements for 400 mW first order Raman pumping (squares) and for 630 mW second order with 100 mW first order (triangles). Lines are results of simulations (broken for first order, solid for dual order).

High-birefringence nonlinearly-chirped fiber Bragg grating for tunable compensation of polarization mode dispersion

S. Lee, R. Khosravani, J. Peng[†], A. E. Willner, V. Grubsky*, D.S. Starodubov**, and J. Feinberg*

Dept. of Electrical Engineering - Systems
University of Southern California, Los Angeles, California, 90089-2565
(213) 740-1488, FAX : (213) 740-8729, sanggeon@scf.usc.edu
*Dept. of Physics, USC, also with D-STAR Technologies, Inc.
**D-STAR Technologies, Inc.
[†]Tsinghua University

Key advances in managing fiber dispersion and nonlinearities have produced astounding results in increasing the capacity of optical systems. However, polarization mode dispersion (PMD) has recently emerged as one of the next critical hurdles in achieving very-high-performance optical transmission systems and networks. This situation has occurred since much of the fiber that was deployed throughout the 1980's had a PMD parameter that is much higher (up to a factor of 100 times) than the more-optimized fiber deployed today. Therefore, any high-performance transmission systems using the embedded fiber base must account for possible PMD problems.

In general, PMD is caused by the different transmission speeds of the two states-of-polarization (SOPs) in the fiber. Since the state-of-polarization of a signal changes randomly along a fiber link, PMD is a statistically random quantity. However, to zeroth order, PMD can be emulated and compensated by simply delaying one state-of-polarization with respect to the other; ***this is more accurately known as differential group delay (DGD) although we will refer to it as PMD for this paper.*** Since PMD can change for a static link and can certainly change for a dynamically reconfigurable network, it is highly desirable to have a ***tunable*** PMD compensator.

One technique for compensating PMD is to use polarization maintaining fiber with polarization controller [1]. The disadvantage of this approach is that it is quite cumbersome and not tunable. Another method is to perform compensation in the electrical domain at the receiver [2], but this technique can only be performed at the receiver, not in-line, and can only compensate for a limited amount of PMD.

We report a nonlinearly-chirped fiber Bragg grating (FBG) that is written into a high-birefringence fiber and can be tuned to compensate for different amounts of PMD. The high-birefringence fiber provides a different delay for different SOPs, and the nonlinear chirp provides the ability for tuning of the specific amounts of differential polarization delay. The differential polarization delay can be tuned by stretching the grating. We use this novel grating to compensate for induced DGD and show good performance at 10 Gb/s signal with 175 ps tunability. This technique has the advantages in that it is tunable, fiber compatible, and compact.

Figure 1 shows a conceptual diagram of our high-birefringence nonlinearly-chirped fiber Bragg grating (HN-FBG). High-birefringence optical fiber (HBF), like polarization maintaining fiber, has a large refractive index difference between fast and slow polarization axes. Due to this large refractive index difference, the reflection position from the chirped grating is different for each polarization direction of an input optical signal at one fixed wavelength within the grating bandwidth. This reflection position difference (ΔL) gives a time delay between the two polarization directions of :

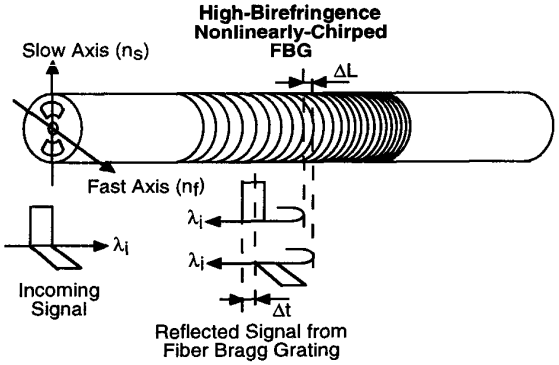

Fig. 1. Diagram of High-Birefringence Nonlinearly-Chirped Fiber Bragg Grating. (Incoming signal is in fast and slow polarization state.)

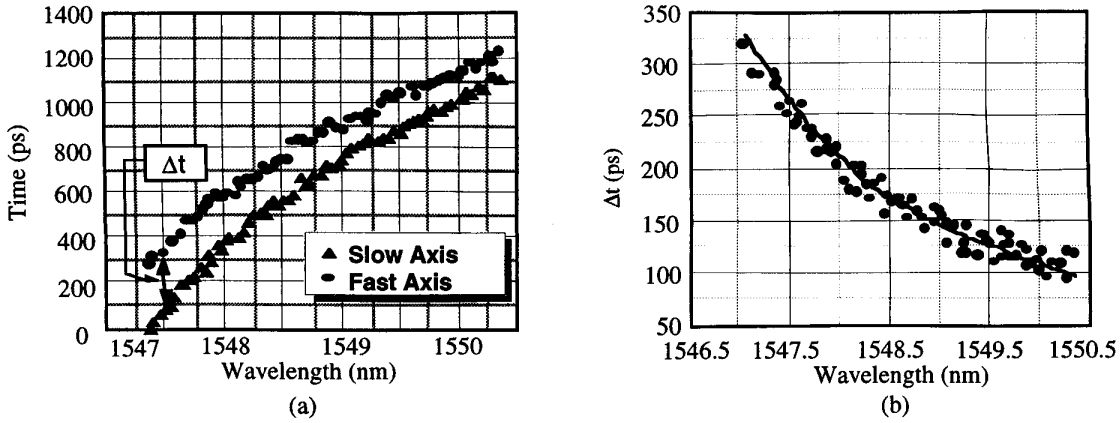

Fig. 2. (a) Reflected time delay curve for slow axis and fast axis polarization, (b) Time Delay between two orthogonal polarizatons. Solid line provides the expected time delay from the curve fitting of Figure 2 (a).

$$\Delta t = \frac{2n}{c}\Delta L \qquad (1)$$

, where c and n are the speed of light and core refractive index respectively. If the grating is written with nonlinear chirp, Δt can be varied with wavelength within the grating bandwidth. These different-delayed optical signals will be combined at the output from the grating without interference since they are orthogonally polarized.

We write a nonlinearly-chirped grating on a photosensitive HBF through nonlinearly-chirped phase mask using 300nm near UV light. High birefringence (i.e. large refractive index difference) gives two almost identical gratings for the orthogonal polarization directions separated by $\Delta\lambda$ which is determined by the refractive index difference between two polarization directions [3, 4, and 5], according to

$$\Delta\lambda = \frac{n_s - n_f}{n - n_{cl}}\lambda_g \qquad (2)$$

where n_s, n_f, n, n_{cl}, and λ_g are slow axis, fast axis, core, cladding refractive indices and average of the fast and slow polarization resonant wavelengths respectively. For our photosensitive HBF, $\Delta\lambda$is around 0.6 nm at 1550 nm. The time delay curves of the reflected signals from our HN-FBG as a function of wavelength are measured for each polarization direction, shown in Figure 2. (a). Note that almost identically-chirped gratings are written for both polarization directions. Since the grating is nonlinearly-chirped, Δt is a function of wavelength as shown at Figure 2. (b). Δt changes from 320 ps to 100 ps when wavelength changes from 1547.03 nm to 1550.34 nm. The solid line provides the expected time delay between the two polarizations, obtained by fitting our experimental data.

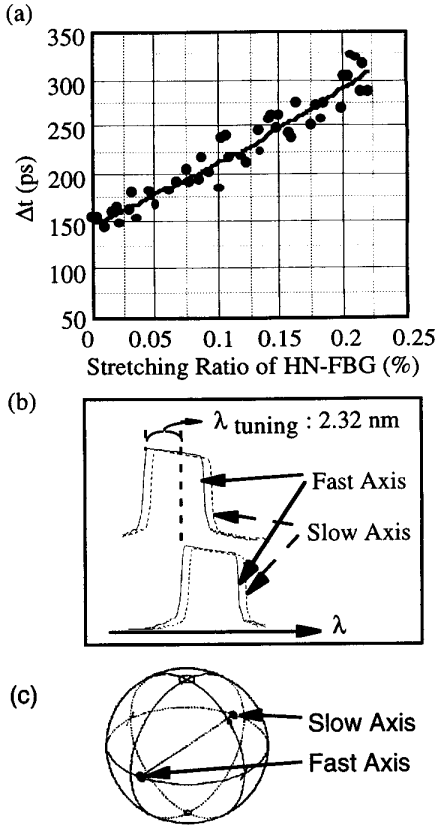

Fig. 3. Tuning of HN-FBG by Stretching at 1549.34 nm (a) Time delay between two polarizations (Δt) curve as a function of stretching. (b) Shifting of reflection spectra of two polarizations through stretching, (c) SOP of the reflected signal on Poincare sphere

We mounted our HN-FBG on a translational stage to investigate the tunability of the grating. With stretching, Figure 3 (b) shows that the shape of reflection spectrum for each polarization direction does not change over 2.32 nm wavelength tuning by stretching. SOP of the reflected signal from the HN-FBG is measured using an HP8509B polarization analyzer during stretching and the reflected SOP on Poincaré sphere for each polarization direction is shown on Figure 3 (c). There is no significant change in polarization due to stretching. We believe that the small amount of change of SOP (± 1.3 %) during stretching comes from imperfect polarization axis alignment to the grating or stretching. Figure 3 (a) shows the Δt change due to stretching the HN-FBG at 1549.33 nm. Approximately 170 ps Δt tuning is achieved by 0.22 % stretching of the grating at 1549.33 nm.

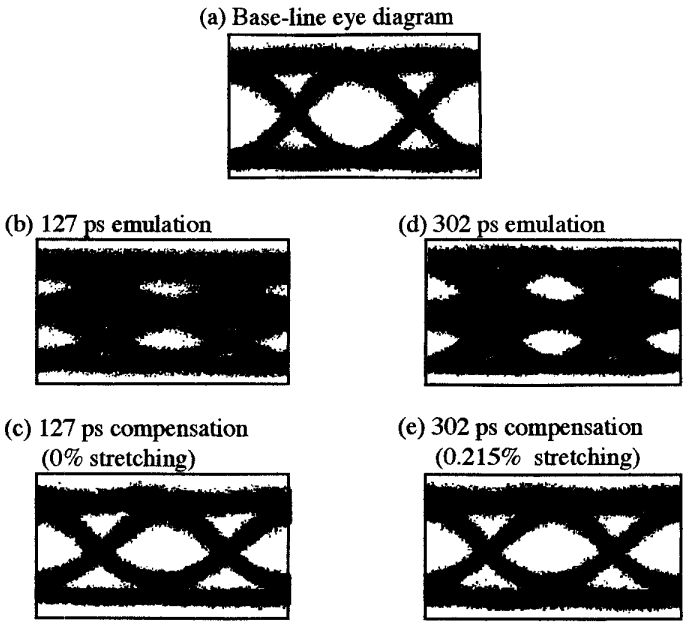

Fig. 4. Tunable PMD compensation of 10Gb/s using HN-FBG

Since the polarization does not change, and Δt is tunable, stretching provides simple potential application for tunable compensation of PMD on long distance high speed optical data transmission. To demonstrate this possibility, a DBR signal laser at 1550.2 nm is externally modulated at 10 Gb/s PRBS non-return-to-zero data format using a 16 GHz electro-optical intensity modulator. Around 127 ps and 302 ps DGD delays are introduced from PMD emulator. A polarization controller is used before the HN-FBG to align the polarization directions to the grating. Figure 4 (a) shows the base eye after the intensity modulator. Figure 4 (b) and (d) show the eye for 127 ps and 302 ps PMD emulations respectively. Both eyes are completely closed because emulation is larger than one bit period. Figure 4 (c) and (d) show the PMD compensation of HN-FBG without tuning and after tuning by 0.215% stretching. The eye is completely recovered after compensation, and bit-error-rate measurements confirm error free operation for both compensated cases.

REFERENCES

1. T. Takahashi, T. Imai and M. Aiki, "Automatic compensation technique for timewise fluctuating polarisation mode dispersion in in-line amplifier systems", *IEE Electronics Letters*, vol. **30**, no. 4, pp. 348-349, 1994
2. B.W. Hakki, "Polarization Mode Dispersion Compensation by Phase Diversity Detection", *IEEE/OSA Photonics Tech. Letters*, vol. **9**, no. 1, pp. 121-123, 1997
3. B. Ortega, L. Dong, W. F. Liu, J. P. de Sandro, L. Reekie, S. I. Tsypina, V. N. Bagratashvili, and R. I. Laming, "High-Performance Optical Fiber Polarizers Based on Long-Period Grating in Birefringent Optical Fibers" , *IEEE/OSA Photonics Tech. Letters*, vol. **9**, no. 10, pp. 1370-1372, 1997
4. A.S. Kurkov, M. Douay, O. Duhem, B. Leleu, J. F. Henninot, J. F. Bayon and L. Rivoallan, "Long-period fiber grating as a wavelength selective polarisation element" , *IEE Electronics Letters*, vol. **33**, no. 7, pp. 616-617, 1997
5. P. Niay, P. Bernage, T. Taunay, M. Douay, E. Delevaque, S. Boj, and B. Poumellec, "Polarization Selectivity of Gratings Written in Hi-Bi Fibers by the External Method" , *IEEE/OSA Photonics Tech. Letters*, vol. 7, no. 4, pp.391-393, 1995

ps/nm and −5,500 ps/nm, respectively. ΔQ^2 in these figures indicates the difference in performance when the pre-emphasis is changed from flat to positive for each channel. As can be clearly seen in these figures, positive pre-emphasis significantly distorts the signal spectrum close to λ_0 whereas the spectral shapes of the channels far away from λ_0 remain basically unaffected as the signal is pre-emphasized. This is yet another indication of a stronger nonlinear behavior of channels in the vicinity of λ_0.

5. Conclusions

We have presented a comparison of orthogonal and parallel polarization launch in a straight-line transatlantic DWDM transmission experiment. We observed more than 1 dB of Q-factor improvement when employing orthogonal launch. Our experimental results agree well with our simulator predictions.

References

1. N.S. Bergano et al., *OFC '1998*, paper PD12, San Jose, USA.
2. D.I. Kovsh et al., *OFC '2001*, paper WT1, Anaheim, USA.
3. J. Hansryd et al., *IEEE Photon. Technol. Lett.*, vol. 12, pp. 1261–1263, 2000.
4. C. Poole et al., *Electron. Lett.*, vol. 22, pp. 1029–1030, 1986.
5. B. Bakhshi et al., *OFC '2001*, paper WF4, Anaheim, USA.

WQ

4:00 pm–6:00 pm
Ballroom A

PMD Compensation

Robert M. Jopson, *Lucent Tech., USA, Presider*

WQ1 **4:00 pm**

Higher-order PMD compensation using a polarization controller and phase modulator in the transmitter

L.-S. Yan, Q. Yu, T. Luo, and A.E. Willner, *Department of Electrical Engineering-Systems, EEB-500, University of Southern California, Los Angeles, CA 90089, Email: lianshay@usc.edu*

Steve Yao, *General Photonics Corporation, 13766 Arapahoe Place, Chino, CA, 91710, Email: syao@generalphotonics.com*

1. Introduction

Polarization-mode-dispersion (PMD) has emerged as a key limitation in: (i) 10-Gbit/s systems that use older legacy fiber, and (ii) 40-Gbit/s systems that use even the newest types of fiber due to the non-zero PMD that appears in most in-line components. Moreover, PMD is characterized as being a random stochastic process for which the system degrading effects change with many environmental conditions.[1–2] For such systems, dynamic PMD compensators would be needed to reduce the probability of network outage.

To first order, PMD can be considered as a simple differential group delay (DGD) between the two polarization axes of the transmission fiber. Therefore, a first-order PMD compensator in the receiver would be a simple DGD element that reverses the time differential caused by the fiber. Typically, this PMD compensator is composed of a polarization controller, a DGD element, and a monitoring feedback loop.[3] The feedback loop is necessary to rotate the state-of-polarization (SOP) of the incoming signal to optimally align to the DGD element. After eliminating the first-order PMD effect, the system performance is essentially limited by higher-order PMD effects.[4] Therefore, higher-order PMD compensation is desired for the more demanding high-performance systems.

Previous reports of higher-order PMD compensators have used two or more DGD sections before the receiver, with each section requiring feedback control.[5–7] This scenario produces a very complex software algorithm of the control feedback signal, in which the DGD elements are correlated and changing one element may perturb the optimal solution on the other element. Therefore, many regions of local power-penalty minima will appear for the feedback control loop, thereby making optimal system performance and tracking extremely difficult.

We demonstrate a novel technique that compensates for the higher-order PMD by using a polarization controller and phase modulator in the transmitter as well as a traditional first-order compensator in the receiver. In our method, the receiver end compensates for first-order PMD, whereas the transmitter end compensates for the higher-order PMD components. These two ends are decorrelated, thereby significantly reducing the possibility of being trapped in a local minimum in the feedback loop. The operation is achieved by using: (i) the receiver end to compensate for first-order, (ii) telemetry from the receiver to the transmitter to give information on the signal's higher-order PMD, (iii) rotating the signal SOP at the transmitter to align with the fiber's higher-order principle axes, and (iv) producing signal chirp and higher-order compression using a phase modulator. Our simulation results show that the PMD tolerance for 40-Gb/s NRZ system can be increased from ~7 ps after first-order compensation to ~10 ps after higher-order compensation according to criterion of the outage probability of 1/18,000 (i.e., 30 min. per year). The experimental demonstration confirms the effectiveness of this approach. We note that the phase modulator at the transmitter side can be shared by many WDM channels, or replaced by only a dual-drive amplitude modulator as the transmitter. The feedback response has the similar requirement as first-order PSP transmission.[8]

2. Higher-order PMD compensation

The basic concept of higher-order PMD compensation is shown in Fig. 1 using a geometric representation of PMD vectors. The first-order PMD vector along the link is denoted by Ω_{link}. By applying an opposite Ω_{comp} at the receiver, we can compensate first-order PMD of the link. The second-order PMD vector Ω_{ω} is approximately perpendicular to Ω_{link}. If we can align the input SOP of the signal S_{sig} in parallel to the direction of Ω_{ω}, the pulse can be compressed by a given amount of chirp and the chromatic dispersion induced by second-order PMD effects,[9] and hence mitigate the system degradation due to higher-order PMD.

3. Experimental demonstration

To demonstrate the effectiveness of our approach, we use the experimental setup shown in Fig. 2(a). The signal from a tunable external cavity laser (ECL) is splitted into two parts. One of them is NRZ modulated at 10-Gb/s (2^{31} − 1 PRBS). A phase modulator driven by the clock signal can introduce a fixed chirp on the signal. A polarization controller (PC1) used to adjust the input SOP is placed right after the phase modulator. An optical switch then is used to switch between the two parts of light (i.e, one is modulated, another is un-modulated). A higher-order PMD emulator being put inside a temperature chamber is composed of 30-section polarization maintaining (PM) fiber spliced at certain angles and provides ~50-ps average PMD. After the PMD emulator, a PMD analyzer is used to measure the instantaneous PMD including first-order (DGD) and second-order PMD by switching the optical path to the un-modulated signal. A traditional first-order PMD compensator that is composed of a polarization controller (PC2) and a variable DGD element (VDGD) is used before the receiver. The DGD value of the first-order compensator is set from the measurement result of the PMD analyzer. By turning the phase modulator on and off, we can compare the compensation performance of first-order and second-order, as the results show in Fig. 2(b). The power penalty after first-order PMD compensation and higher-order PMD compensation are compared with respect to the second order PMD measured from the PMD analyzer. Here the power penalty is compared with the back-to-back sensitivity measured at 10^{-9} bit-error-ratio (BER) using an optical pre-amplifier before the receiver to increase the sensitivity. Note that these samples are not statistically distributed, we select 100 typical samples by sweeping the wavelength of the tunable laser. We can see that the relationship between the power penalty after the first-order PMD compensation is strongly correlated to the second-order PMD even though we set PC1 to

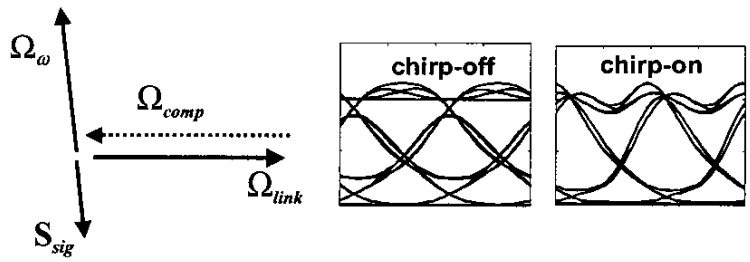

WQ1 **Fig. 1.** Schematic diagram illustrating the concept of proposed higher-order PMD compensation.

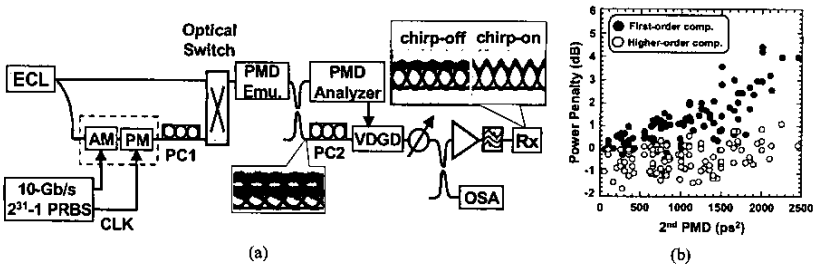

WQ1 **Fig. 2.** Higher-order PMD compensation using emulator that consists of 30-section PM fiber. (a) Experimental setup (b) First-order and higher-order compensation results as a function of the second-order PMD.

random polarization states for the first-order PMD compensation case.

4. Simulation Results

PMD compensation is modeled for NRZ 40-Gb/s transmission over a fiber link that has Maxwellian PMD statistics.[1] The link is modeled by 25 cascaded segments, each having a randomly distributed DGD (Maxwellian) and a randomly oriented PSP (uniform on the Poincaré sphere). We assume chromatic dispersion and fiber nonlinearities do not accumulate along the link since we are trying to isolate the effect of PMD separately. The PMD-induced Q-factor penalty for each fiber sample is calculated from the simulated BER versus the receiver decision threshold, assuming that amplified spontaneous emission (ASE) is the dominant noise source. First-order PMD compensation is achieved by compensating the link DGD to exactly zero at the signal spectral center, and the signal input SOP is controlled by a feedback loop of two control variables to maximize the simulated eye opening.

The purpose of PMD compensation is to reduce the probability of inducing large system penalties or link outages due to PMD. Under the assumption that an outage occurs when the Q-penalty is greater than 2.5 dB, Fig. 3(a) shows the outage probability as a function of the average DGD for an ensemble of independent fiber samples. Simulations show that, similar to first-order PSP transmission, the feedback loop controlling the input SOP does not suffer from the local-optima. As a result, the outage probability calculated using a local optimization algorithm (open circles in Fig. 3a) basically agrees with the probability calculated from a global optimization of input SOP over the whole Poincare sphere (solid circles). According to the criterion of the outage probability of 1/18,000, the system tolerance to PMD can be increased from 7.5 ps after first-order compensation to 10 ps after higher-order compensation. The Q penalty distributions for both first-order and higher-order compensation at 12.5-ps average PMD are shown in Fig. 3(b).

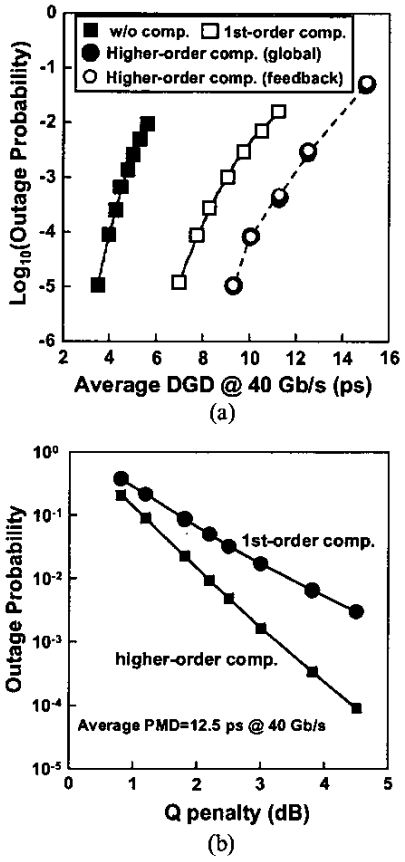

WQ1 **Fig. 3.** Simulation results for 40-Gb/s NRZ transmission (a) Probability of Q-penalties exceeding 2.5 dB, here for the higher-order compensation, the open circles is calculated from the compensation based on feedback control and the solid circle is based on global optimization. (b) Outage probability as a function of Q penalty for first-order compensation and higher-order compensation with 12.5-ps link average PMD.

References

1. C.D. Poole, and J. Nagel, *Optical Fiber Telecommunications,* San Diego: Academic, vol. III-A, chapter 6, pp. 114–161, (1997).
2. R.M. Jopson, L.E. Nelson, G.J. Pendock, A.H. Gnauck, "Polarization-mode dispersion impairment in return-to-zero and nonreturn-to-zero systems," OFC '99, paper WE3, (1999).
3. F. Heismann, D.A. Fishman, and D.L. Wilson, "Automatic compensation of first-order polarization mode dispersion in a 10 Gb/s transmission system," ECOC '98, 529–530, (1998).
4. H. Bülow, "Limitation of Optical First-order PMD Compensation," OFC '99, paper WE1, (1999).
5. Q. Yu, L.-S. Yan, Y. Xie, M. Hauer and A.E. Willner, "Higher order polarization mode dispersion compensation using a fixed time delay followed by a variable time delay," IEEE Photonics Technol. Lett., 8, 863–865, (2001).
6. M. Shtaif, A. Mecozzi, M. Tur, and J.A. Nagel, "A Compensator for the Effects of High-Order Polarization Mode Dispersion in Optical Fibers," IEEE Photonics Technol. Lett., 12, 434–435, (2000).
7. R. Noé, D. Sandel, M. Yoshida-Dierolf, S. Hinz, et al. "Polarization mode dispersion compensation at 10, 20, and 40 Gb/s with various optical equalizers," J. of Lightwave Technol., 17, 1602–1616, (1999).
8. T. Ono, Y. Yano, L.F. Garrett, J.A. Nagel, M.J. Dickerson and M. Cvijetic, "10 Gb/s PMD compensation field experiment over 452 km using principal state transmission method," OFC '2000, paper PD44, (2000).
9. William Shieh, "On the Second-Order Approximation of PMD," IEEE Photonics Technol. Lett, 12, 290–292, (2000).

WQ2 **4:15 pm**

Coherent heterodyne frequency-selective polarimeter for error signal generation in higher-order PMD compensators

I. Roudas, *Corning Inc., 2200 Cottontail Ln., Somerset, NJ 0887, USA. Tel. (732) 748-3716. Email: roudasj@corning.com*

G. Piech, M. Mlejnek, Y. Zhu, and D.Q. Chowdhury, *Corning Inc., Corning, NY 14831, USA*

1. Introduction

Polarization-mode dispersion (PMD) is a major impairment for the achievement of ultra-high capacity transmission over installed legacy optical fibers. For this purpose, several optical and electronic adaptive PMD compensation schemes are proposed in the bibliography.[1–7] All aforementioned techniques comprise a form of PMD monitoring device, which generates an error signal for driving the control unit of the adaptive PMD compensator. Frequency-selective polarimeters, i.e., devices which can measure the variation of Stokes parameters as a function of frequency,[6,8,9] are especially attractive candidates for PMD monitoring in higher-order PMD compensators because frequency-resolved Stokes parameters can provide, at least in principle, information about all PMD orders.

In this article we propose a novel coherent heterodyne receiver architecture, which can operate as a frequency-selective polarimeter. An original and efficient algorithm is used for the estimation of the Stokes parameters of the received signal spectrum. We demonstrate the operation of the coherent receiver by measuring the Stokes parameters of a 10 Gb/s NRZ signal after propagation through a polarization-maintaining (PM) fiber. To illustrate the potential use of the coherent heterodyne receiver as PMD monitoring device in adaptive PMD compensators, we generate